PhD Thesis

Metal Ion Based Assemblies of Gold Nanoclusters with Tuneable Photoluminescence

Submitted by

Manideepa Paul

for the award of the degree of

Doctor of Philosophy

Department of Chemistry

Indian Institute of Technology Guwahati

Guwahati-781039

Assam, India

September, 2023

Metal Ion Based Assemblies of Gold Nanoclusters with Tuneable Photoluminescence

A Thesis Submitted by

Manideepa Paul

Roll No. 176122049

Under the Supervision of

Prof. Arun Chattopadhyay

for the award of the degree of

Doctor of Philosophy

Department of Chemistry

Indian Institute of Technology Guwahati

Guwahati-781039

Assam, India

Statement

I hereby declare that the thesis entitled, "**Metal Ion Based Assemblies of Gold Nanoclusters with Tuneable Photoluminescence**" is an outcome of investigations and research work carried out by me in the Department of Chemistry, under the supervision of **Prof. Arun Chattopadhyay, Department of Chemistry, Indian Institute of Technology Guwahati, Assam, India** for the award of the degree of Doctor of Philosophy.

I further declare, the present thesis has not been submitted for the award of any degree, diploma or associateship to any other Institute or University or elsewhere to my knowledge.

Manideepa Paul

Date: 01/09/2023

Place: Guwahati

Manideepa Paul
Department of Chemistry
IIT Guwahati
Assam, India

भारतीय प्रौद्योगिकी संस्थान गुवाहाटी
INDIAN INSTITUTE OF TECHNOLOGY GUWAHATI

Certificate

This is to certify that the thesis entitled, "**Metal Ion Based Assemblies of Gold Nanoclusters with Tuneable Photoluminescence**" being submitted by **Manideepa Paul**, a Ph.D. student of **Department of Chemistry, Indian Institute of Technology Guwahati**, Assam, India for the award of the degree of **Doctor of Philosophy** in **Chemistry**. The data and information reported are the results of her work and has been carried out under the guidelines of laboratory. The work has not been submitted elsewhere for the award of any degree or diploma.

Prof. Arun Chattopadhyay
Department of Chemistry
Indian Institute of Technology Guwahati
Guwahati-781 039, INDIA

Date: 01/09/2023
Place: Guwahati

Prof. Arun Chattopadhyay
Thesis Supervisor
Department of Chemistry
IIT Guwahati
Assam, India

Dedicated to

My Parents and Brother

Acknowledgements

I am grateful to reach this destination, and I owe this journey to the guidance, support and encouragement of numerous individuals who have contributed along the way.

First and foremost, I extend my deepest gratitude to my Ph.D. supervisor and mentor Prof. Arun Chattopadhyay. His patience and willingness to take time to explain with unwavering calmness has not only broadened my horizons but also my intellectual growth. His dedication and expertise, his feedback and constructive insights have been pivotal in shaping my academic perception and re-igniting a sense of ambition in me. I am fortunate to have the opportunity to work under his supervision. Thank you, Sir!

I am thankful to my esteemed Ph.D. committee chairperson, Dr. Sunanda Chatterjee for her encouragement and constructive feedback. I am also thankful to my DC members Dr. Akshai Kumar A. S and Dr. Partha Sarathi Guha Pattadar, for their valuable suggestions, and thorough evaluation of my work.

I would like to extend my acknowledgment to the Department of Chemistry, Central Instrumentation Facility and Centre for Nanotechnology, IIT Guwahati for providing me the timely instrumentation facilities.

My heartfelt thanks also extend to my seniors and current lab members for the exchange of ideas and the mutual support we've shared.

To my well-wishers and friends, your belief and encouragement have been a source of strength during this stressful time. Your occasional distractions have lightened the difficulties of this academic journey.

Last but certainly not least, I am profoundly grateful to my parents for their boundless love, care, and self-less sacrifices. I am fortunate to have a younger brother who believed in me and poured me with unwavering support throughout the years.

I am thankful to the almighty for blessings.

Manideepa

Table of Contents

Chapter 1

Introduction and Literature Review

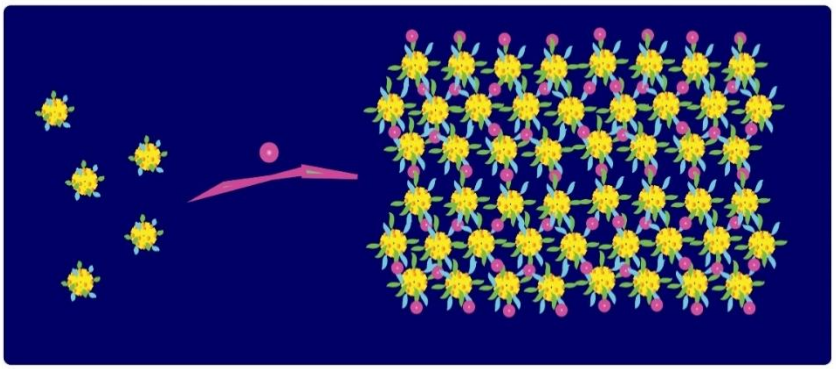

This chapter briefly gives an overview on metal nanoclusters, their properties. It concisely highlights the importance and applications in the field of nanoscience. Further brief discussions on methodologies to obtain higher ordered structures from nanoclusters, and implications in various fields have been mentioned.

1. Introduction

"There's plenty of room at the bottom", as delivered in his widely recognized lecture by Richard Feynman, envisioning manipulating individual atoms and molecules to produce new materials at the nanoscale. The field of nanoscience is a relentless chronicle of understanding the matter at the tiniest scale, scientific curiosity, and technological innovations. Nanoscience, a multidisciplinary research area delves into the widespread behaviours of nanoscale particles. Nanoscale particles are referred to as tiny units of matter at the nanometre scale, typically considered in the range of 1-100 nanometre. Due to quantum effects and increased surface area, the properties of nanoscale materials are different from their larger counterparts. Continuous advancements in synthetic chemistry, and the prominence of nanoscale particles (for example nanoclusters, nanoparticles, quantum dots. etc) have greatly expanded the horizon in science. The dynamic field of nanoscale particles spurs research to drive and underpin applications in the fields of energy conversion, bioimaging, chemical sensors, catalysis, and drug delivery.

1.1 Metal Nanoclusters

The advancement in the field of nanoscience have led to the development of numerous nanoparticles varying in shape, size, and composition. Metal nanoclusters (NCs) have progressed in research of nanoscale materials and related fields due to their distinctive properties. Elucidation of their properties and control of the synthesis procedure have been explored in recent years. They exhibit an intermediate state between an atom and a solid, that is apparent in their atomic configurations and electronic structures. The discrete electronic structures of metal NCs induce a plethora of unique chemical and physical properties. New methodologies owing to the successful development of atomically precise metal NCs are emerging. Based upon the attributes, NCs have important potential in catalysis, luminescent-based devices, chemical sensors, light harvesting materials, and other applications.

1.1.1 Brief Idea

Metal NCs are sub-nanometre-sized (2-3 nm in diameter) particles of atomic precision and represent an intermediate state of matter. As the size approaches the fermi wavelength of electrons, it bestows them to bridge between isolated metal atoms and metal nanoparticles

having plasmonic properties. Metal NCs are manifested in their molecular-like characteristics such as HOMO-LUMO transitions, tuneable photoluminescence, and intrinsic magnetism. Owing to the discrete energy levels, NCs exhibit unique chemical properties that are dependent on their geometric structures and compositions. [1-2]

1.1.2 Luminescent Metal Nanoclusters

Metal NCs of gold (Au), copper (Cu), and silver (Ag) have been extensively studied, owing to their different electronic, chemical, and optical properties in terms of small size, photoluminescence, quantum yield, large surface-to-volume ratio and photostability. Numerous factors such as NC size, the design of surface ligands, NC assembly structure, etc affect the photoluminescence properties.[3-6]

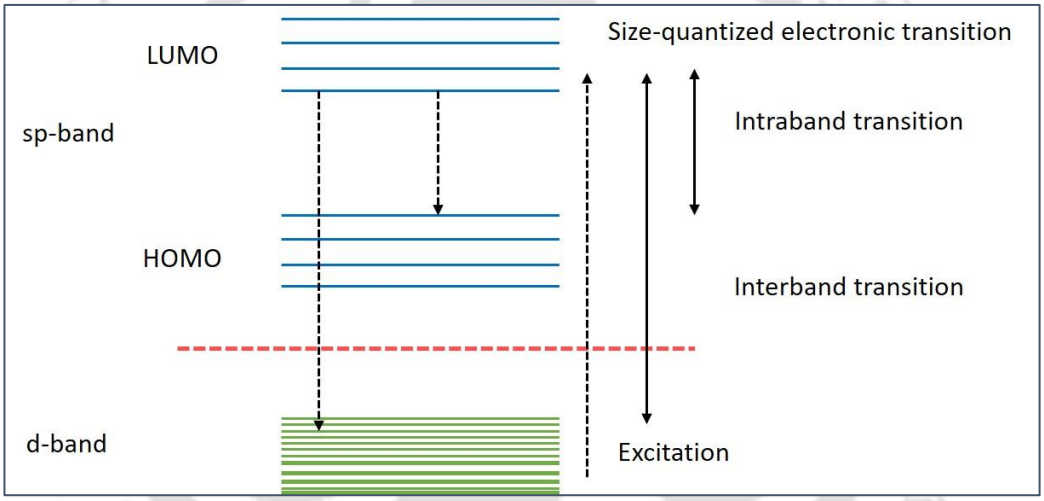

Figure 1.1. Solid-state model for the origin of the two luminescence bands: The high-energy band is due to the radiative inter-band transition between the sp and d-bands, while the low-energy band is originated from radiative intra-band transitions within the sp-band across the highest occupied molecular orbital (HOMO) and lowest unoccupied molecular orbital (LUMO) gap. Modified from Reference 7. Copyright (2002) American Chemical Society.

The primary explanations for the mechanism of photoluminescence have been recognized. The quantum confinement mechanisms of metal, not exhibiting plasmonic properties are observed in a few atom NCs. The continuous energy band is broken down to discrete energy levels, as the size of metal NCs approaches the fermi wavelength of electron (typically <1 nm). The motion of electrons is restricted leading to the breakup of continuous energy

bands to discrete energy levels, and no longer supporting SPR but resulting in molecule-like properties. The origin of electron transition process and metal NCs' photoluminescence emissions are fundamentally attributed to intra band (sp - sp) transition and/or inter-band (sp - d) transition.[7] Other parameters like charge transfer mechanism on the shell of metal NCs following interaction between metal core and functional ligands have a significant effect on emission properties. Ligand to metal charge transfer (LMCT) or ligand to metal-metal charge transfer (LMMCT) is based on the concept of photoluminescence emission of organometallic complexes of transition metals.

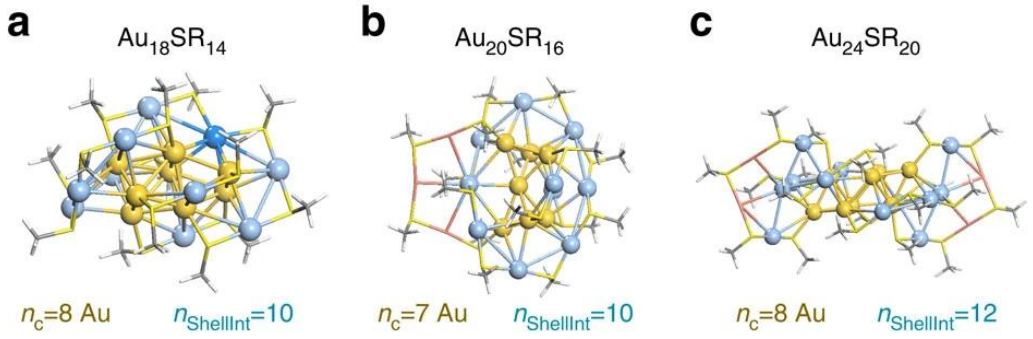

Figure 1.2. Optimized geometries of the experimentally synthesized metal nanoclusters. (a) $Au_{18}SR_{14}$, (b) $Au_{20}SR_{16}$, (c) $Au_{24}SR_{20}$. Here, n_c represents the number of core metal atoms while $n_{ShellInt}$ represents the number of shell-to-core interactions. Representation of ligands (S-CH_3) is shown in stick, core, and shell atoms, in ball and stick, colored yellow and blue, respectively. Reprinted with permission from reference 14. Copyright 2017 Springer Nature.

However, these explanations also are challenged when accounting for size-dependent and independent emissions is concerned. Metal NCs' properties are sensitive to the number of atoms, and hence control at the atomic level is required. Therefore, the synthesis of NCs requires suitable reducing agents and surface capping and/or protecting ligands for surrounding the NC core acting as stabilizers. These stabilizing ligands with different functional moieties are important to determine the structure and photoluminescence properties of NCs. Generally, NCs are composed of a metal core allied by stable motifs, which is further stabilized by ligands like thiolates, carbenes, phosphines, or a mixture of ligands.[7-14]

The thiol-protected NCs have been demonstrated to have excellent stability in photoluminescence properties, by taking advantage of the strong coordination between Au/Ag and sulfur atoms. The luminescence properties of NCs can be influenced by surface capping ligands in two ways to prevent aggregation: (a) ligand to sulphur (S) charge transfer and then to Au through Au-S bond (LMCCCT) and (b) direct donation of electron (of electron rich atom/group in ligands) to Au core.[3] Different thiol (-SH) containing functional groups such as glutathione (GSH), 3-mercaptopropionic acid (MPA), p-mercaptobenzoic acid, cysteine, etc have been used to synthesize luminescent NCs. GSH-protected clusters have high quantum yield attributed to the presence of functional groups (-COOH, $-NH_2$) with contains of electron-rich (O, N, etc) atoms that facilitate LMCCT. Also, ligand stabilized metal NCs, for instance, $Au_{102}(SR)_{44}$, $Au_{144}(SR)_{60}$, and $[Ag_{25}(SR)_{18}]^-$ exhibit precise molecular formulas, with uncharged or charged species.[15-17] Examples include chemical reactivity, chirality, and well-defined emission and absorption resulting from quantized energy levels. The existence of various types of ligands on the metal core allows the possibility to form specific non-covalent interactions with metal NCs, and other molecules.

1.2 Application of metal NCs

1.2.1 Catalysis

NCs of size 1-2 nm with strong quantum confinement are crucial for nanocatalysis. It is possible to correlate the structural properties of atomically precise NCs with well-defined structures and precise composition with their catalytic properties. High enhancement efficiency due to high surface-to-volume ratio and extreme control over specific site selectivity are major factors of NCs. For example, poly(N-vinyl-2-pyrrolidone) Au NCs were used as homogeneous catalysts for various aerobic oxidation reactions of alcohol as well as formal Lewis acid reactions.[18] Au NC deposited on TiO_2 nanotube arrays with enhanced activity have been used for water splitting and photocatalytic decomposition of pollutants.[19] Selective organic transformation for controllable synthesis of chemicals is important. So, Au_{38} NC with excellent activities in the selective oxidation of sulfides and amines were developed.[20,21] $Au_{25}(SR)_{18}$ as a model catalyst has been developed for selective reduction of α, β-unsaturated ketones and aldehydes.[22] Au NCs have been explored as catalyst for electrocatalytic reactions in fuel cells, and for organic reactions including coupling reactions, oxidation, and reduction reactions.[23-30]

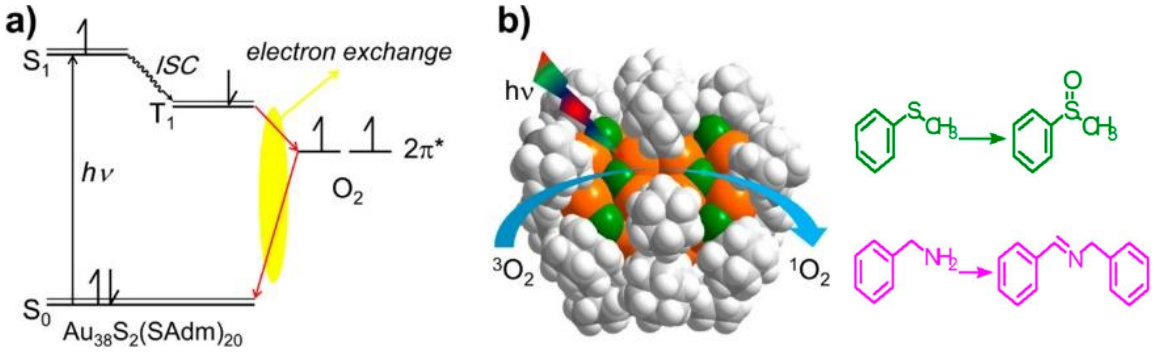

Figure. 1.3. Demonstration of $Au_{38}S_2(SAdm)_{20}$ NCs in the generation of activated singlet oxygen for selective catalytic reactions. (a) Mechanism of the dexter-type electron exchange coupling between $Au_{38}S_2(SAdm)_{20}$ and oxygen molecule for generation of singlet oxygen and (b) Illustrations of the $^1O_2$ generation process and catalysing the oxidation of sulfide to sulfoxide and benzylamines to imines. Reprinted with permission from reference 21. Copyright 2017 American Chemical Society.

1.2.2 Sensors

The sensing of different small molecules and ions using NCs has been reported. The optical properties and luminescence of metal NCs are responsive to the local environment and are influenced by interaction with external analytes and hence act as "turn-on" or "turn-off" sensors.[31] For instance, fluorescent NCs were used for ultrasensitive detection of Hg (II) ions at nanomolar concentrations.[32,33] The GSH -Au NC and BSA-Au NC as fluorescent sensors for highly selective detection of Cu (II) ions were reported.[34-36] In another example, Au NC and Ag NCs as nanosensors for selectivity towards cyanide ion and halide ions with a limit of detection in the nanomolar range were developed.[37,38] From literature surveys, fluorescent Au NCs have been reported to be used for the detection of amino acids and their derivatives such as urea, cysteine, dopamine, and cholesterol.[39-42]

1.2.3 Biological applications

Owing to the nontoxicity of Au particles, they are widely used in biological and biomedical applications such as cancer treatment, bio-labelling, drug delivery, etc. Biocompatible Au NCs for cancer radiotherapy and high tumor specificity were reported.[43,44] For instance, near-IR emitting fluorescent Au NC as biomarkers were incorporated into cancer cells

(HeLa) by endocytosis and featured excellent intracellular thermal sensitivity.[45] Also, conjugated Au NC nano bio probe for targeted flow-cytometric detection of acute myeloid leukaemia cells were reported.[46] Even Au-gadolinium nanocluster showed high tumour accumulation and in vivo renal clearance.[47] In another example, oligoarginine capped Au NC as a nanocarrier can also be applied for the delivery of biological drugs-nerve growth factor, small interfering RNA in pancreatic cancer.[48]

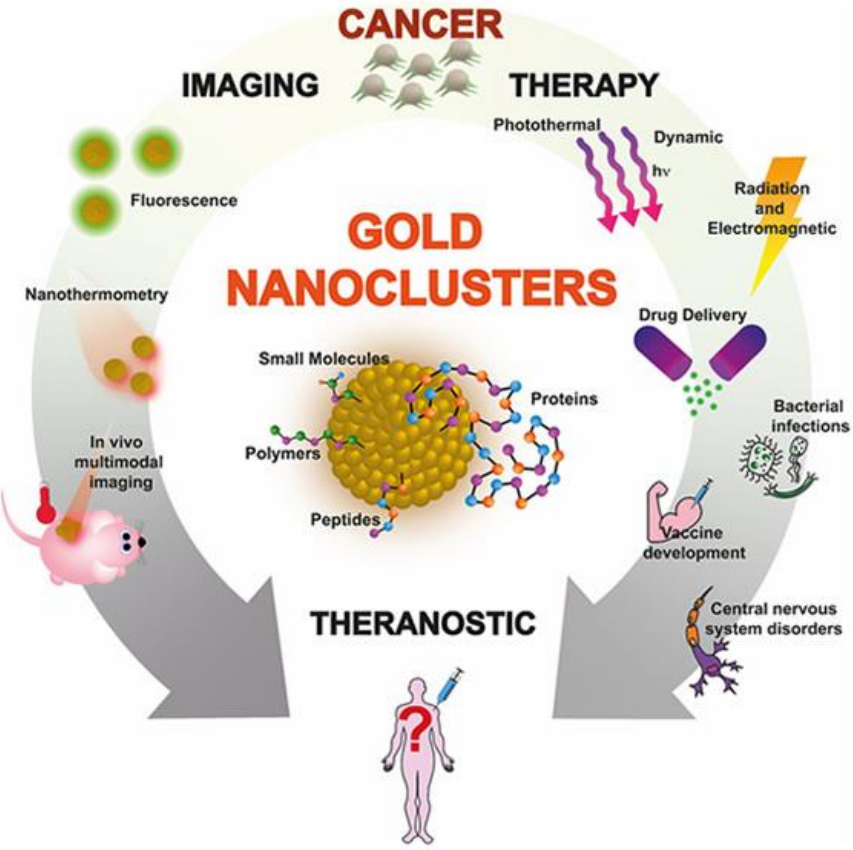

Figure. 1.4. Schematic illustration of Au NCs with various classes of capping ligands, investigated for potential use in imaging, therapy, and theranostic roles in biomedical applications. Reprinted with permission from reference 53. Copyright 2022 American Chemical Society (open access).

BSA capped Au NCs were used for the delivery of the hydrophilic drug doxorubicin (DOX) to cancer cells with concurrent single-photon or two photon imaging.[49] Au NCs have been reported as a drug delivery tool, without light activation as well. For example, protein protected Au NCs were tested for anticancer therapeutics in lung cancer cells.[50] Numerous studies have concentrated in particular on integrating imaging and therapy into a single platform. A variety of biomolecules are employed as capping ligands for metal NCs. This

provides options for toxicity reduction, and biocompatibility and making NCs a desirable and adaptable tool for biomedical applications.[51-53]

1.2.4. Light emitting diodes

Metal NCs synthesis and characterization at atomic precision further renders the tailorable cluster emission based on cluster size and structure. Such tunability of emission also greatly adds metal NCs in white light emitting diode (WLED) applications. Active absorption and emission make metal NCs to be used in the field of electroluminescent devices. For example, aggregation-induced emission of Au NC by ionic liquid (IL) for WLED and multiple ion probe applications were reported.[54] Also, Cu NCs with long luminescence lifetime, and high quantum yield, were utilized as WLEDs with white light properties.[55] Protein present in unicellular bacteria as a stabilizer for the synthesis of Au NC was utilized for white light emission.[56] In a nutshell, both Cu NCs and Au NCs have been utilized extensively for WLEDs.

1.3. Self-assembly of metal NCs

Metal NCs are focus of interest due to their strong size dependent properties, giving rise to different applications, and the possibility to study the evolution of various structures as a function of size. The use of mono-dispersed NCs as building blocks for superior structures offers possibilities for designing new materials. In this regard, the physicochemical properties of assembled NCs are found to be superior to those of non-assembled NCs, attributed to the combined properties of the constituents. As a result, an upsurge in the generation of complex nanostructures by using NCs as building units has been reported in the literature. The assemblies of such NCs could be achieved because of their improved stability and well-defined molecular compositions. In this aspect, the assembly into superior hierarchical structures utilizing the molecular nature of metal clusters with discrete energy levels would confer them with new collective functions. Hence, the development in creating higher-order structures could be a significant step toward applications in the field of noble metal NCs. Self-assembly of NCs has been categorized into different sections including template-free assembly, and template-directed assembly.

Different interactions for such assemblies of NCs have been accomplished, among which a few from the literature are summarized below-

1.3.1 Template-free assembly of metal NCs

The role of surface forces (ligands) on the self-assembly of metal NCs in their colloidal forms such as electrostatic interactions, hydrogen bonding, C-H···Π/Π···Π, van der Waals, and metallophilic interactions have been discussed in the literature.

For example, Jadzinsky et al. reported the crystallization of Au_{102}(*p*-MBA)$_{44}$ induced by hydrogen bonding for the first time. [16] In another example, Nonappa et al. demonstrated the self-assembly of Au_{102}(*p*-MBA)$_{44}$ monodisperse NC into two-dimensional (2D) colloidal crystals. Also, by changing the kinetics of crystallization via electrostatic interactions, the shapes of the assembled structure could be tuned.[57,58] Also, electrostatic interactions to demonstrate self-assembly in NCs are introduced by charge separation in neighboring cluster units. For example, the interaction between negatively charged Au@SG NCs and positively charged modified silicon nanoparticles to form dual emitting spherical superstructures was reported.[59]

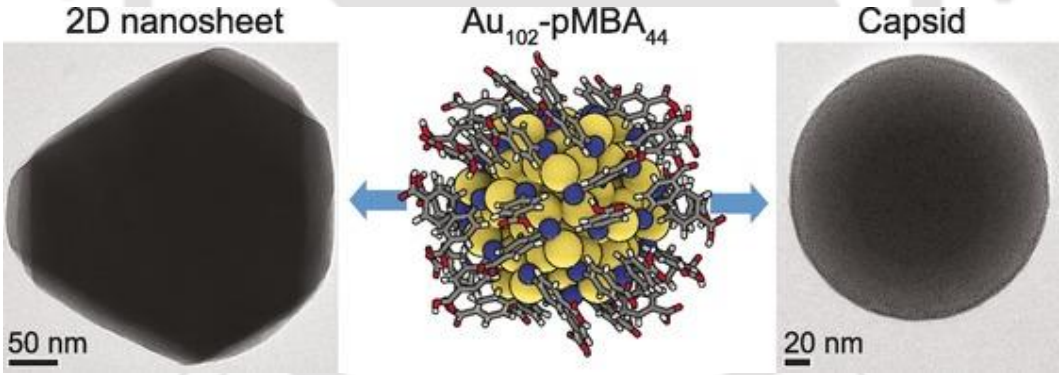

Figure 1.5. (a) TEM images of colloidal assembly of Au_{103}(*p*-MBA)$_{44}$ NCs into 2D crystalline nanosheets showing the stacked layer. (b) Internal structure extracted from the solid-state structure of Au_{102}(*p*-MBA)$_{44}$ NCs. (c) TEM images of spherical capsids of aqueous Au_{102}-*p*MBA$_{44}$ nanoclusters. Reprinted with permission from Reference 57. Copyright 2016 John Wiley and Sons.

Self-assembly of cationic and anionic bimetallic Au-Ag NCs in one pot method was also demonstrated.[60] Wu et al. demonstrated the 2D self-assembly of ligand-assisted Au_{15} NC into a few, multilayered nanosheets in colloidal dispersions at higher temperatures in a vacuum based on the hydrophobic interaction between the ligands.[61] In this case, the

asymmetric distribution of ligands generates the anisotropic van der Waals attraction into 2D assemblies, thus allowing further control of the thickness and morphologies of Au_{15}NC.

The C-H···Π/Π···Π interactions were further extended to demonstrate the crystallization of larger NCs. For example, Higaki et al. reported the crystal structure of $Au_{103}S_2(S\text{-}NAP)_{41}$ NC via vapor diffusion method.[62] The weak inter and intra NC interaction between the ligands is the primary reason behind such type of assembly. Also, metallophilic interactions such as Au-Au interaction and their structure-directed assemblies are also known.[63] For example, Nardi et al. demonstrated the one-dimensional (1D) linear assembly of $Au_{25}(SBu)_{18}$ via aurophilic interactions.[64] Wu et al. also reported the three-dimensional (3D) colloidal assembly of $[Au_{25}(p\text{-}MBA)]^-$ into nanoribbons with enhanced PL and quantum yield. In another example, Li et al. reported hierarchical 1D to a 3D assembly of Au_{21} nanoparticles.[65]

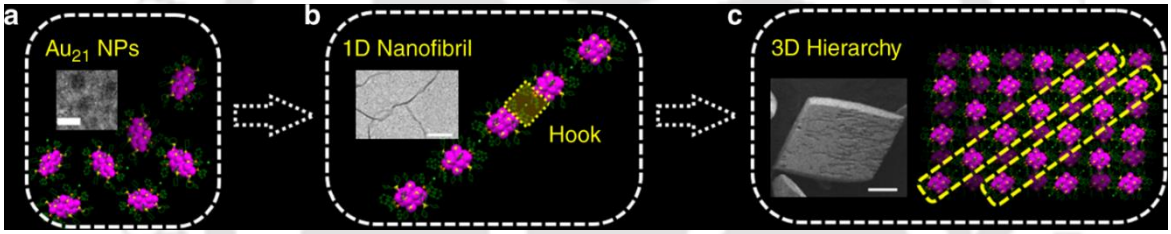

Figure 1.6 Schematic picture of the hierarchical (1D to 3D) assembly of Au_{21} NPs. (Inset: TEM image of individual Au_{21} NPs). (b) TEM image of the 1D nanofibril assembled from Au_{21} NPs (c) scanning electron microscopic (SEM) image of 3D crystals assembled from Au_{21} NPs. Reprinted with permission from Ref 65. Copyright 2018 Springer Nature.

1.3.2 Template-directed assembly of metal NCs

Templates considered substrates consisting of active sites such as macromolecules, polymers, and DNA can bind with NCs to induce assembly. Quantum confinement of NCs (replacing metallic NP) and PL properties of NCs add advantage to template-based assembly. In the recent past, new properties of NCs have been observed in different forms of hybrid assemblies. Such assemblies depend on the stability of NC and the interaction of the template and NCs. For example, Yang et al. demonstrated the self-assembly of Au@SG NC inside poly(amidoamine) dendrimer with enhanced PL for bioimaging.[66] Ju et al. demonstrated pH-dependent assembly-disassembly with similar Au NC with bacterial

protein that was further used for protein delivery and cell imaging.[67] However, polymer templates often lead to uncontrolled aggregation. Later, Wang et al. reported the self-assembled Au NC-DNA complex in cancer cells and used it for diagnosis and theranostics.[68] Also, combined host-guest interaction also produces assembled NCs with superior photophysical properties. For example, Jiang et al. demonstrated Au_{22}NC for self-assembled spheres of NC by utilizing non-covalent ligand interaction with host cavities of cucurbituril.[69]

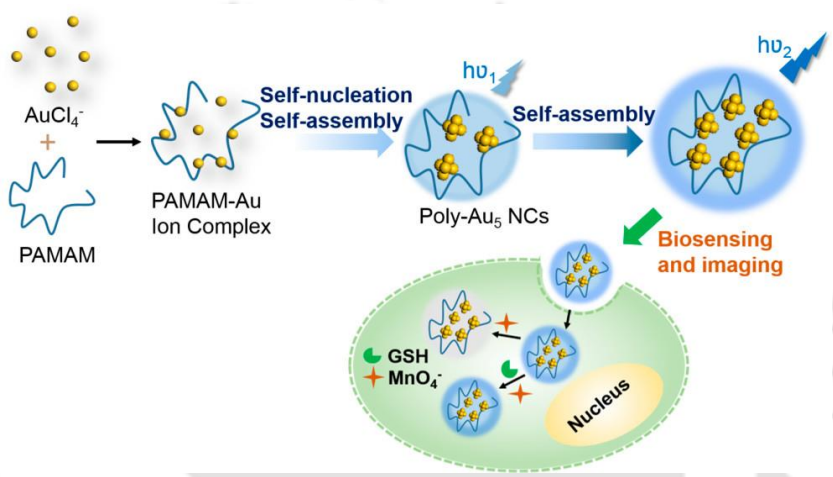

Figure 1.7. Schematic pictorial representation of growth process and the structure of Au_5 self-assemblies in PAMAM matrix used for sensitive and stable intracellular fluorescent imaging. Reprinted with permission from Reference 66. Copyright 2018 American Chemical Society.

In another example, Huang et al. reported a supramolecular assembly of cyclodextrin -Cu NC with di(adamantane-1-yl) phosphine molecule triggered by host-guest interaction.[70] Synthesis and assemblies of noble metals of Au, Pt, and Pd NCs into well-defined geometry were achieved with carriable micellar templates.[71]

1.4 Potential applications of higher order assembled metal NCs

Further, assembly-induced properties of NCs amplify applications in the field of optical devices, catalysis, luminescent sensing, energy storage, and biological imaging, are of significant progress. For example, Wu et al demonstrated the WLED fabricated from a combination of $Cu_{14}(DT)_{10}$ NCs nanosheets and Au@NC sheets and $Cu_{14}(DT)_{10}$ nanoribbon.[72] Later, from NC assembly, multi-colored LEDs were fabricated. For example, Huang et al. through zinc coordinated assemblies of GSH-Au NC fabricated WLED.[73]

Here, the blending of yellow-orange emitting Au NC and green emitting carbon dots facilitated WLED. Also, the assembled NCs have been efficient for use in molecular sensors.[74] The self-assembled NCs were further explored for bioimaging and therapeutic applications. For example, the cellular uptake of assembled NCs was higher than constituent NCs, where assembled Au NCs were fabricated using a cationic template (polymer) for drug delivery and cancer cell imaging.[75] Also, metal coordinated assemblies of Au NC have been studied for application in biomedicine. [76-78]

1.5 Context of the Thesis Work

With the pursuit of literature surveys done in the field of assembly of metal NCs, a significant step may emerge from advancement towards the combined properties of constituent NCs. To direct the assembly of such NCs, a keen understanding of the interaction of ligands based on the functional groups would be essential to develop new material based on the assembly of constituent NCs and ions. Through the envision of inorganic complexation reaction, the assembly of ligand-stabilized nanocluster is possible with metal ions, which supersedes the non-assembled clusters in terms of tailorable structural properties. In this context, studying the effects of transition metal ions and lanthanide metal ions for assembling NCs would offer a platform to develop higher-order structures that may be promising and desirable.

The current thesis covers the approach of an exploration of higher-dimensional crystalline assembly of gold clusters driven by the complexation of specific metal ions with the functional group of the surface ligands. Such formation of crystalline nanostructures could induce the possibility of amplification in multifunctional properties. And integrating such nanoparticles into assembly could have potential in the field of supramolecular chemistry.

1.6 Thesis Overview

The details of the current works incorporated in the thesis are elaborated in the form of five chapters. In the thesis, works including the synthesis, and formation of crystalline assemblies and it's their superior properties have been discussed. A brief discussion of the work is summarised below-

Chapter 1 covers an overview of metal NCs including their syntheses, characteristics, and structural assembly. The formulation of nanocluster-based hierarchical assembly with amplification on molecular physio-chemical properties is highlighted. The key applications in various fields based on the literature are also incorporated.

Chapter 2 describes the formation of a two-dimensional (2D) multi-layered assembly of dual ligand-stabilized gold nanoclusters (Au NCs) via the coordination of zinc metal ion (Zn^{2+}) and the terminal groups of ligands stabilizing the clusters. The complexation reaction between Au NCs (stabilized by mercaptopropionic acid and L-phenyl alanine) with Zn^{2+} resulted in the formation of near-uniform nanosheets of Zn Au NCs with an average thickness of 3.80 ± 1.65 nm. The 2D nature of nanosheets was confirmed by atomic force microscopy (AFM) and field emission scanning electron microscopy (FESEM) analyses. Transmission electron microscopy (TEM) in conjugation with selected area diffraction (SAED) and high-resolution transmission electron microscopy (HRTEM) analyses revealed the single crystalline assembly of the constituents organized hexagonally. A plausible organization of 2D assembly of Au NC is proposed based on computational optimization and allied with experimental evidence. The experimental demonstration of photoluminescent 2D layered nanosheets of zinc Au NCs was efficient in storing molecular oxygen with a capacity of 0.266 ± 0.004 mM/g of Zn Au NCs, which could be used reversibly at an ambient condition of 20 ºC and pressure limit ranging from 0 to 20 bar.

Chapter 3 demonstrates the delayed fluorescence enhancement of europium (Eu^{3+}) ion with prolonged lifetime through interactions of ligand-stabilized Au NCs. The different Eu-centric emissions following complexation with Au NCs had selective augmentation in spectral lines attributed to the modulation of the $^5D_0 \rightarrow {}^7F_j$ transitions. The photoluminescent (PL) properties - that included delayed Eu emission - from each component could be modulated through the functionalization of phosphate ions (Pi) leading to crystallization. The assembled crystalline structure of europium containing Au NCs (Eu Au NCs) was

corroborated by electron diffraction (TEM and SAED) and high-resolution transmission electron microscopy (HRTEM) analyses. Based on PL measurements and experimental evidence, the two different lifetimes arising from the components - prompt emission of Au NCs and delayed emission of Eu were present in the assembled nanostructure. Such design offers the possibility for developing an optical system by conjugating molecular NCs and atomic luminescent probes into superior nanomaterials with potential usage in various fields.

Chapter 4 presents the generation of synchronous tri-color (orange, green and blue) emission from a single excitation wavelength out of inorganic surface complexation reaction on gadolinium-based 2D single crystalline assembly of gold clusters (Gd-Au NCs). The independent emissions at three colors were achieved from the Au NC assembly and the complexes with dual ligands acetylsalicylic acid and fluorescein. The assembled crystalline superstructure with augmented lifetime and quantum yield, emitted white light at λ_{exc} ~325 nm to give a color chromaticity coordinate of (0.34,0.33) in the dispersed phase. The color rendering index (CRI) value >85 obtained from the white light emitting (WLE) nanostructure is important and would offer innovative entrants in the field of LEDs. The crystallinity of the 2D structure was established by XRD and TEM, SAED, and HRTEM analyses. The optical and magnetization properties of the nanosheet from experimental observations have been investigated by photoluminescence measurements and VSM analysis.

Chapter 5 comprises the summary and future prospects of the present thesis work.

1.7 Bibliography

1. Varnavski, O.; Ramakrishna, G.; Kim, J.; Lee, D.; Goodson, T., Critical Size for the Observation of Quantum Confinement in Optically Excited Gold Clusters. *J. Am. Chem. Soc.* **2010,** *132* (1), 16-17.
2. Negishi, Y.; Nobusada, K.; Tsukuda, T., Glutathione-Protected Gold Clusters Revisited: Bridging the Gap between Gold(I)−Thiolate Complexes and Thiolate-Protected Gold Nanocrystals. *J. Am. Chem. Soc.***2005,** *127* (14), 5261-5270.
3. Wu, Z.; Jin, R., On the Ligand's Role in the Fluorescence of Gold Nanoclusters. *Nano Lett.* **2010,** *10* (7), 2568-2573.
4. Yuan, X.; Luo, Z.; Zhang, Q.; Zhang, X.; Zheng, Y.; Lee, J. Y.; Xie, J. Synthesis of Highly Fluorescent Metal (Ag, Au, Pt, and Cu) Nanoclusters by Electrostatically Induced Reversible Phase Transfer *ACS Nano* **2011**, 5, 8800– 8808.
5. Xu, H.; Suslick, K. S., Sonochemical Synthesis of Highly Fluorescent Ag Nanoclusters. *ACS Nano* **2010,** *4* (6), 3209-3214.
6. Luo, Z.; Yuan, X.; Yu, Y.; Zhang, Q.; Leong, D. T.; Lee, J. Y.; Xie, J., From Aggregation-Induced Emission of Au(I)–Thiolate Complexes to Ultrabright Au(0)@Au(I)–Thiolate Core–Shell Nanoclusters. *J. Am. Chem. Soc.***2012,** *134* (40), 16662-16670.
7. Link, S.; Beeby, A.; FitzGerald, S.; El-Sayed, M. A.; Schaaff, T. G.; Whetten, R. L., Visible to Infrared Luminescence from a 28-Atom Gold Cluster. *J. Phys. Chem. B* **2002,** *106* (13), 3410-3415.
8. Takano, S.; Ito, S.; Tsukuda, T., Efficient and Selective Conversion of Phosphine-Protected $(MAu_8)^{2+}$ (M = Pd, Pt) Superatoms to Thiolate-Protected $(MAu_{12})^{6+}$ or Alkynyl-Protected $(MAu_{12})^{4+}$ Superatoms via Hydride Doping. *J. Am. Chem. Soc.***2019,** *141* (40), 15994-16002.
9. Zhu, M.; Aikens, C. M.; Hollander, F. J.; Schatz, G. C.; Jin, R., Correlating the Crystal Structure of a Thiol-Protected Au_{25} Cluster and Optical Properties. *J. Am. Chem. Soc.* **2008,** *130* (18), 5883-5885.
10. Yi, H.; Osten, K. M.; Levchenko, T. I.; Veinot, A. J.; Aramaki, Y.; Ooi, T.; Nambo, M.; Crudden, C. M., Synthesis and enantioseparation of chiral Au_{13} nanoclusters protected by bis-N-heterocyclic carbene ligands. *Chem. Sci.* **2021,** *12* (31), 10436-10440.

11. Narouz, M. R.; Osten, K. M.; Unsworth, P. J.; Man, R. W. Y.; Salorinne, K.; Takano, S.; Tomihara, R.; Kaappa, S.; Malola, S.; Dinh, C.-T.; Padmos, J. D.; Ayoo, K.; Garrett, P. J.; Nambo, M.; Horton, J. H.; Sargent, E. H.; Häkkinen, H.; Tsukuda, T.; Crudden, C. M., N-heterocyclic carbene-functionalized magic-number gold nanoclusters. *Nat. Chem.* **2019,** *11* (5), 419-425.

12. Jin, S.; Du, W.; Wang, S.; Kang, X.; Chen, M.; Hu, D.; Chen, S.; Zou, X.; Sun, G.; Zhu, M., Thiol-Induced Synthesis of Phosphine-Protected Gold Nanoclusters with Atomic Precision and Controlling the Structure by Ligand/Metal Engineering. *Inorg. Chem.* **2017,** *56* (18), 11151-11159.

13. Zhang, Q.-F.; Williard, P. G.; Wang, L.-S., Polymorphism of Phosphine-Protected Gold Nanoclusters: Synthesis and Characterization of a New 22-Gold-Atom Cluster. *Small* **2016,** *12* (18), 2518-2525.

14. Taylor, M. G.; Mpourmpakis, G., Thermodynamic stability of ligand-protected metal nanoclusters. *Nat. Commun* **2017,** *8* (1), 15988.

15. Ghosh, A.; Ghosh, D.; Khatun, E.; Chakraborty, P.; Pradeep, T., Unusual reactivity of dithiol protected clusters in comparison to monothiol protected clusters: studies using $Ag_{51}(BDT)_{19}(TPP)_3$ and $Ag_{29}(BDT)_{12}(TPP)_4$. *Nanoscale* **2017,** *9* (3), 1068-1077.

16. Jadzinsky, P. D.; Calero, G.; Ackerson, C. J.; Bushnell, D. A.; Kornberg, R. D., Structure of a Thiol Monolayer-Protected Gold Nanoparticle at 1.1 Å Resolution. *Science* **2007,** *318* (5849), 430-433.

17. Joshi, C. P.; Bootharaju, M. S.; Alhilaly, M. J.; Bakr, O. M., $[Ag_{25}(SR)_{18}]^-$: The "Golden" Silver Nanoparticle. *J. Am. Chem. Soc.***2015,** *137* (36), 11578-11581.

18. Tsukuda, T.; Tsunoyama, H.; Sakurai, H. Aerobic Oxidations Catalyzed by Colloidal Nanogold *Chem. Asian J.* **2011**, 6, 736– 748.

19. Xiao, F. X.; Hung, S. F.; Miao, J.; Wang, H. Y.; Yang, H.; Liu, B. Metal-cluster-decorated TiO_2 nanotube arrays: a composite heterostructure toward versatile photocatalytic and photoelectrochemical applications. *Small* **2015**, *11*, 554– 567.

20. Li, G.; Qian, H.; Jin, R. Gold nanocluster-catalyzed selective oxidation of sulfide to sulfoxide. *Nanoscale* **2012**, *4*, 6714– 6717.

21. Li, Z.; Liu, C.; Abroshan, H.; Kauffman, D.R.; Li, G. $Au_{38}S_2(SAdm)_{20}$ Photocatalyst for One-Step Selective Aerobic Oxidations. *ACS Catal.* **2017**, *7*, 3368– 3374.

22. Zhu, Y.; Qian, H.; Drake, B. A.; Jin, R., Atomically Precise $Au_{25}(SR)_{18}$ Nanoparticles as Catalysts for the Selective Hydrogenation of α, β-Unsaturated Ketones and Aldehydes. *Angew. Chem. Int. Ed.* **2010,** *49* (7), 1295-1298.

23. Chakraborty, S.; Babanova, S.; Rocha, R. C.; Desireddy, A.; Artyushkova, K.; Boncella, A. E.; Atanassov, P.; Martinez, J. S., A Hybrid DNA-Templated Gold Nanocluster for Enhanced Enzymatic Reduction of Oxygen. *J. Am. Chem. Soc.***2015,** *137* (36), 11678-11687.

24. Abroshan, H.; Li, G.; Lin, J.; Kim, H. J.; Jin, R., Molecular mechanism for the activation of $Au_{25}(SCH_2CH_2Ph)_{18}$ nanoclusters by imidazolium-based ionic liquids for catalysis. *J. Catal.* **2016,** *337*, 72-79.

25. Fu, F.; Xiang, J.; Cheng, H.; Cheng, L. J.; Chong, H. B.; Wang, S. X.; Li, P.; Wei, S. Q.; Zhu, M.; Li, Y. D. A Robust and Efficient Pd_3 Cluster Catalyst for the Suzuki Reaction and Its Odd Mechanism. *ACS Catal.* **2017**, *7*, 1860– 1867.

26. Nie, X.; Qian, H.; Ge, Q.; Xu, H.; Jin, R. CO Oxidation Catalyzed by Oxide-Supported $Au_{25}(SR)_{18}$ Nanoclusters and Identification of Perimeter Sites as Active Centers. *ACS Nano* **2012**, *6*, 6014– 6022.

27. Takahashi, M.; Koizumi, H.; Chun, W.-J.; Kori, M.; Imaoka, T.; Yamamoto, K. Finely controlled multimetallic nanocluster catalysts for solvent-free aerobic oxidation of hydrocarbons. *Sci. Adv.* **2017**, *3*.

28. Zhang, J.; Li, Z.; Huang, J.; Liu, C.; Hong, F.; Zheng, K.; Li, G. Size dependence of gold clusters with precise numbers of atoms in aerobic oxidation of d-glucose. *Nanoscale* **2017**, *9*, 16879– 16886.

29. Li, G.; Jin, R. Gold Nanocluster-Catalyzed Semihydrogenation: A Unique Activation Pathway for Terminal Alkynes. *J. Am. Chem. Soc.* **2014**, *136*, 11347– 11354.

30. Li, G.; Abroshan, H.; Chen, Y.; Jin, R.; Kim, H. J. Experimental and Mechanistic Understanding of Aldehyde Hydrogenation Using Au_{25} Nanoclusters with Lewis Acids: Unique Sites for Catalytic Reactions. *J. Am. Chem. Soc.* **2015**, *137*, 14295– 14304.

31. Yuan, X.; Luo, Z.; Yu, Y.; Yao, Q.; Xie, J. Luminescent Noble Metal Nanoclusters as an Emerging Optical Probe for Sensor Development *Chem. - Asian J.* **2013**, 8, 858– 871.

32. Adhikari, B.; Banerjee, A. Facile Synthesis of Water-Soluble Fluorescent Silver Nanoclusters and Hg (II) Sensing *Chem. Mater.* **2010**, 22, 4364– 4371.

33. Shang, L.; Yang, L.; Stockmar, F.; Popescu, R.; Trouillet, V.; Bruns, M.; Gerthsen, D.; Nienhaus, G. U. Microwave-assisted Rapid Synthesis of Luminescent Gold Nanoclusters for Sensing Hg^{2+} in Living Cells Using Fluorescence Imaging *Nanoscale* **2012**, 4, 4155– 4160.

34. Zhang, G.; Li, Y.; Xu, J.; Zhang, C.; Shuang, S.; Dong, C.; Choi, M. M. F., Glutathione-protected fluorescent gold nanoclusters for sensitive and selective detection of Cu^{2+}. *Sens. Actuators B Chem.* **2013,** *183*, 583-588.

35. Durgadas, C. V.; Sharma, C. P.; Sreenivasan, K. Fluorescent Gold Clusters as Nanosensors for Copper Ions in Live Cells *Analyst* **2011**, 136, 933– 940.

36. Chen, W.; Tu, X.; Guo, X. Fluorescent Gold Nanoparticles-based Fluorescence Sensor for Cu^{2+} ions *Chem. Commun*. **2009**, 1736– 1738.

37. Yang, H., Yang, Y., Liu, S. *et al.* Ratiometric and sensitive cyanide sensing using dual-emissive gold nanoclusters. *Ana.l Bioanal. Chem.* **2020**, 412, 5819–5826.

38. Ma, Y.; Shen, X.-F.; Liu, F.; Pang, Y.-H., Colorimetric detection toward halide ions by a silver nanocluster hydrogel. *Talanta* **2020,** *211*, 120717.

39. Nair, L.V., Philips, D.S., Jayasree, R.S. and Ajayaghosh, A. A Near-Infrared Fluorescent Nanosensor (AuC@Urease) for the Selective Detection of Blood Urea. *Small*, **2013**, 9, 2673-2677.

40. Cui, M.-L.; Liu, J.-M.; Wang, X.-X.; Lin, L.-P.; Jiao, L.; Zhang, L.-H.; Zheng, Z.-Y.; Lin, S.-Q., Selective determination of cysteine using BSA-stabilized gold nanoclusters with red emission. *Analyst* **2012,** *137* (22), 5346-5351.

41. Ban, R.; Abdel-Halim, E. S.; Zhang, J.; Zhu, J.-J., β-Cyclodextrin functionalised gold nanoclusters as luminescence probes for the ultrasensitive detection of dopamine. *Analyst* **2015,** *140* (4), 1046-1053.

42. Chen, X.; Baker, G. A., Cholesterol determination using protein-templated fluorescent gold nanocluster probes. *Analyst* **2013,** *138* (24), 7299-7302.

43. Zhang, X.-D.; Luo, Z.; Chen, J.; Shen, X.; Song, S.; Sun, Y.; Fan, S.; Fan, F.; Leong, D. T.; Xie, J. Ultrasmall $Au_{10–12}(SG)_{10–12}$ Nanomolecules for High Tumor Specificity and Cancer Radiotherapy. *Adv. Mater.* **2014**, 26, 4565– 4568.

44. Zhang, X.-D.; Chen, J.; Luo, Z.; Wu, D.; Shen, X.; Song, S.-S.; Sun, Y.-M.; Liu, P.-X.; Zhao, J.; Huo, S.; Fan, S.; Fan, F.; Liang, X.-J.; Xie, J. Enhanced Tumor

Accumulation of Sub-2 nm Gold Nanoclusters for Cancer Radiation Therapy *Adv. Healthcare Mater.* **2014**, 3, 133– 14.

45. Shang, L.; Stockmar, F.; Azadfar, N.; Nienhaus, G. U. Intracellular Thermometry by Using Fluorescent Gold Nanoclusters *Angew. Chem. Int. Ed.* **2013**, 52, 11154– 11157.

46. Retnakumari, A.; Jayasimhan, J.; Chandran, P.; Menon, D.; Nair, S.; Mony, U.; Koyakutty, M., CD33 monoclonal antibody conjugated Au cluster nano-bioprobe for targeted flow-cytometric detection of acute myeloid leukaemia. *Nanotechnology* **2011,** *22* (28), 285102.

47. Hu, D. H.; Sheng, Z. H.; Zhang, P. F.; Yang, D. Z.; Liu, S. H.; Gong, P.; Gao, D. Y.; Fang, S. T.; Ma, Y. F.; Cai, L. T. Hybrid Gold-Gadolinium Nanoclusters for Tumor-Targeted NIRF/CT/MRI Triple-Modal Imaging in Vivo. *Nanoscale* **2013**, *5* (4), 1624– 1628,

48. Lei, Y.; Tang, L.; Xie, Y.; Xianyu, Y.; Zhang, L.; Wang, P.; Hamada, Y.; Jiang, K.; Zheng, W.; Jiang, X. Gold Nanoclusters-Assisted Delivery of NGF SiRNA for Effective Treatment of Pancreatic Cancer. *Nat. Commun.* **2017**, *8* (1), 1– 15,

49. Khandelia, R.; Bhandari, S.; Pan, U. N.; Ghosh, S. S.; Chattopadhyay, A. Gold Nanocluster Embedded Albumin Nanoparticles for Two-Photon Imaging of Cancer Cells Accompanying Drug Delivery. *Small* **2015**, *11* (33), 4075– 4081.

50. Govindaraju, S.; Roshini, A.; Lee, M.-H.; Yun, K. Kaempferol Conjugated Gold Nanoclusters Enabled Efficient for Anticancer Therapeutics to A549 Lung Cancer Cells. *Int. J. Nanomed.* **2019**, *14*, 5147– 5157.

51. Govindaraju, S.; Rengaraj, A.; Arivazhagan, R.; Huh, Y. S.; Yun, K. Curcumin-Conjugated Gold Clusters for Bioimaging and Anticancer Applications. *Bioconjugate Chem.* **2018**, *29* (2), 363– 370.

52. Cifuentes-Rius, A.; Deepagan, V. G.; Xie, J.; Voelcker, N. H. Bright Future of Gold Nanoclusters in Theranostics. *ACS Appl. Mater Interfaces* **2021**, *13* (42), 49581– 49588.

53. van de Looij, S. M.; Hebels, E. R.; Viola, M.; Hembury, M.; Oliveira, S.; Vermonden, T., Gold Nanoclusters: Imaging, Therapy, and Theranostic Roles in Biomedical Applications. *Bioconjug. Chem.* **2022,** *33* (1), 4-23.

54. Zhu, M.; Yao, Q.; Liu, Z.; Liu, J.; Liu, M.; Long, M.; Xie, J., Aggregation-Induced Emission of Gold Nanoclusters by Ionic Liquids for White Light-Emitting Diode

and Multiple-Ion Probe Applications. *J. Phys. Chem. Lett.* **2022,** *13* (33), 7722-7730.

55. Zhang, C.; Shao, C.; Wang, J.; Li, Z.; Liang, M.; Wang, Y.; Liu, D.; Lu, S., Multifunctional Fluorescent Copper Nanoclusters for Ag^{+} Sensing, Anticounterfeiting, and Blue/White Light-Emitting Diodes. *ACS Appl. Nano Mater.* **2022,** *5* (5), 7449-7459.

56. Goswami, U.; Basu, S.; Paul, A.; Ghosh, S. S.; Chattopadhyay, A., White light emission from gold nanoclusters embedded bacteria. *J. Mater. Chem. C* **2017,** *5* (47), 12360-12364.

57. Nonappa, T. Lahtinen, J. S. Haataja, T.-R. Tero, H. Häkkinen, O. Template-Free Supracolloidal Self-Assembly of Atomically Precise Gold Nanoclusters: From 2D Colloidal Crystals to Spherical Capsids , *Angew. Chem. Int. Ed.* **2016**, *55*, 16035.

58. Nonappa; Ikkala, O., Hydrogen Bonding Directed Colloidal Self-Assembly of Nanoparticles into 2D Crystals, Capsids, and Supracolloidal Assemblies. *Adv. Funct. Mater.* **2018**, *28* (27), 1704328.

59. Xue, F.; Qu, F.; Han, W.; Xia, L.; You, J., Aggregation-induced emission enhancement of gold nanoclusters triggered by silicon nanoparticles for ratiometric detection of protamine and trypsin. *Anal. Chim. Acta* 2019, *1046*, 170-178.

60. L. He, Z. Gan, N. Xia, L. Liao, Z. Wu, Alternating Array Stacking of $Ag_{26}Au$ and $Ag_{24}Au$ Nanoclusters *Angew. Chem. Int. Ed.* 2019, *58*, 9897.

61. Wu, Z.; Liu, J.; Li, Y.; Cheng, Z.; Li, T.; Zhang, H.; Lu, Z.; Yang, B., Self-Assembly of Nanoclusters into Mono-, Few-, and Multilayered Sheets via Dipole-Induced Asymmetric van der Waals Attraction. *ACS Nano* **2015,** *9* (6), 6315-6323.

62. Higaki, T.; Liu, C.; Zhou, M.; Luo, T.-Y.; Rosi, N. L.; Jin, R., Tailoring the Structure of 58-Electron Gold Nanoclusters: $Au_{103}S_2(S\text{-}Nap)_{41}$ and Its Implications. *J. Am. Chem. Soc.***2017,** *139* (29), 9994-10001.

63. Li, Q.; Russell, J. C.; Luo, T.-Y.; Roy, X.; Rosi, N. L.; Zhu, Y.; Jin, R., Modulating the hierarchical fibrous assembly of Au nanoparticles with atomic precision. *Nat. Commun.* **2018,** *9* (1), 3871.

64. De Nardi, M.; Antonello, S.; Jiang, D.-e.; Pan, F.; Rissanen, K.; Ruzzi, M.; Venzo, A.; Zoleo, A.; Maran, F., Gold Nanowired: A Linear (Au_{25}) n Polymer from Au_{25} Molecular Clusters. *ACS Nano* **2014,** *8* (8), 8505-8512.

65. Li, Q., Russell, J.C., Luo, TY. *et al.* Modulating the hierarchical fibrous assembly of Au nanoparticles with atomic precision. *Nat. Commun.* **2018,** *9*, 3871 (2018).

66. Yang, L.; Wang, H.; Li, D.; Li, L.; Lou, X.; Liu, H., Self-Nucleation and Self-Assembly of Highly Fluorescent Au_5 Nanoclusters for Bioimaging. *Chem. Mater.* **2018,** *30* (15), 5507-5515.

67. Ju, E.; Li, T.; Ramos da Silva, S.; Gao, S.-J., Gold Nanocluster-Mediated Efficient Delivery of Cas9 Protein through pH-Induced Assembly-Disassembly for Inactivation of Virus Oncogenes. *ACS Appl. Mater. Interfaces.* **2019,** *11* (38), 34717-34724.

68. Wang, M.; Chen, Y.; Cai, W.; Feng, H.; Du, T.; Liu, W.; Jiang, H.; Pasquarelli, A.; Weizmann, Y.; Wang, X., In situ self-assembling Au-DNA complexes for targeted cancer bioimaging and inhibition. *Proc. Natl. Acad. Sci.* **2020,** *117* (1), 308-316.

69. Jiang, T.; Qu, G.; Wang, J.; Ma, X.; Tian, H., Cucurbiturils brighten Au nanoclusters in water. *Chem. Sci.* **2020,** *11* (13), 3531-3537.

70. Huang, Y.; Ji, J.; Zhang, J.; Wang, F.; Lei, J., Host–guest recognition-regulated aggregation-induced emission for in situ imaging of MUC1 protein. *Chem. Commun.* **2020,** *56* (2), 313-316.

71. Zhou, Y.; Zeng, H. C., Simultaneous Synthesis and Assembly of Noble Metal Nanoclusters with Variable Micellar Templates. *J. Am. Chem. Soc.* **2014,** *136* (39), 13805-13817.

72. Wu, Z.; Liu, J.; Gao, Y.; Liu, H.; Li, T.; Zou, H.; Wang, Z.; Zhang, K.; Wang, Y.; Zhang, H.; Yang, B., Assembly-Induced Enhancement of Cu Nanoclusters Luminescence with Mechanochromic Property. *J. Am. Chem. Soc.* **2015,** *137* (40), 12906-12913.

73. Huang, HY., Cai, KB., Talite, M.J. *et al.* Coordination-induced emission enhancement in gold-nanoclusters with solid-state quantum yields up to 40% for eco-friendly, low-reabsorption nano-phosphors. *Sci Rep***. 2019**, 9, 4053 (2019).

74. Basu, S.; Paul, A.; Chattopadhyay, A., Zinc-Coordinated Hierarchical Organization of Ligand-Stabilized Gold Nanoclusters for Chiral Recognition and Separation. *Chem. Eur. J.* **2017,** *23* (38), 9137-9143.

75. Yahia-Ammar, A.; Sierra, D.; Mérola, F.; Hildebrandt, N.; Le Guével, X., Self-Assembled Gold Nanoclusters for Bright Fluorescence Imaging and Enhanced Drug Delivery. *ACS Nano* **2016,** *10* (2), 2591-2599

76. Hou, W.; Xia, F.; Alfranca, G.; Yan, H.; Zhi, X.; Liu, Y.; Peng, C.; Zhang, C.; de la Fuente, J. M.; Cui, D., Nanoparticles for multi-modality cancer diagnosis: Simple protocol for self-assembly of gold nanoclusters mediated by gadolinium ions. *Biomater.* **2017,** *120*, 103-114.

77. Basu, S.; Goswami, U.; Paul, A.; Chattopadhyay, A., Crystalline assembly of gold nanoclusters for mitochondria targeted cancer theranostics. *J. Mater. Chem. B* **2018,** *6* (11), 1650-1657.

78. Wang, L.; Zhang, C.; Li, T.; Duan, M.; Xia, F.; Li, X.; Song, C.; Pan, S.; Liu, B.; Cui, D., A modular approach for cytosolic protein delivery: metal ion-induced self-assembly of gold nanoclusters as a general platform. *Nanoscale* **2019,** *11* (46), 22237-22242.

Chapter 2

Complexation Reaction based Two-dimensional Luminescent Crystalline Assembly of Atomic Clusters for Recyclable Storage of Oxygen

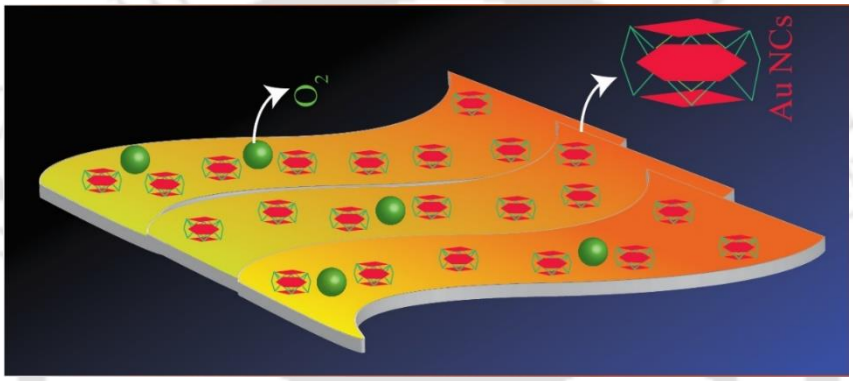

In this work, we report the storage of oxygen in two-dimensional crystalline nanosheets comprising luminescent gold nanoclusters. Complexation reaction between gold nanoclusters (stabilized by L phenylalanine and mercaptopropionic acid) and zinc ions led to the formation of crystalline assembly of gold nanocluster (Au NCs). The crystalline nature of the assembly of Au NCs was confirmed through transmission electron microscopic (TEM), High-resolution TEM, and selected area electron diffraction (SAED) analysis. Atomic force microscopic (AFM) analysis, in conjunction with field emission scanning electron microscopic (FESEM) analysis, confirmed the two-dimensional (2D) nature of the assembly of Au NCs. The 2D crystalline nanosheets formed out of the reaction between Au NCs and Zn^{2+} were found to be of near-uniform thickness, with an average value of 3.8 ± 1.65 nm. These 2D nanosheets constituting hierarchically organized Au NCs, were further used for reversible storage of oxygen at ambient conditions of 20 °C and 20 bar pressure.

Paul et al. Langmuir 2020, 36, 3, 754–759. Reproduced with permission from American Chemical Society.

2.1 Introduction

Superstructures of nanoscale particles have emerged as a class of advanced materials with application potential in domains as diverse as theranostics and energy-efficient devices.[1-10] In this regard, nanoclusters, with uniform structural integrity provide unique opportunities for the formation of deterministic assemblies, akin to the organization of "atoms to molecules". To this end, our research group has lately introduced the concept of the formation of crystalline assembly of gold clusters via "complexation reaction.[11-15] Through this strategy of assembly formation, it could be demonstrated that zinc-mediated assembly of nanoclusters supersedes the non-assembled clusters in terms of optical properties and application potential. Further, the self-assembly of gold nanoparticles has been achieved via supramolecular interactions like hydrogen bonding interactions. In addition, the formation of three-dimensional superlattices of gold nanoparticles has been pursued at air-water interfaces.[16,17]

On the other hand, a persistent interest of researchers pursuing spatial organization of nanoscale materials is to be able to form two-dimensional (2D) nanomaterials owing to superior chemical stability, improved optical properties, and ease of functionalization vis-à-vis materials with other dimensionalities.[18] For example, 2D quantum dots derived from phosphorene, graphene, and metal chalcogenides have been used for catalysis, bioimaging, and therapeutics.[19,20] Notably, 2D assemblies of Au nanoclusters (Au NCs) formed using principles of inorganic complexation reactions were envisioned to feature further intriguing characteristics. In recent work, we have achieved the formation of two-dimensional arrangements of Au NCs via complexation between zinc ions and the carboxylate groups of ligands stabilizing the clusters. The so-formed 2D organization of gold clusters exhibited unprecedented delayed fluorescence at room temperature with a lifetime of 0.5 ms in comparison to that of the as-synthesized clusters being a few hundred μs.[15] In this regard, the localization of atomic clusters onto nanosheets of double hydroxides has been pursued to achieve augmented luminescence. Furthermore, 2 D layered crystalline materials have been demonstrated to exhibit highly efficient phosphorescence energy transfer. In an allied vein, surface-enhanced Raman scattering

(SERS) 2 D materials have been fabricated by localization of gold nanoparticles onto sodium polyacrylate nanosheets. In addition, chalcogenide quantum dot decorated g-C_3N_4 micro ribbons have been demonstrated for highly efficient hydrogen evolution. Moreover, the importance of the hierarchical arrangement of individual components into higher-order dimensions, to achieve desirable physicochemical properties, has been demonstrated.[21-25]

A key application of the current concern, which is being methodically addressed, is with regard to energy storage. Although there are numerous examples, storage of oxygen at ambient pressure and temperature is of particular importance, given the potential utility in the survival of marine divers, Fighter pilots, military personnel, and medical patients with critical oxygen demand.[26] To this end, zeolites and porous carbons have been a popular choice for oxygen storage.[27, 28] However, their use for gas storage has been largely limited by the heterogeneous nature of their pore sizes. Thus, the advent of materials with well-defined geometries, where gas storage could be possible based on interactions between the gas molecules and constituents of the storage materials may be considered as an important alternative. This may lead to greater control over the amount of gas storage and the conditions (especially pressure and temperature) required for gas storage and release. It has been demonstrated in our laboratory that metal ion-mediated superstructures of atomic gold clusters are potent for the storage of gases (hydrogen and carbon dioxide) with concomitant visual sensing of the storage process.[11,13] Further, given the widespread recognition of 2D nanomaterials in gas storage, synthetic fabrication of 2D assemblies of atomic clusters for expedient storage of oxygen at pliant conditions could be intriguing. As mentioned before, 2D nanomaterials with high lateral size and thickness comparable to that of atoms are gaining prominence owing to their unique features - high chemical stability and ease of functionalization, as opposed to materials of higher dimensions. For example, in the current case, oxygen stored in 2D nanosheets of luminescent atomic clusters may be further used for pursuing catalytic oxygenation reactions at ambient pressure and temperature. Since in the case of 2D nanomaterials, exposure of the surface atoms is very high, the best utilization of the oxygen stored in the 2D nanosheets of the assembled gold clusters may be achieved for oxygenation reactions with concomitant sensing of the catalytic reaction, which may otherwise be difficult in materials assemblies with other dimensionalities.

2.2 Outline of the present work:

Herein, we report the formation of 2D multi-layered nanosheets of Au NCs via coordination with zinc ions. As per AFM (atomic force microscopic) analysis, the thickness of the nanosheets was measured to be 3.80 ± 1.65 nm. Transmission electron microscopic, in conjunction with field emission scanning electron microscopic (FESEM), analyses also featured the presence of layered crystalline structures. Selected area electron diffraction (SAED) in conjunction with high-resolution transmission electron microscopic (HRTEM) analyses revealed that the constituents of the crystalline assembly were arranged in a hexagonal manner. Further, a probable organization of the 2D crystalline assembly of Au NCs could be proposed based on computational optimization, in addition to experimental evidence. Also, it has been experimentally demonstrated that these multi-layered nanosheets of zinc-ligated assemblies of Au NCs could store molecular oxygen reversibly at the ambient conditions of 20 °C and 20 bar pressure.

2.3 Experimental Details:

2.2.1 Materials:

Ethanol, tetra chloroauric acid ($HAuCl_4$, Sigma Aldrich), L-phenyl alanine (Sigma Aldrich), mercaptopropionic acid (Sigma Aldrich), zinc acetate dihydrate (Merck), potassium bromide (Sigma Aldrich) and methanol (HPLC grade) were used as received.

2.2.2 Analytical Methods:

(a) Optical measurements: UV-visible spectra and photoluminescence spectra for all samples were recorded using PerkinElmer Lamda 35 UV/Vis Spectrometer and HORIBA FluoroMax-4 spectrofluorometer respectively.

(b) Fourier transform infrared spectroscopy (FTIR): FT-IR analyses were performed using PerkinElmer (Spectrum Two) FT-IR Spectrometer. The pellets were prepared by washing the acquired precipitate with ethanol and evaporating the solvent to dryness.

(c) Transmission electron microscopy (TEM) and selected area electron diffraction (SAED) analysis: TEM, high-resolution TEM, and SAED (selected area electron

diffraction) analysis were done with JEOL JEM-2100F transmission electron microscope (operated at a maximum accelerating voltage of 200 kV). Samples were prepared by drop casting appropriate diluted dispersions on carbon carbon-coated copper grid.

(d) Time-resolved photoluminescence study: Time-resolved PL analysis was performed by using a Life-Spec-II spectrofluorometer (Edinburgh Instrument) under the continuous stirring condition to avoid settlement of the samples.

(e) Quantum Yield Calculation: To calculate the quantum yield of Zn Au NCs, three samples of Zn Au NCs were synthesized in three different batches following the same protocol. The quantum yields of these three dispersions of Zn Au NCs nanosheets were calculated separately using quinine sulfate (in 0.1M H_2SO_4) as a reference. The quantum yield of Zn Au NCs nanosheets was calculated using the following equation.

Q.Y of Zn Au NCs =

$$Q.Y_{ref}\ X\ (Area\ under\ the\ emission\ spectrm\ of\ Zn\ Au\ NCs\ /\ Area\ under\ the\ emission\ spectrum\ of\ QS)X$$
$$(Absorbance\ of\ QS\ /\ Absorbance\ of\ Zn\ Au\ NCs)X$$
$$(\mathrm{Re}\ fractive\ index\ of\ Zn\ Au\ NCs\ /\ \mathrm{Re}\ fractive\ index\ of\ QS)$$

In the current case, water was used as a solvent for calculating the quantum yield of Zn Au NCs. The refractive index of water is reported to be 1.33. Also, quinine sulphate (at low concentration) was dissolved in water. Hence, the ratio of the refractive indices of quinine sulphate solution and Zn Au NC dispersion was taken to be 1. Given the quantum yield of quinine sulphate to be 0.54, the luminescence quantum yield of Zn Au NCs has been calculated to be 0.83 ± 0.08 %.

(f) Atomic force microscopic analysis (AFM): AFM analysis was performed using Oxford Cypher AFM Instrument. The samples were prepared by appropriate dilution of the dispersion of Zn Au NCs nanosheets. Further, 0.2 mL of the diluted dispersion of Zn Au NCs was spin-coated on a Silicon Wafer, which was dried and used for further analysis.

(g) Field emission Scanning electron microscope (FESEM) analysis: FESEM analysis was performed using JEOL JSM-7610F. The sample was prepared by diluting the

dispersion of Zn Au NC nanosheets and drop casting 0.3 mL of this dispersion on an aluminium foil enfolded in a glass slide. The sample was dried overnight under ambient conditions for analysis.

(h) Computational analysis: The structure of Zn Au NCs was optimized using Avogadro software.

(i) Oxygen adsorption analysis: For probing oxygen adsorption, firstly the crystalline assembly of Au NCs was prepared by following the procedure as discussed above with ethanol as the solvent. The acquired precipitate was washed with ethanol and dried by evaporating the solvent. To perform the O_2 adsorption analysis, 125.8 mg of the sample was purged with nitrogen at a temperature of 90 $^{\circ}$C. The sample was then used for the O_2 adsorption experiment in the pressure range of 0.2 bar to 20 bar and at a temperature of 20 $^{\circ}$C, using the isorbHP1-XKRLSPN100 machine.

2.2.3 Synthetic methods:

(a) Synthesis of gold nanoclusters: 1 mL $HauCl_4$ (10 mM) was added to 10 mL ethanol. To this solution of $HAuCl_4$ 0.4 mL mercaptopropionic acid was added. This led to the gradual formation of a colorless dispersion. The resultant solution was thereafter added with ~ 5 mg of L-phenylalanine, which consequently resulted in the formation of a luminescent dispersion. This dispersion was centrifuged for 10 min at 10 °C. The speed of centrifugation was set at 10,000 rpm. This pellet, following re-dispersion in one mL water, was used for further experiments.

(b) Synthesis of assembly of gold clusters: To the above-obtained dispersion of Au NCs (obtained following centrifugation), ~ 100 mg zinc acetate dihydrate was added, which led to the formation of a highly luminescent dispersion exhibiting emission at 590 nm (λ_{ex} = 330 nm). The dispersion was centrifuged for 10 min at 10 °C. The speed of centrifugation was set at 10,000 rpm. The obtained pellet was re-dispersed in one mL of water and used for further experiments.

2.4 Result and discussion

Adding mercaptopropionic acid (MPA) and L-phenylalanine (Phe) to tetrachloroauric acid ($HAuCl_4$) in ethanol resulted in the formation of a colourless dispersion.

The UV-vis absorption spectrum of the dispersion did not feature the presence of any significant maximum (Figure 2.1.A). Further, the dispersion was observed to be luminescent, exhibiting an emission maximum at 590 nm (λ_{ex} 330 nm) (Figure 2.1.B). This could be indicative of the successful synthesis of Au NCs.

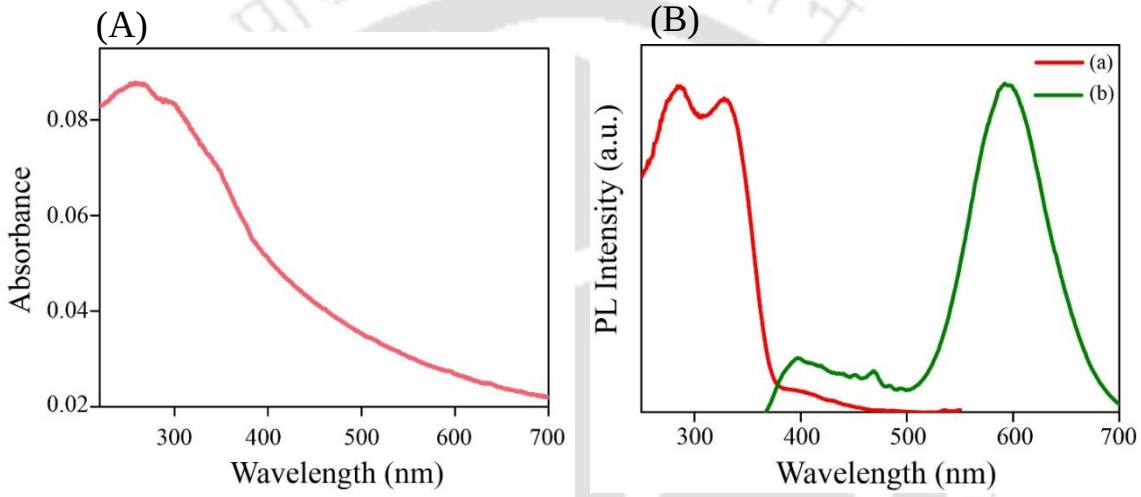

Figure 2.1. (A) UV-vis spectrum of MPA and L phe Au NCs. (B) Excitation and emission spectra of MPA and L phe stabilized Au NCs.

TEM analysis was performed to confirm the formation of particles with a size of 2 nm (Figure 2.2.A). These particles were observed to be non-crystalline (Figure 2.2.B). Moreover, electrospray ionization mass spectrometric (ESI-MS) analysis confirmed the formation of Au_{14} NCs. The ESI-MS spectrum featured a peak at 1489.8962, which has been assigned to the presence of Au_{14} species. The formula of the aforementioned species has been attributed to $[Au_{14}MPA_{10}Phe_4]^{3+}$ (Figure A.2.1).

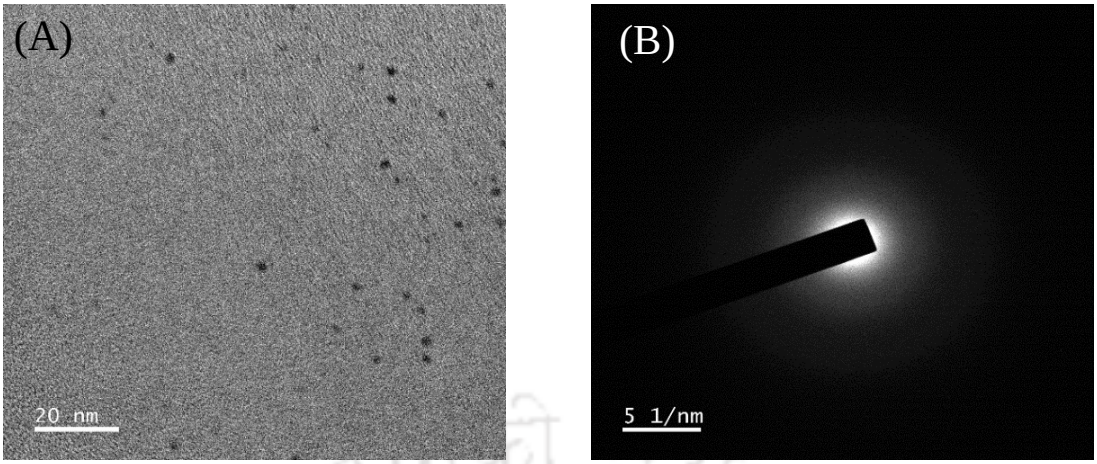

Figure 2.2. (A) TEM image of MPA and L phe stabilized Au NCs. (B) SAED of a typical collection of particles shown in (A).

Principles of reaction chemistry were used to achieve the synthesis of "a few layered" 2D assemblies of Au NCs. Given the scope of facile chemical bonding between the carboxylate groups of ligands stabilizing the Au NCs and transition divalent metal ions, the formation of metal ion coordinated extended network of Au NCs was deemed possible. Further, the possibility of π- π interaction between the Phe moieties stabilizing the Au NCs provided an opportunity for assemblies with close intermolecular packing and sheet forming propensity. Thus, a combined methodology of coordination and supramolecular chemistry was pursued for the formation of a few layered two-dimensional assemblies of Au NCs. Complexation of Phe and MPA stabilized Au NCs and zinc ions was carried out at room temperature. This led to the formation of dispersion with augmented luminescence intensity and lifetime as compared to the constituent Au NCs (Figure 2.3, 2.4, and Table 2.1). Further, the dispersion of zinc-added Au NCs was centrifuged and the so-obtained pellet was found to retain the enhanced luminescence intensity.

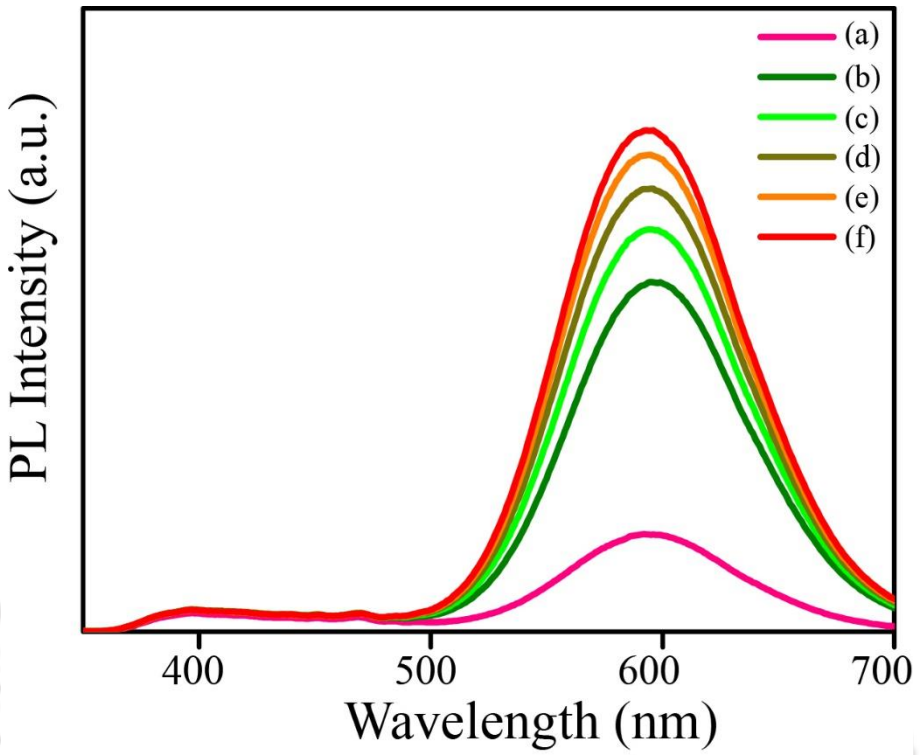

Figure 2.3. Emission spectrum of (a) MPA and L phe stabilized Au NCs and of that following the addition of (b) 0.05 mL (c) 0.1 mL, (d) 0.20 mL, (e) 0.30 mL and (f) 0.40 mL of ~ 100 mg/mL of zinc acetate dehydrate.

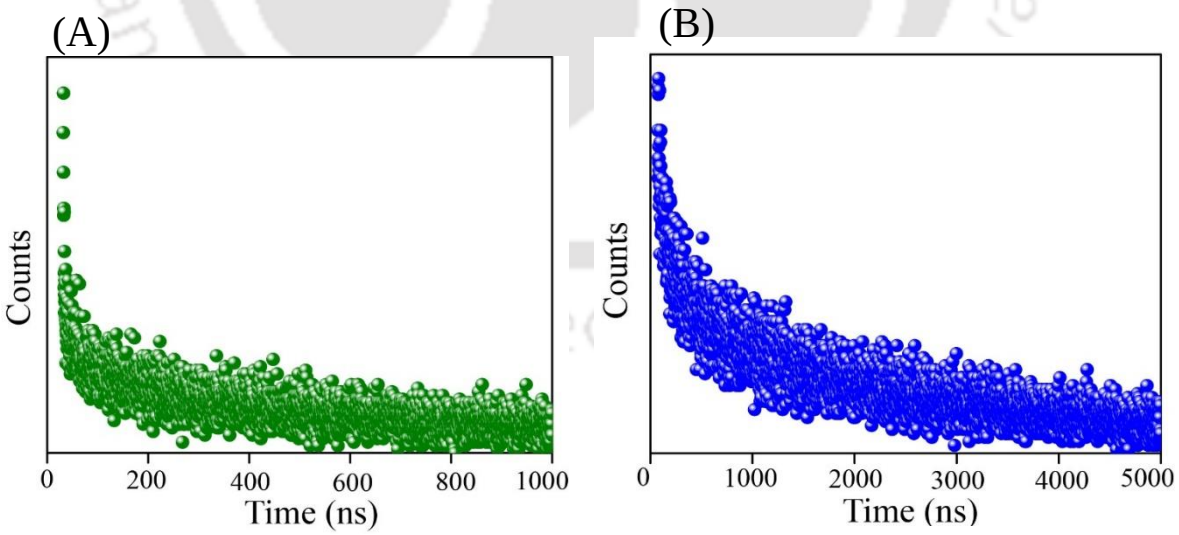

Figure 2.4. TRPL decay profile of (A) MPA and L phe stabilized Au NCs. (B) TRPL decay profile of Zn Au NCs.

Table 2.1. Decay parameters obtained from TRPL analysis of Au NCs and Zn Au NCs obtained following biexponential fitting.

Sample	A_1	ΔA_1	τ_1(ns)	A_2	ΔA_2	τ_2(ns)	χ^2
Au NCs	96.241	1.39	276.734	3.759	0.28	4.675	1.249
Zn Au NCs	92.798	0.28	1804.670	7.202	1.36	133.771	1.141

This could possibly indicate the binding of zinc ions with the Phe and MPA moieties stabilizing the Au NCs. To this end, Fourier transformed infrared (FTIR) analysis was performed to understand the nature of binding between the terminal groups of ligands stabilizing Au NCs and zinc ions. As it may be noted in the FTIR spectrum of Au NCs, a peak at 1704 cm^{-1}, owing to the asymmetric stretching of carboxylate groups of Phe and MPA was observed to be absent in the FTIR spectrum of Zn Au NCs. This indicated the possible role of carboxylate groups of Phe and MPA in bonding with zinc ions (Figure A.2.2).

The formation of complexation reaction-based 2D assemblies of Au NCs linked via zinc ions was confirmed through TEM analysis. Intriguingly, TEM analysis of zinc-assisted assemblies of Au NCs (Zn Au NCs) showed the presence of two-dimensional "sheet-like" structures (Figure 2.5). Each sheet-like structure was found to comprise multiple sheets resulting in the appearance of a stacked structure. Selected area electron diffraction (SAED) analysis performed on typical nanosheets, highlighted their crystalline nature. The SAED pattern indicated the hexagonal positioning of constituents Au NCs (Figure 2.5.A). The edge length of the hexagonal assembly (as obtained from the diffraction) was measured to be 4.7 Å. Further, high-resolution TEM (HRTEM) analysis revealed the presence of lattice spacing with values of 5.7 Å and 2.7 Å on such nanosheets (Figure 2.5 E- F). Additionally, FESEM analysis, also corroborated the presence of 2D nanosheets (Figure A.2.3). STEM analysis and elemental mapping further confirmed the simultaneous presence of Au and zinc in the so-formed nanosheets (Figure A.2.4).

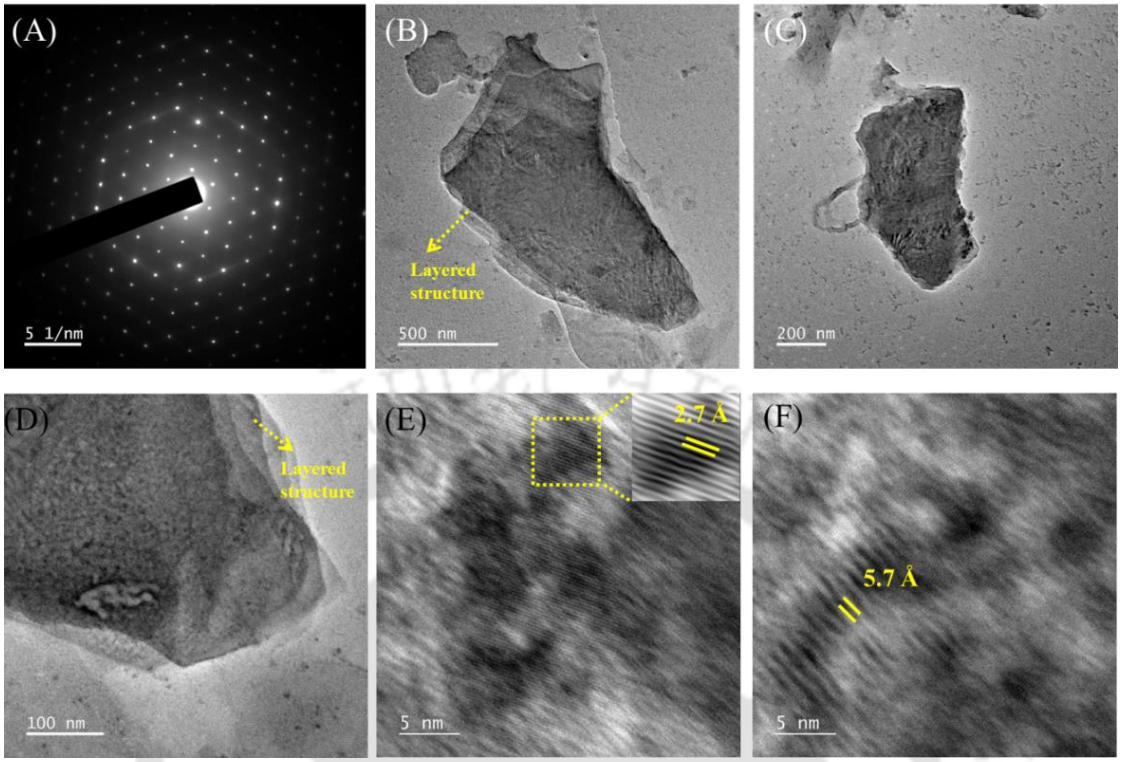

Figure 2.5. (A) Selected area electron diffraction (SAED) pattern of the crystalline assembly of two-dimensional nanosheets obtained from the reaction between ligand stabilized Au NCs and zinc ions. (B-D) TEM image of a typical stack of sheets of Zn Au NCs. (E-F) High-resolution TEM image of Zn Au NCs.

Further, AFM analysis was pursued to confirm the 2D nature of Zn Au NCs. Interestingly, several nanosheets with an average height of 3.80 ± 1.65 nm could be observed in a typical AFM image (Figure 2.6). It is important to note here that the heights of typical sheet like structures of boron nitride and sulphides of molybdenum and tungsten are reported to be in the range of 1 nm to 3 nm. Thus, in the current case, it may be claimed that in addition to single-layered nanosheets, multi-layered 2D nanosheets could also be present. This observation is in fair agreement with the TEM analysis featuring the presence of multi-layered nanosheets. Moreover, based on TEM analysis, supported by AFM analysis, a plausible structure of Zn Au NCs could be proposed. Briefly, ten MPA and four phe ligands stabilized a single unit of cluster, in accordance with ESI MS analysis. Six such Au NCs (stabilized by ligands) were arranged hexagonally with an additional Au NC positioned at the center of the hexagon. Further, in the XY plane, each of these hexagonally placed

clusters was connected to each other via zinc ions following coordination with the MPA ligands. Thus, the XY plane of the 2D nanosheets comprised of hexagonally arranged Au_{14} clusters linked through zinc ions via coordination with MPA stabilizing the clusters. Based on computational studies (Figure A.2.5), the distance between the clusters was found to be 5.2 Å, which matched well with the observed distance of 4.5 Å. On the other hand, the growth of the crystal in the z direction was defined by the coordination of l phe with zinc ions, in conjunction with π- π interaction between l phe moieties. The distance was found to be 2.7 Å, which was rather small compared to the distance in the XY plane, resulting in plausible 2D structures. Further, the distance between Au_{14} cluster-zinc ions - Au_{14} cluster bonded through l phe was computationally found to be 6.5 Å, which was in good agreement with the observed distance of 5.7 Å. Schematic illustrations of such a plausible bonding scheme and structure of Zn Au NCs are shown below (Figure 2.6 B, D). Given the distance between each layer of the 2 D crystalline assembly of Au NCs to be ~ 0.57 nm, the layer number distribution was calculated to be seven units per sheet. Further AFM analyses were performed to understand whether the thickness of the nanosheets could be tuned by varying the amount of zinc acetate dihydrate. Interestingly, when ~100 mg of zinc acetate dihydrate was added to a dispersion of Au NCs, the heights of the nanosheets were found to be in the range of 4-6 nm. However, when ~ 200 mg of zinc acetate dehydrate was added to Au NCs, nanosheets with thickness ranging from 4 to 12 nm were formed. Moreover, upon the addition of ~ 300 mg of zinc acetate dihydrate to Au NCs, nanosheets with heights ranging from 7-10 nm were primarily formed (Figure A.2.6).

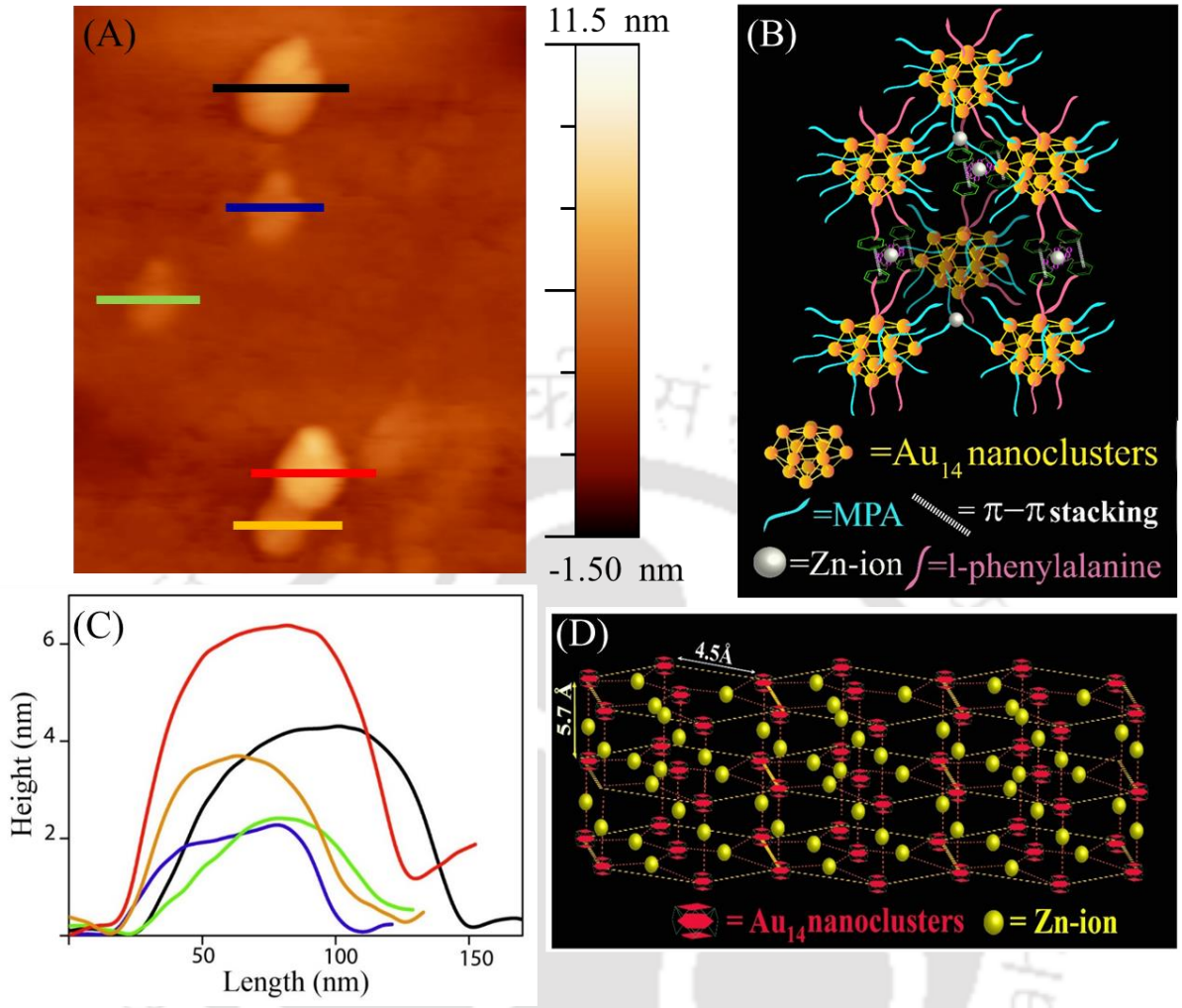

Figure 2.6. (A) AFM images of Zn Au NCs featuring the presence of 2D nanosheets. (B) Schematic representation of possible bonding modes between ligands (Phe and MPA) stabilizing Au NCs and zinc ions. (C) Corresponding height profiles of Zn Au NCs as obtained. (D) Schematic representation of a plausible two-dimensional structure of Zn Au NCs.

The as-prepared nanosheets of Zn Au NCs were tested for their efficacy in oxygen storage. The oxygen storage ability of Zn Au NCs nanosheets was found to be 0.266 ± 0.004 mM/g of Zn Au NCs at 20 ˚C and 20 bar (Figure 2.7). Further, the effect of oxygen adsorption and desorption on the luminescence of Zn Au NCs was monitored. Interestingly, Zn Au NCs showed a decrease in luminescence intensity in the presence of oxygen. However, upon reducing the oxygen pressure, the luminescence of Zn Au NCs was found to recover (partially). (Figure A.2.7)

The reversible nature of changes in luminescence in the presence of oxygen provides further support to the interaction Thus, the 2D assemblies of Au NCs mediated by zinc ions could not only be used for oxygen storage but also served as a visual indicator for adsorption and desorption of oxygen. Further, the practical utility of a gas storage material is not only realized in terms of its gas storage efficiency but also the retention of its gas storage capacity, following repeated cycles of use. Thus, the recyclability of Zn Au NCs nanosheets was also tested. Interestingly, the oxygen storage capacity of Zn Au NCs nanosheets was retained following the completion of one cycle of adsorption and desorption (Figure 2.7). Also, literature reports suggest the reactivity of Au atoms towards molecular oxygen and the interaction is likely to be attributed to the physisorption of oxygen molecules on Au atoms present in Zn Au NCs nanosheets.

Notwithstanding the several advantages of Zn Au NCs as a novel system for storage and sensing of oxygen, a major premise of concern with the practical utility of Zn Au NCs lies in their limited storage capacity of oxygen as compared to other well-known systems (Table A.2.1). Thus, significant efforts are to be made in modulating the oxygen storage capacity of Zn Au NCs. A possible way to circumvent the limited oxygen storage capacity of assembled gold nanoclusters may emerge from using redox active metal ions for complexation-mediated assembly of clusters. In principle, as observed in the case of haemoglobin, ions like Fe^{2+}, which upon binding with oxygen are transformed to Fe^{3+}, may lead to enhancement in the oxygen storage capacity of the assembled Au NCs. Also, species like vanadate molybdate and europium – exhibiting extended coordination capacity may be useful as complexation agents for assembling gold nanoclusters for enhanced oxygen storage vis-à-vis Zn Au NCs. Importantly, our laboratory is currently involved in the exploration of various possibilities to maximize the performance of assembled atomic clusters.

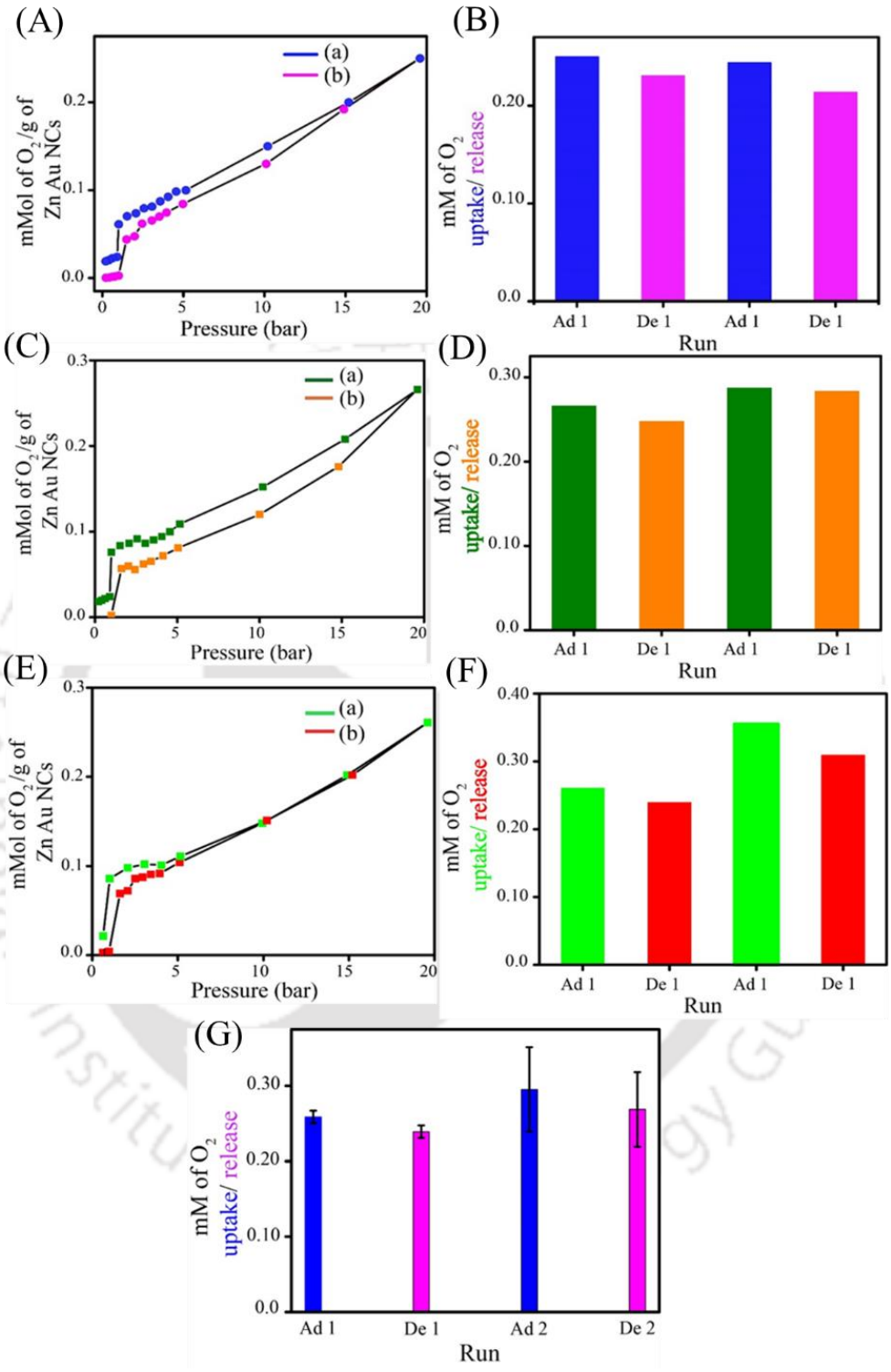

Figure 2.7. (A) Adsorption and desorption isotherms of O_2 on Zn Au NC nanosheets, (B) Bar diagram showing reusability of Zn Au NC nanosheets for reversible storage of O_2. (C) Additional data on adsorption and desorption isotherms of O_2 on Zn Au NC nanosheets. (D) Bar diagram showing reusability of Zn Au NC nanosheets for reversible storage of O_2.

(E) Additional data on adsorption and desorption isotherms of O_2 on Zn Au NC nanosheets. (F) Bar diagram showing reusability of Zn Au NC nanosheets for reversible storage of O_2. (C-D) and (E-F) are the results of two different experiments performed on different days using two different samples of Zn Au NCs nanosheets. (G) Bar diagram (with error bars) showing the reusability of Zn Au NCs nanosheets for reversible storage of O_2. The oxygen storage ability of Zn Au NCs nanosheets was found to be 0.266 ± 0.004 mM/g of Zn Au NCs at 20 ˚C and 20 bar. We observed the measurements were reproducible within 89%, measured over three different samples.

2.5 Conclusion

The generation of 2D nanosheets of Au NCs (stabilized by l-phenylalanine and mercaptopropionic acid) was achieved based on principles of coordination and supramolecular chemistry. Complexation reaction between zinc ions and ligand-stabilized Au NCs resulted in the formation of nanosheets with an average height of 3.80 ± 1.65 nm. The 2D nanosheets were thoroughly characterized by TEM, AFM, and FESEM analyses. A possible structure of such 2D assembly was proposed, based on experimental evidence and computational analysis. Further, the 2D nanosheets could be used for recyclable storage of oxygen at ambient conditions with a storage capacity of 0.266 ± 0.004 mM/ g of Zn Au NCs.

2.6 Bibliography

1. Mao, X.; Wang, Z.; Zeng, D.; Cao, H.; Zhan, Y.; Wang, Y.; Li, Q.; Shen, Y.; Wang, J. Self-Assembled Chiral Nanoparticle Superstructures and Identification of their Collective Optical Activity from Ligand Asymmetry. *ACS Nano* **2019**, *13*, 2879-2887.
2. Chou, L. Y. T.; Zagorovsky, K.; Chan, W. C. W. DNA Assembly of Nanoparticle Superstructures for Controlled Biological Delivery and Elimination. *Nat. Nanotechnol*. **2014**, *9*, 148-155.
3. Hove, J. B. T.; Leeuwen F. W. B. V.; Velders, A. H. Manipulating and Monitoring Nanoparticles in Micellar Thin Film Superstructures. *Nat Commun*. **2018**, *9*, 5207.
4. Nagaoka, Y.; Tan, R.; Li, R.; Zhu, H.; Eggert, D.; Wu, Y. A.; Liu, Y.; Wang Z.; Chen, O. Superstructures Generated from Truncated Tetrahedral Quantum Dots. *Nature* **2018**, *561*, 378-382.
5. Wintzheimer, S.; Granath, T.; Oppmann, M.; Kister, T.; Thai, T.; Kraus, T.; Vogel, N.; Mandel, K. Supraparticles: Functionality from Uniform Structural Motifs. *ACS Nano*, **2018**, *12*, 5093-5120.
6. Chen, C. L.; Rosi, N. L. Preparation of Unique 1-D Nanoparticle Superstructures and Tailoring their Structural Features. *J. Am. Chem. Soc*. **2010**, *132*, 6902-6903.
7. Disch, S.; Wetterskog, E.; Hermann, R. P.; Korolkov, D.; Busch, P.; Boesecke, P.; Lyon, O.; Vainio, U.; Alvarez, G. S.; Bergstrom, L.; Bruckel, T. Structural Diversity in Iron Oxide Nanoparticle Assemblies as Directed by Particle Morphology and Orientation. *Nanoscale* **2013**, *5*, 3969-3975.
8. Lewis, R. B.; Corfdir, P.; Li, H.; Herranz, J.; Pfüller, C.; Brandt O.; Geelhaar, L. Quantum Dot Self-Assembly Driven by a Surfactant-Induced Morphological Instability. *Phys. Rev. Lett*. **2017**, *119*, 086101.
9. Yang, M.; Chan, H.; Zhao, G.; Bahng, J. H.; Zhang, P.; Král P.; Kotov, N. A. Self-Assembly of Nanoparticles into Biomimetic Capsid-like Nanoshells. *Nat. Chem*. **2017**, *9*, 287-294.
10. Shen, J.; Wang, Z.; Sun, D.; Liu, G.; Yuan, S.; Kurmoob, M.; Xin, X. Self-Assembly of Water-Soluble Silver Nanoclusters: Superstructure Formation and Morphological Evolution. *Nanoscale* **2017**, *9*, 19191-19200.

11. Basu, S.; Paul, A.; Chattopadhyay, A. Zinc Mediated Crystalline Assembly of Gold Nanoclusters for Expedient Hydrogen Storage and Sensing. *J. Mater. Chem. A* **2016**, *4*, 1218-1223.

12. Basu, S.; Goswami, U.; Paul A.; Chattopadhyay, A. Crystalline Assembly of Gold Nanoclusters for Mitochondria Targeted Cancer Theranostics. *J. Mater. Chem. B* **2018**, *6*, 1650-1657.

13. Basu, S.; Bhandari, S.; Pan, U. N.; Paul A.; Chattopadhyay, A. Crystalline Nanoscale Assembly of Gold Clusters for Reversible Storage and Sensing of CO_2 via Modulation of Photoluminescence Intermittency. *J. Mater. Chem. C* **2018**, *6*, 8205-8211.

14. Basu, S.; Paul A.; Chattopadhyay, A. Zinc-Coordinated Hierarchical Organization of Ligand-Stabilized Gold Nanoclusters for Chiral Recognition and Separation. *Chem. Eur. J*. **2017**, *23*, 9137-9143.

15. Basu, S.; Chattopadhyay, A. Room-Temperature Delayed Fluorescence of Gold Nanoclusters in Zinc-Mediated Two-Dimensional Crystalline Assembly. *Langmuir* **2019**, *35*, 5264-5270.

16. Yao, H.; Kojima, H.; Sato, S.; Kimura, K.; Interparticle Spacing Control in the Superlattices of Carboxylic Acid-Capped Gold Nanoparticles by Hydrogen-Bonding Mediation. *Langmuir* **2004**, *20*, 10317-10323.

17. Wang, S.; Yao, H.; Sato, S.; Kimura, K.; Inclusion-Water-Cluster in a Three-Dimensional Superlattice of Gold Nanoparticles. *J. Am. Chem. Soc.* **2004**, *126*, 7438-7439.

18. Xu, Y.; Wang, X.; Zhang, W. L.; Lv, F.; Guo, S. Recent Progress in Two-Dimensional Inorganic Quantum Dots. *Chem. Soc. Rev*. **2018**, *47*, 586-625.

19. Yong, Y.; Cheng, X.; Bao, T.; Zu, M.; Yan, L.; Yin, W.; Ge, C.; Wang, D.; Gu, Z.; Zhao, Y. Tungsten Sulfide Quantum Dots as Multifunctional Nanotheranostics for In Vivo Dual-Modal Image-Guided Photothermal/Radiotherapy Synergistic Therapy. *ACS Nano* **2015**, *9*, 12451-12463.

20. Gao, W.; Wang, M.; Ran, C.; Li, L. Facile One-Pot Synthesis of MoS_2 Quantum Dots–Graphene–TiO_2 Composites for Highly Enhanced Photocatalytic Properties. *Chem. Commun*. **2015**, *51*, 1709-1712.

21. Tian, R.; Zhang, S.; Li, M.; Zhou, Y.; Lu, B.; Yan, D.; Wei, M.; Evans, D. G.; Duan, X. Localization of Au Nanoclusters on Layered Double Hydroxides Nanosheets:

Confinement-Induced Emission Enhancement and Temperature- Responsive Luminescence. *Adv. Funct. Mater.* **2015**, *25*, 5006-5015.

22. Tian, R.; Li, M.; Teng, H.; Luo, H.; Yan, D.; Wei, M. Surface enhanced Raman scattering based on Au nanoparticles/layered double hydroxide ultrathin films. *J. Mater. Chem. C* **2015**, *3*, 5167-5174.

23. Yao, L.; Wei, D.; Ni, Y.; Yan, D.; Hu, C. Surface localization of CdZnS quantum dots onto 2D *g*-C_3N_4 ultrathin microribbons: Highly efficient visible light-induced H_2-generation. *Nano Energy* **2016**, *26*, 248-256.

24. Yan, D.; Evans, D. G. Molecular crystalline materials with tunable luminescent properties: from polymorphs to multi-component solids. *Mater. Horiz.* **2014**, *1*, 46.

25. Gao, R.; Yan, D. Layered host–guest long-afterglow ultrathin nanosheets: high-efficiency phosphorescence energy transfer at 2D confined interface. *Chem. Sci.* **2017**, *8*, 590.

26. DeCoste, J. B.; Weston, M. H.; Fuller, P. E.; Tovar, T. M.; Peterson, G. W.; LeVan, M. D.; Farha, O. K. Metal–Organic Frameworks for Oxygen Storage. *Angew. Chem. Int. Ed*. **2014**, *53*, 14092-14095.

27. Reid, C. R.; O'Koye, I. P.; Thomas, K. M. Adsorption of Gases on Carbon Molecular Sieves Used for Air Separation. Spherical Adsorptives as Probes for Kinetic Selectivity. *Langmuir* **1998**, *14*, 2415-2425.

28. Helvensteijn, B. P. M.; Wang, Y.; LeVan, M. D.; Luna, B.; Kashani, A. Adsorption of Oxygen onto Zeolites at Pressures up to 15 MPa. *AIP Conf Proc* **2012**, *1434*, 1245.

Appendix: A.2

Chapter 2

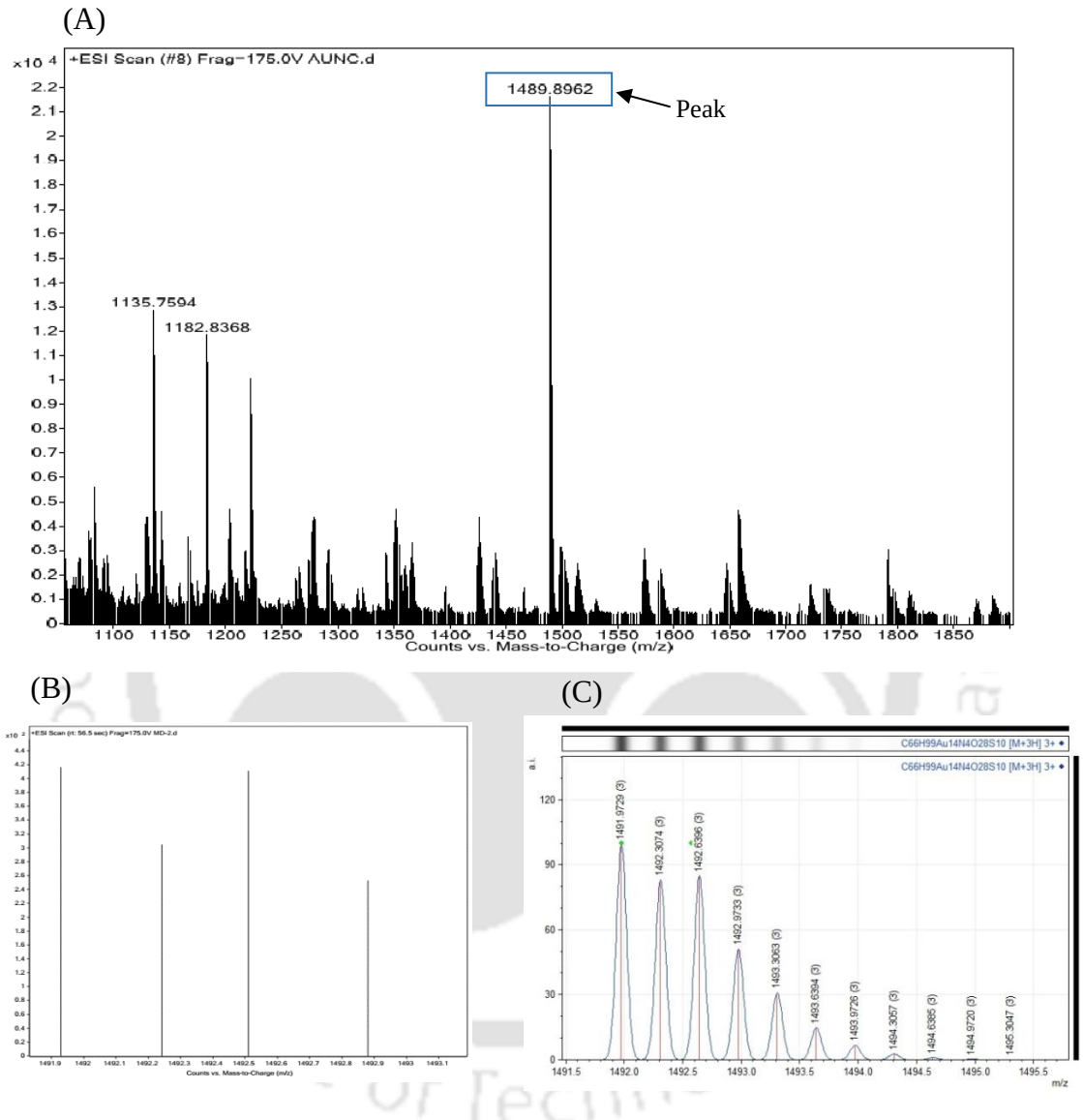

Figure A.2.1. (A) ESI-MS spectrum of MPA and L phe stabilized Au NCs. (B) Experimental mass spectrum of $Au_{14}MPA_{10}Phe_4$. (C) Simulated mass spectrum of $Au_{14}MPA_{10}Phe_4$.

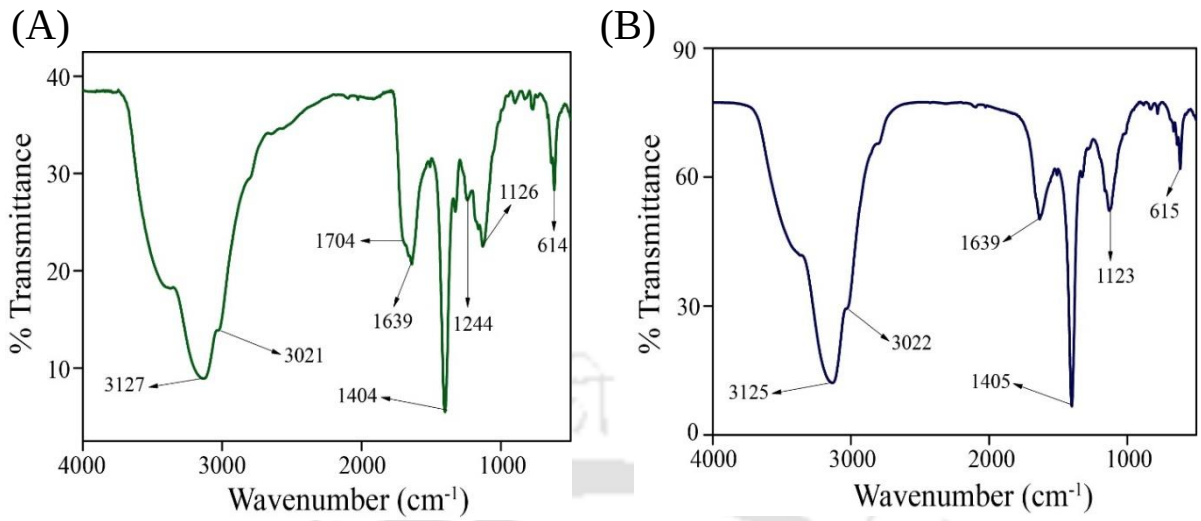

Figure. A.2.2. Fourier transformed infrared spectrum of (A) MPA and L phe stabilized Au NCs. (B) FTIR spectrum of Zn Au NCs.

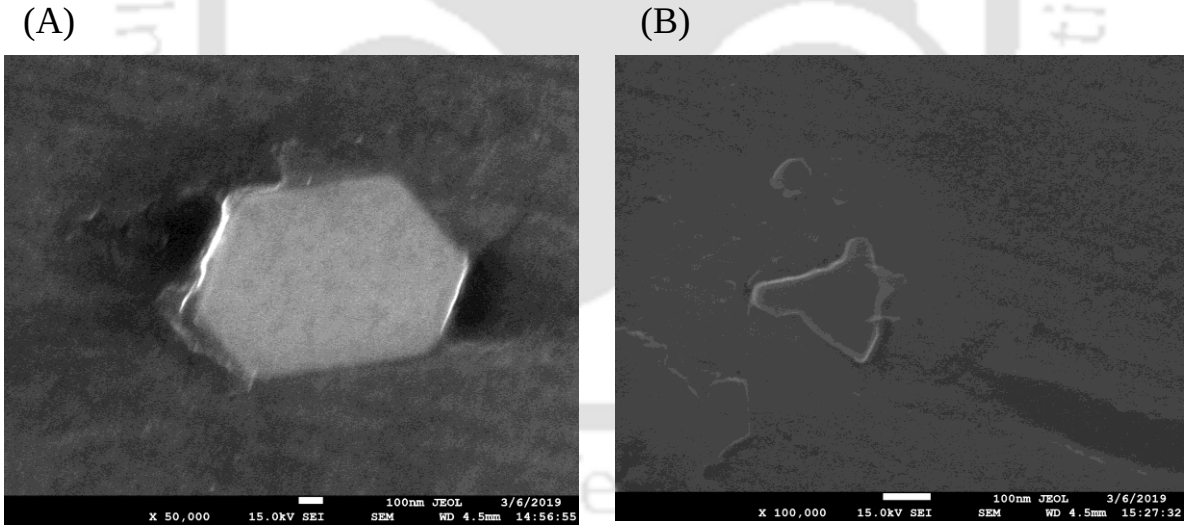

Figure. A.2.3 (A-B) Representative FESEM images of Zn Au NCs.

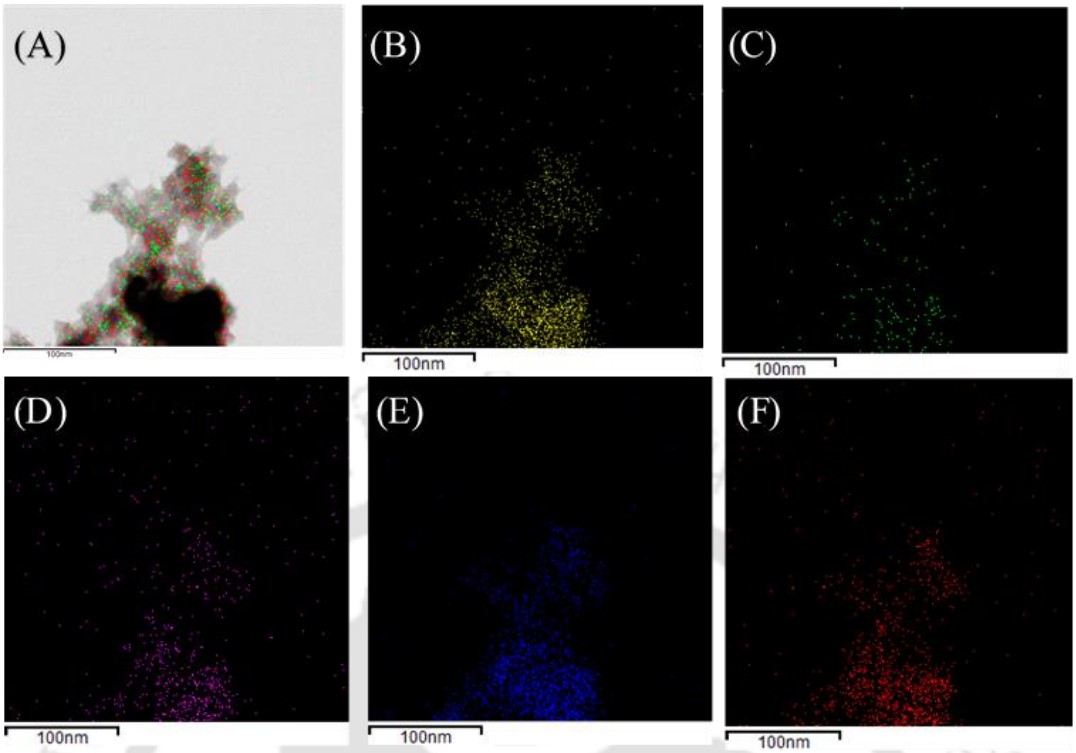

Figure. A.2.4. (A) STEM image of the product of reaction between MPA and L phe Au NCs and zinc ions and. Elemental mapping analysis of (B) Au, (C) N, (D) O, (E) S, (F) Zn obtained from the STEM image of Zn Au NCs.

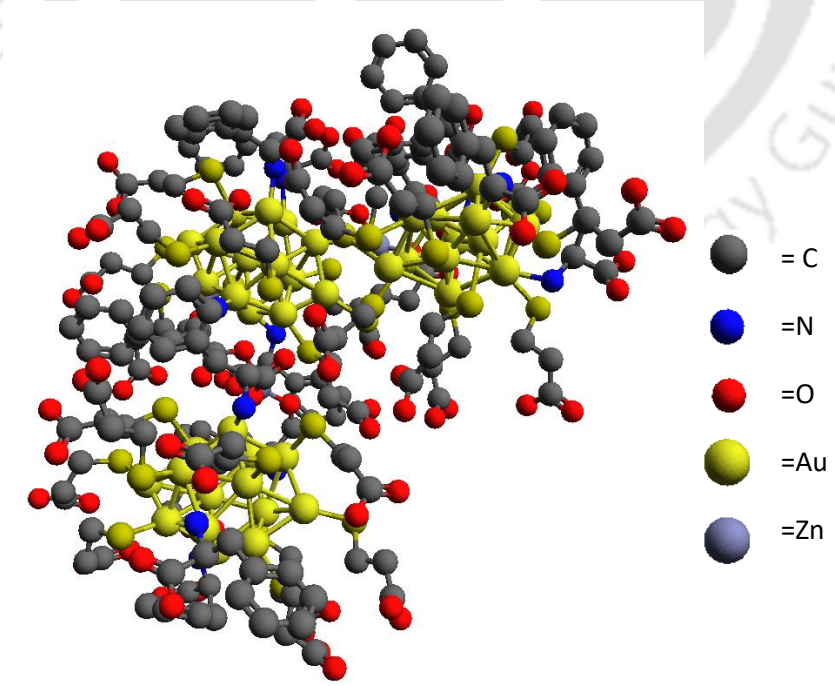

Figure. A.2.5. Computationally optimized structure of Zn Au NCs.

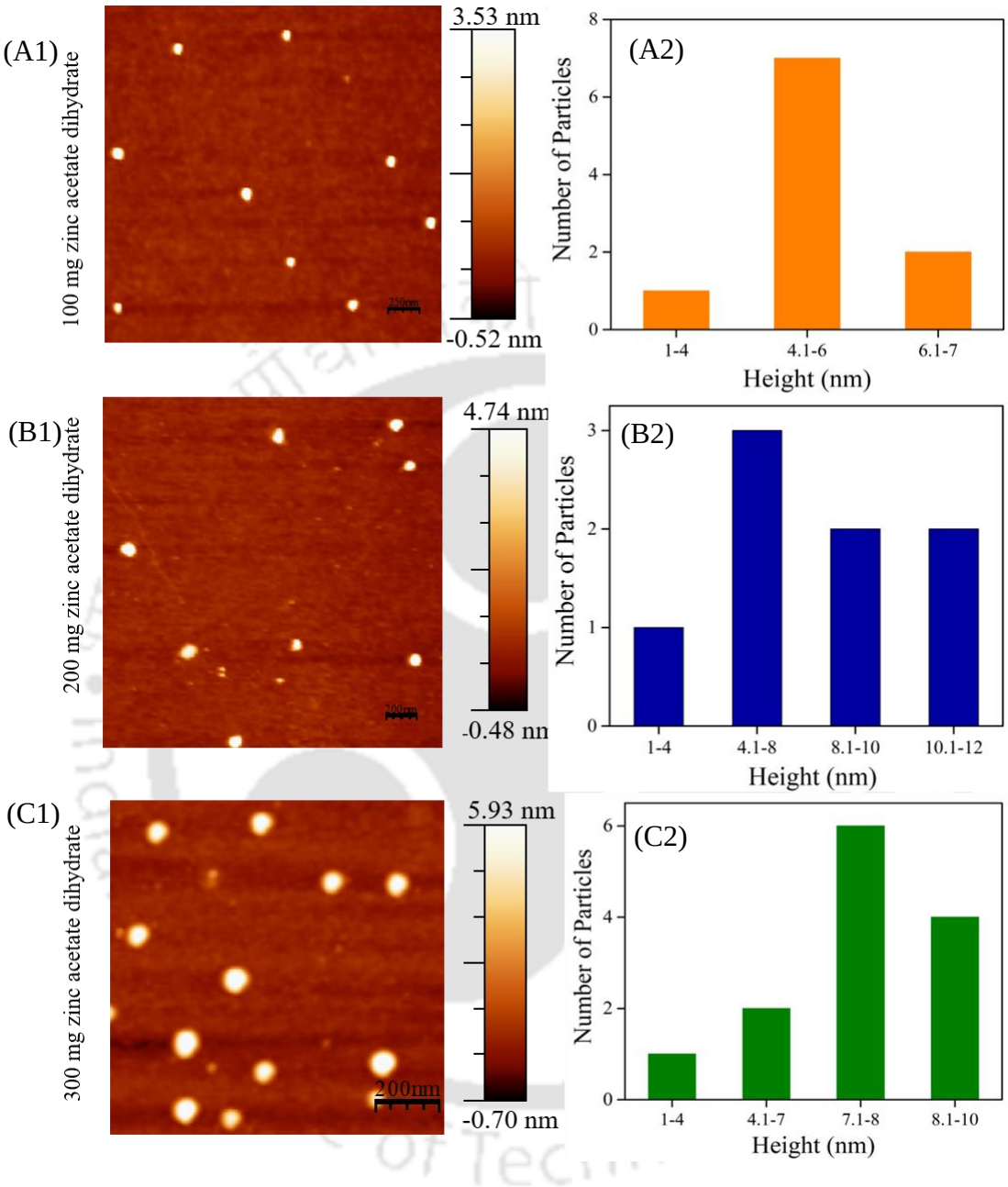

Figure. A.2.6. AFM image of (A1) Zn Au NCs nanosheets formed using ~ 100 mg of zinc acetate dihydrate. (A2) Corresponding height distribution of Zn Au NCs nanosheets. AFM image of (B1) Zn Au NCs nanosheets formed using ~ 200 mg of zinc acetate dihydrate. (B2) Corresponding height distribution of Zn Au NCs nanosheets. AFM image of (C1) Zn Au NCs nanosheets formed using ~ 300 mg of zinc acetate dihydrate. (C2) Corresponding height distribution of Zn Au NCs nanosheets.

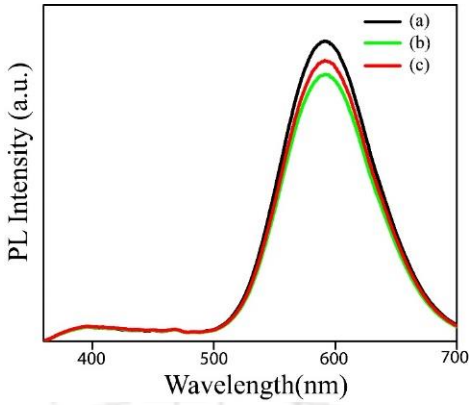

Figure. A.2.7. (a) Luminescence spectrum of (a) Zn Au NCs and of that following (b) purging by oxygen for ~ 5 min and (c) withdrawal of oxygen flow.

Table A.2.1. Table comparing the oxygen storage abilities of several materials reported in the literature.

Reference	Materials	Oxygen storage Capacity	Advantages	Disadvantages
(i) He, H.; Dai, H. X.; Au, C. T. *Catal. Today* **2004**, *90*, 245. (ii) DiMonte, R.; Fornasiero, P.; Graziani, M.; Kašpar, J. *J. Alloys Compd.* **1998**, *275*, **887.**	$Ce_{1-x}Zr_xO_{2+\delta}$	0.4 – 0.5 mMol/g of sample	Appreciable oxygen storage capacity	Operates at high temperature of ~ 500 °C.
Nagai, Y; Yamamoto, T.; Tanaka, T.; Yoshida, S.; Nonaka, T.; Okamoto, T.; Suda, A.; Sugiura, M. *Catal. Today* **2002**, *74*, 225.	CeO_2–ZrO_2 mixtures	1.5 mMol/g of sample	Appreciable oxygen storage capacity	(i) The materials are synthesised are harsh conditions like very high temperature. (ii) Low BET surface area
DeCoste, J. B.; Weston, M. H.; Fuller, P. E.; Tovar, T. M.; Peterson, G. W.; LeVan, M. D.; Farha, O. K. *Angew. Chem. Int. Ed.* **2014**, 53, 14092-14095.	(i) Metal organic framework (MOF) - NU-125 (ii) Zeolites	(i) 10.1 mMol/g of sample (ii) 3 mMol/g of sample	(i) Excellent oxygen storage capacity (ii) Operates at room temperature Appreciable oxygen storage capacity	Operates at high pressure of about 140 bar.
Current work	Luminescent Assembly of nanoclusters	0.266 mM/g of sample	(i) Moderate oxygen storage capacity. (ii) Luminescent indicator for oxygen storage and de-storage (iii) Operates at 20 °C and 20 bar pressure i.e., at ambient conditions (iv) The material for oxygen storage may be synthesised under pliant conditions.	-------

Chapter 3

Modulating Photoluminescence of Europium Through Crystalline Assembly Formation with Gold Nanoclusters and then Phosphate Ions

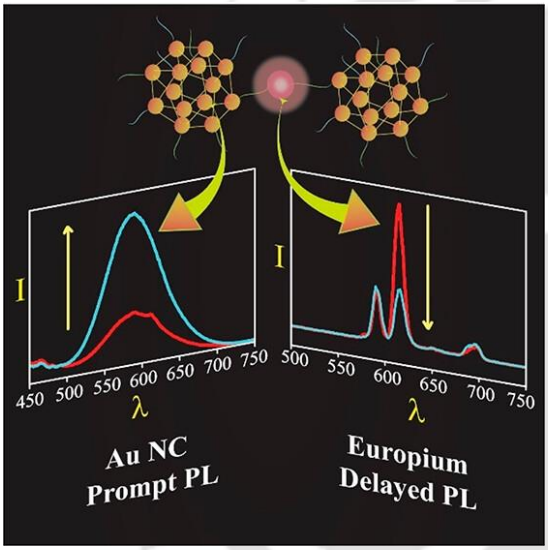

Herein we report delayed fluorescence enhancement of europium (Eu^{3+}) ion through complexation with ligand-stabilized gold nanoclusters (Au NCs). The different Eu^{3+} centric emissions following complexation with Au NCs had selective augmentation in spectral lines attributed to the modulation of the $^5D_0 \rightarrow {}^7F_j$ transitions. The photoluminescence (PL) properties - that included delayed Eu emission - from each component could be modulated through further functionalization of phosphate ions (Pi) leading to crystallization. The assembled crystalline structure of europium containing Au NCs (Eu Au NCs) was corroborated by electron diffraction analyses (TEM and SAED) and high-resolution transmission electron microscopy (HRTEM) analyses. Based on PL measurements and other experimental evidence, the two different lifetimes arising from the components - prompt emission of Au NCs and delayed emission of Eu were affected in the assembled nanostructure. Such design offers a possibility for developing an optical system by conjugating molecular NCs and atomic luminescent probes with potential usage in imaging.

Paul et al. J. Phys. Chem. Lett. 2023, 14, 50, 11250–11257. Reproduced with permission from American Chemical Society.

3.1 Introduction

Deterministic multicomponent assembly of atomic and molecular species offers the opportunity of designing nanoscale matter with the highest precision of functionality. In this regard, the advent of few-atom metal nanoclusters (NCs) having discrete energy levels and inherent feature of molecule-like properties has generated significant interest in the pursuit of their higher-order organization. The atomic clusters exhibit distinctive structures made up of metal core and surface ligands. Typical utilization of organic ligands containing thiols, carboxylate, and amines as functional groups, for surface functionalization, provides convenient options for higher-order assembly through chemical reactions, especially complexation reactions. Recent results suggest that such organization into higher dimensional structures and their subsequent supers-stacking bring in novel properties that are absent in the constituent clusters or metal complexes and even in the 2D assemblies. The transition metal ions such as those of Zn^{2+} play a critical role in bringing structural order to the assembly that leads to superior physical and chemical properties. For example, the crystalline 2D assembly of Au nanoclusters based on complexation reaction with Zn^{2+} ions were efficient for reversible storage of gaseous carbon dioxide, hydrogen, and oxygen and, for recognition and separation of chiral molecules.[1-4] On the other hand, similar crystalline 2D assembly of Au and Cu nanoclusters exhibited properties of delayed fluorescence at room temperature and near white light emitter with superior quantum yield.[5,6] Additionally, 2D crystalline hexagonal Cu nanocluster assemblies - when chemically stacked at 30º- resulted in superior chemical stability and delayed photoluminescence.[7] The cited literature indicates the prominence of the property of the atomic clusters in the assembly with the transition metal ion acting as the bridging species. However, if the metal ion also could add to the overall physical and chemical properties of the assembly through its distinctive features, the multifunctionality could be more advantageous. Such an assembly is yet to be introduced.

An important choice of the metal ion could be based on rare-earth elements with their specific chemical and physical properties. The lanthanides exhibit properties that are unique to their electronic configurations and are disparate from the transition metal and main group elements.[8-11] However, the low absorption coefficient of the lanthanide ion results from their parity forbidden *f-f* transition, and causes low-intensity luminescence emission. This emission can be enhanced by bonding with ligands, which help overcome

the low absorption of lanthanide (III), and serve as sensitizers that effectively transfer energy from the ligand to the 4f metal center.[12-15] Because of atomic-like emission, long excited states (up to millisecond timescale) and great photostability, lanthanide complexes are potential candidates for application as molecular imaging agents, electroluminescent materials, and as luminescent optical probes.[16-21] For instance, co-doped clusters of gold and silver with lanthanide in silicate glasses show potential as bright light-emitting devices.[22] Also, europium-coordinated gold nanoparticle probes have been developed for sensing heavy metal toxins.[23]

Thus, complexation reaction involving ligand-stabilized atomic gold nanoclusters (Au NCs) and lanthanides may provide assembled structures with complementary optical properties of both components. The luminescent lanthanide, in particular, europium (III) is prominent with strong luminescence, which includes narrow-band emission ($^5D_0 \rightarrow {}^7F_J$) and prolonged excited state lifetime (due to delayed emission) in μs-ms time scales.[24] The emission is induced by configurational 4f electronic transitions, which are sensitive to the structure and symmetry of the complex.[25,26] Contrast to typically used molecular fluorophores, these aspects make them appealing as they enable the cut-off of scattering of light and auto-fluorescence of short-lived background photoluminescence generally in ns range and hence improve the signal-to-noise ratio through as overcome time-resolved detection. The europium (III) specific luminescence is indeed important and desirable for optical sensing [27,28] and light-emitting devices[29,30]. For example, a europium hybrid complex of nanoparticle and polymer dots were developed for biological imaging and assays.[31-32] Also, the long luminescence lifetime of europium complex was efficient as a selective anion sensor with a potential for biosensing.[33-34]

Although europium-based inorganic complexes or compounds offer an avenue for materials with tuneable properties, however, the synergy of action that is due to the optoelectronic properties of the components may be either insignificant or difficult to achieve. On the other hand, when both the components are active with their specific optoelectronic properties then the synergy of action may be more prominent. This would be even more significant when the components are assembled based on molecular chemistry principles with molecules contributing to both structural and functional aspects of the assembly. One way forward would be to conjugate ligand-stabilized atomic clusters with Eu^{3+} ions through complexation reaction. The Eu^{3+} ions would bind through chelation

to carboxylate groups present in the ligands of the Au-NC surface and serve as links between the Au-NCs, leading to the formation of an assembly. It is also known that the oxo-philic nature of the Eu^{3+} allows the ions to bind with species such as phosphate ions. Thus, the already-assembled Au-NCs through Eu^{3+} ions may further react with phosphate ions to form superstructure that may have superior optoelectronic properties. This provides an opportunity to explore the crucial attributes of the luminescent characteristics of the atomic clusters and functionalized metal in a single-nanocomplex, which are correlated and could also be modulated in a supramolecular assembly. To the best of our knowledge, the combination of correlated luminescence of an atomic species and that of atomic clusters in a crystalline superstructure is yet to be reported. It is also plausible that the emission wavelengths and lifetimes of the emitting species would bring newer aspects of a multifunctional property hitherto unreported.

3.2 Outline of the present work:

We herein report a crystalline super-assembly that consists of ligand-stabilized Au-NCs, Eu^{3+} ions bonded through complexation with the ligands, and finally phosphate (Pi) ions that played crucial roles in the formation of the superstructure. We also observed that the emission properties of the Eu^{3+} ions and Au-NCs in the assembly were different from the components when isolated. Functionalization with Pi ions not only contributed to the crystallinity of the structure but also to the optical properties of both the Au-NCs and Eu^{3+} ions. Importantly, the difference in lifetimes of the Au-NCs and Eu^{3+} ions provided an opportunity to have two different emissions in the same composite - with the prompt emission of the NCs and the delayed emission of the atomic ions. Transmission electron microscopy (TEM) analyses indicated the hexagonal arrangement of crystalline assembly of Eu-Au-NC-Pi composite with an edge length of 4.5 Å. Interestingly, in the super-assembly, the Eu-Au-NCs were present as single crystalline particles with the Pi ions bridging them through a hexagonal crystal structure.

3.3 Experimental Section:

3.3.1 Chemicals:

Tetrachloroauric acid (Sigma-Aldrich, assay = 99.99%), mercaptopropionic acid (Sigma-Aldrich, assay ≥ 99%), D-tryptophan (Sigma-Aldrich, assay ≥ 98.0 %), europium (III) chloride hexahydrate (Sigma-Aldrich, assay = 99.9 %), *ortho*-phosphoric acid (Merck, assay ≥ 85.0%), ethanol(assay ≥ 99.9%), acetonitrile (Merck, assay ≥ 99.9 %), potassium bromide (Sigma-Aldrich, assay ≥ 99%), sulphuric acid (Merck, assay = 95% - 98%), and Milli-Q grade water was used as procured for experimental work.

3.3.2 Analytical Methods:

(a) Optical Measurements: All measurements related to fluorescence experiments of Au clusters and europium assembly of Au clusters were performed using Horiba Jobin Yvon Fluoromax-4 spectrofluorometer. UV measurements were performed using Perkin Elmer, Lamda 750 UV-Visible spectrophotometer.

(b) Time-resolved photoluminescence study: TRPL analysis was performed under continuous stirring of Au clusters and europium assembly of Au clusters to avoid precipitation of samples. TRPL analysis was done using an Edinburgh Life spec-II spectrofluorometer.

(c) Delayed fluorescence spectroscopy: Delayed fluorescence spectra and decay lifetime measurements were acquired using Horiba Jobin Yvon Fluoromax-4P. Delayed fluorescence measurements were performed under settings of-

Initial delay time- 0.05 ms; sample window- 0.5 ms; maximum delay- 2 ms; flash count-100, time/flash-61 ms, excitation slit- 5 nm; and emission slit- 5 nm.

(d) Fourier transform infrared spectroscopy: FTIR analysis of Au clusters and europium assembly of Au clusters were done using a Thermo scientific Perkin Elmer FTIR spectrometer.

(e) Field emission transmission electron microscopy (TEM) and selected area electron diffraction analysis: TEM and SAED analyses of all the samples were acquired using

JEOL JEM 2100F FETEM Instrument with an acceleration voltage of 200 kV. An aqueous dispersion of the sample was drop-casted in the carbon-coated copper grid and allowed to dry in a vacuum.

(f) Thin film X-ray diffraction study: Thin film XRD analysis was done using Rigaku TTRAX III diffractometer running with CuKα source (λ=1.54 Å).

(g) Simulation of Electrospray ionization mass spectrometric study: ESI-MS of Au clusters was simulated using mMass spectrometry tool.

3.3.3 Synthetic methods:

(a) Synthesis of Au nanoclusters: D-tryptophan stabilized gold clusters were synthesized following a previously reported approach.[4] 1 mL of $HAuCl_4$ (10 mM) was added to 10 mL of ethanol, followed by 0.4 mL of MPA (0.11M), and the medium was stirred continuously, leading to a colorless dispersion. Following that, ~10 mg of D-tryptophan was added to the above resultant solution and agitated continuously. The luminescent dispersion obtained was centrifuged at 10 °C for 10 min at a speed of 10,000 rpm to remove the free ligands existing in the supernatant. The pellet obtained was utilized for further experiments.

(b) Synthesis of Europium Au nanocluster (Eu Au NCs): 10 mM of salt europium (III) chloride hexahydrate was added to the Au NCs dispersion obtained after centrifugation. For the next 60 minutes, the solution was allowed to stir, which led to dispersion with decreasing luminescence intensity. The resulting dispersion was centrifuged multiple times at 10°C for 10 min at a speed of 10,000 rpm. The final pellet produced after centrifugation was utilized for further experiments.

(c) Synthesis of phosphate-mediated crystalline assembly of Eu Au NCs: 1 mL of *ortho*-phosphoric acid (5 mM) was added dropwise to the above dispersion of Eu Au NCs resulting in opaque dispersion of Eu-Au NC-Pi. For the next 60 minutes, the solution was allowed to stir. The resulting luminescent color-less dispersion was then centrifuged at 10°C for 10 minutes at a speed of 12,000 rpm. Finally, the pellet obtained was washed multiple times, later re-dispersed in 1 mL water, and used for characterization and measurements.

3.4 Results and discussions

The consecutive addition of mercaptopropionic acid (MPA) followed by D- tryptophan (Try) to an ethanolic solution containing tetrachloroauric acid ($HAuCl_4$) resulted in colorless dispersion of Au nanoclusters. The colorless dispersion exhibited photo-luminescent emission maximum at 590 nm at excitation at 340 nm. (Figure 3.1) The UV-vis spectrum marked the absence of any possible significant peak beyond the range of 500 nm, suggestive of the presence of any gold nanoparticle. (Figure A.3.1) Transmission electron microscopy (TEM) and selected area electron diffraction (SAED) analyses confirmed the formation of non-crystalline atomic Au NCs. (Figure 3.2) Additionally, the formation of Au_{14} NCs species was confirmed from the electrospray ionization spectrometric (ESI-MS) analyses. The isotopic distribution featuring peak at m/z=1366.0416 was assigned to the formula of Au_{14} $(MPA)_5$ $(Try)_4$ with the assigned ionization $[Au_{14}(MPA)_5(Try)_4 +3H]^{3+}$. The simulated pattern of the obtained molecular formula was characterized by mMass software. ((Figure 3.3).

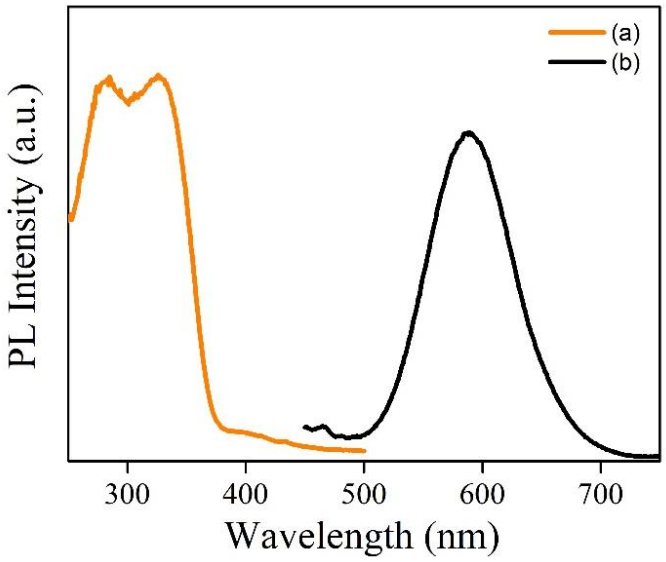

Figure 3.1. (A) Photoluminescence (a) excitation (with the emission fixed at 590 nm) and (b) emission (with the excitation fixed at 340 nm) spectra of MPA and D-tryptophan, ligand stabilized Au NCs.

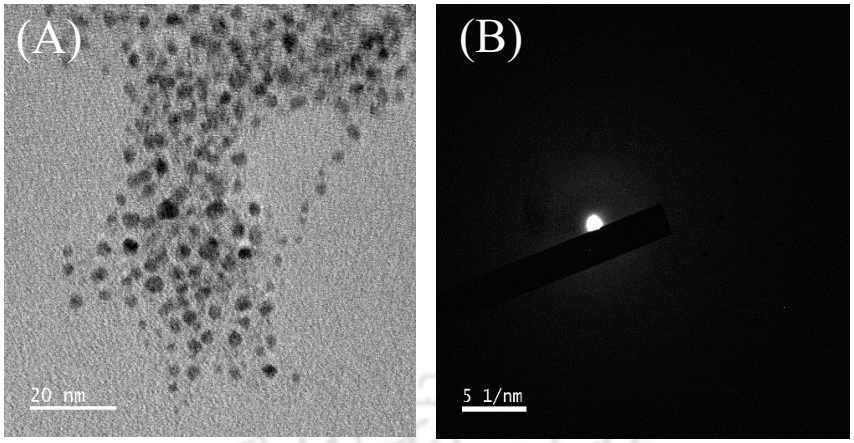

Figure 3.2. (A) TEM image of Au NCs stabilized by MPA and D-tryptophan in 20 nm scale. (B) SAED of the collection of particles being devoid of any distinct diffraction pattern.

With the increase in the concentration of Eu^{3+} ions, the fluorescence emission intensity of Au NCs at 590 nm was reduced in the solution. (Figure 3.4.A) The appearance of a weak peak at 615 nm suggested the coordination of Eu^{3+} with Au NCs. The typical emission peak at ~ 615 nm is attributed to the transition from excited state $^5D_0$ to lower state $^7F_2$ of Eu^{3+} ions. The centrifuged pellet of Eu^{3+} coordinated Au NCs obtained following re-dispersion retained the diminished luminescence intensity i.e., a perceptible peak at 615 nm. (Figure A.3.2) There was a change in fluorescence (FL) lifetime from 244.23 ns to 223.64 ns (Figure 3.4.B, Table A.3.1). This also supported the coordination of the ions to the NCs. Through TEM investigation, the europium-coordinated Au NCs were then analyzed, which exhibited aggregated larger-size particles in comparison to the NCs. The results indicated possible aggregation of NCs through bridging between neighbouring clusters via europium ions. The aggregated particle sizes were in the range of 8-12 nm. (Figure 3.4 C, D). Inverse fast Fourier transform (IFFT) images obtained from the high-resolution transmission electron microscopy (HRTEM) analysis indicated a lattice spacing value of 2.5 Å as obtained from the particles. (Figure A.3.4) The d-spacing corresponds to the intra Au-Au distance in an Au_{14} cluster. The confirmation of associated gold and europium atoms was examined by scanning transmission electron microscopy (STEM) analysis and was shown by elemental mapping that corroborated the associated elements (Eu and Au) present in Eu-Au NCs nanoparticles. (Figure A.3.5).

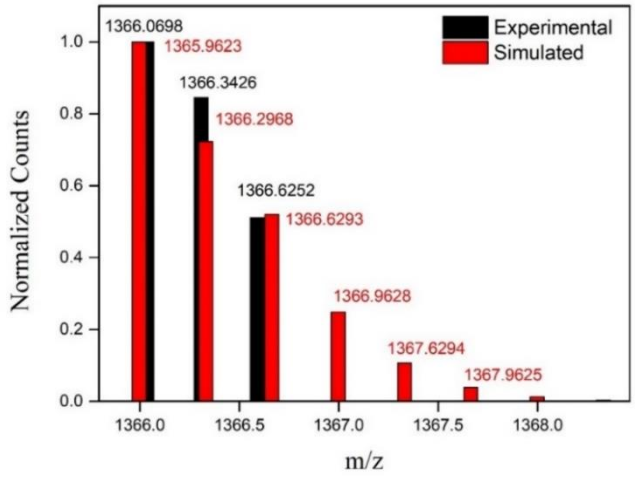

Figure 3.3. Experimental and simulated histograms of the mass spectrum depicting the isotopic distribution of Au NCs species with formula $[Au_{14}(MPA)_5(Try)_4 + 3H]^{3+}$.

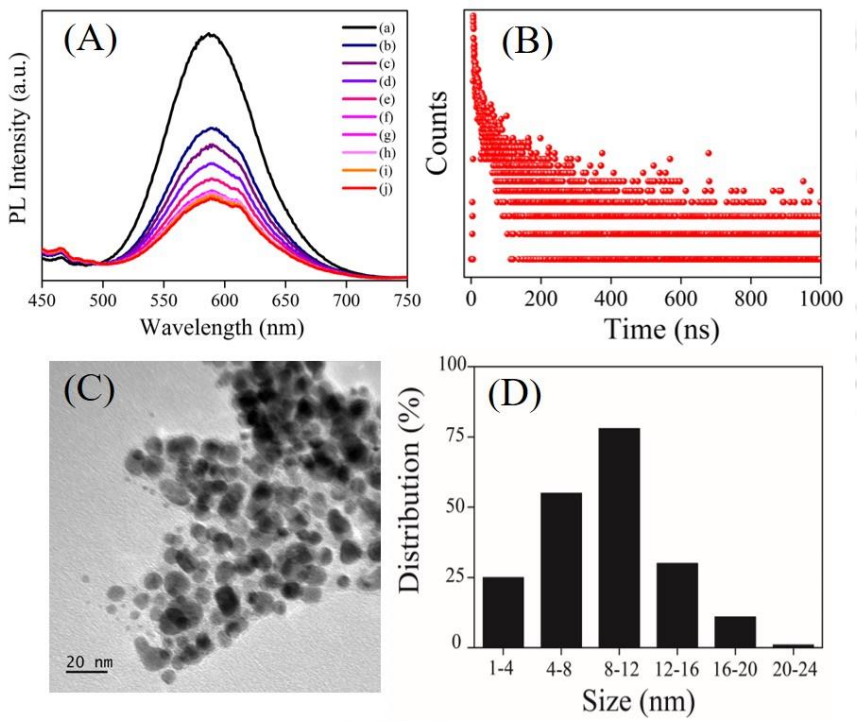

Figure 3.4. (A) Emission spectra of (a) tryptophan-MPA Au NCs, and of that following addition of (b) 10 µL, (c) 20 µL, (d) 30 µL, (e) 50 µL, (f) 70 µL, (g) 90 µL, (h)120 µL, (i)150 µL and (j) 200 µL of 50 mM europium chloride hexahydrate. TRPL decay profile of (B) europium mediated assembly of tryptophan-MPA Au NCs. (C) TEM image of Eu Au NC crystals obtained from the reaction between Eu^{3+} ions and Au NCs and (D) corresponding particle size histogram.

Fourier transform infrared spectroscopy (FT-IR) revealed the binding nature of terminal groups in ligands MPA and tryptophan stabilizing the Au NCs assembled by europium ion. (Figure 3.5) As observed in the FT-IR spectrum, the asymmetric stretch at 1704 cm^{-1} for the carboxylate group of MPA shifted to 1608 cm^{-1}, and peak at 1630 cm^{-1} owing to the asymmetric stretch of the carboxylate group of D-tryptophan shifted to 1541 cm^{-1} after coordinating to Eu^{3+} ion in the assembly now known Eu-Au NC. (The peak at 1385 cm^{-1} is symmetric stretching of C-O present in ligands (D-tryptophan and MPA). Thus, it is evident from the observation that the carboxylate group of ligands stabilizing the Au NCs were bound to the europium ions.

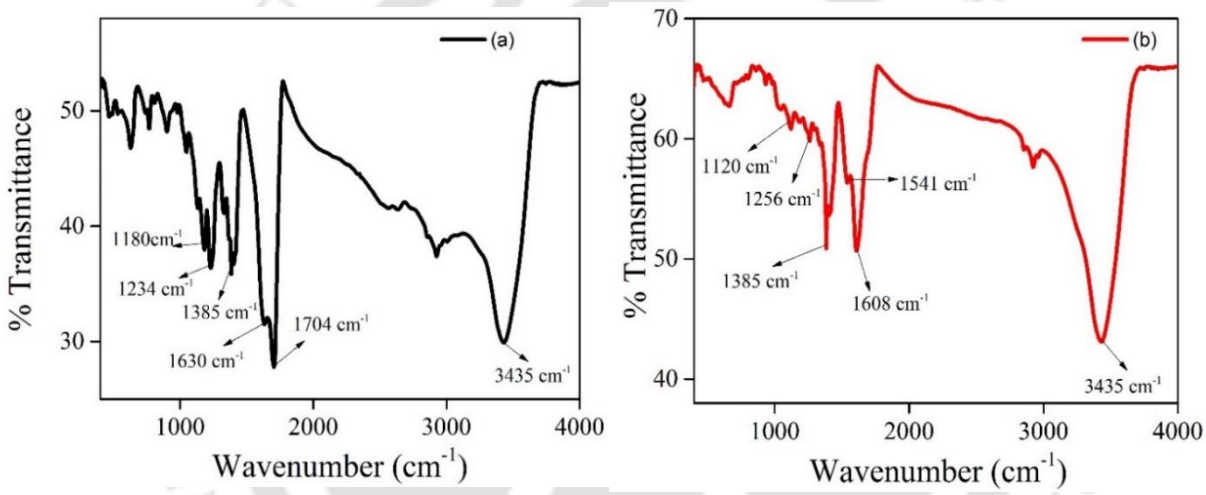

Figure 3.5. Fourier transform infrared spectra of (a) MPA and D-tryptophan stabilized Au NCs. (b) FTIR spectrum of Eu Au NCs.

The absorptions of lanthanide (Eu) cations as a consequence of Laporte forbidden 4f transition are weak, which restricts their practical applicability in the visible region. The europium emission is delayed for an extended period owing to the long excited state and efficient energy transfer between the excited emissive state ($^5D_0$) and ground state ($^7F_2$). Thus, the delayed fluorescence characteristics of europium in the "aggregated" Eu Au NC ensemble were measured, which could be effectively modulated by taking leverage of its high flexible coordination number. So, combined with the time-gated method, that eliminates the short-lived background autofluorescence, the long-lived europium emission significantly contributes to the emission of the assembly.

Interestingly, owing to the effective complexation between Au_{14}NCs and Eu^{3+} ions, the distinctive luminescent metal-centred emission confirmed the coordination of cluster and Eu metal ion. The excitation spectrum of Eu- Au NC particles exhibited a collection of peaks in the broad wavelength range of 250 - 500 nm. (Figure A.3.6) An intense red emission was observed for the Au NCs after strong coordination with Eu ions. Hence, only the assembled nanoscale particles of Eu Au NC were affecting the emission from the Eu (III) excited state. A schematic representation of Au NC aggregated by europium ion is represented in Figure 3.6A. The intense narrow peak at 393 nm in the visible range corresponding to $^7F_0 \rightarrow {}^5L_6$ transition was identified from a sequence of peaks. Following excitation, Eu Au NCs exhibited emissions at 590, 615, 650, and 699 nm structured to the metal-centric europium emission ascribed to the *4f-4f* transitions $^5D_0 \rightarrow {}^7F_1$, $^5D_0 \rightarrow {}^7F_2$, $^5D_0 \rightarrow {}^7F_3$ and $^5D_0 \rightarrow {}^7F_4$, respectively. (Figure 3.6.B) The presence of these significant peaks supported the interactions between the Au NCs and Eu^{3+} in the aggregated particles. The peaks at 580 nm and 650 nm correspond to $^5D_0 \rightarrow {}^7F_0$ and $^5D_0 \rightarrow {}^7F_3$ transitions that are forbidden in electric and magnetic dipole transitions. The $^5D_0 \rightarrow {}^7F_2$ transition is observed with the highest intensity, dominating the whole spectrum followed by the $^5D_0 \rightarrow {}^7F_1$ transition. The intense electric dipole transition at 615 nm of the Eu^{3+} ions is sensitive to a polarizable chemical environment. Strong interaction with the ligands stabilizing the Au NCs led to a non-symmetrical local environment around Eu ions. The asymmetric ratio was evaluated from the ratio of emission intensities ($r = I_{j=2}/I_{j=1}$) of the integrated $^5D_0 \rightarrow {}^7F_2$ transition to $^5D_0 \rightarrow {}^7F_1$ transition peaks.[25] The asymmetric intensity ratio obtained for Eu Au NCs in the dispersion was 3. That was the highest calculated value compared to 0.5 and 0.6 for Eu salt solution, and a mixture of ligand and Eu salt, respectively. (Table A.3.2).

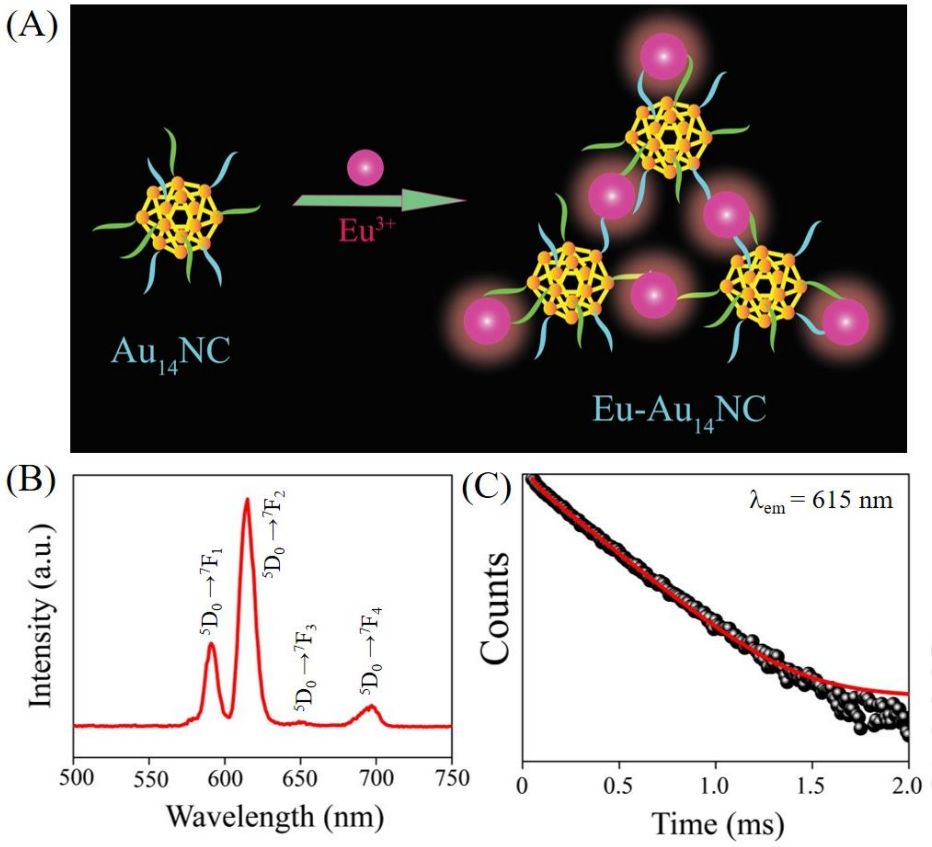

Figure 3.6. (A) Schematic illustration of luminescence process of europium-mediated ligand-stabilized Au NC producing europium delayed fluorescence emission. (B) Delayed fluorescence emission spectrum of Eu Au NCs recorded fixing excitation at 393 nm. (C) Time-resolved decay spectrum of Eu Au NC nanoparticles fixing at emission 615nm. [black-experimental and red-fitted graphs] The average lifetime calculated is 0.230 ±0.005 ms at an emission of 615 nm.

Interestingly, the as-synthesized Eu-Au NC nanoparticles with an average emission lifetime of 0.230 ±0.005 ms being attributed to *f⟶f transition* (at 615 emission), indicated the presence of delayed fluorescence of Eu (III) ion. (Figure 3.6.C) Also, for the intense peak at 590 nm corresponding to the $^5D_0 \rightarrow ^7F_1$ transition, the calculated decay lifetime was 0.236±0.009 ms. Remarkably, the longest lifetime was observed for the aggregated Eu Au NCs as compared to other possible compositions as pursued in control experiments. (Table A.3.4). The overall quantum yield of Eu-Au NCs aggregated particles was observed to have been 33.99 ±1.56 %. The long emission decay and quantum yield accounted for the strong coupling of europium ions to $Au_{14}NC$ through complexation with the stabilizing ligands. The generated ensemble effectively combined the dual characteristics of molecular

atomic cluster and Eu^{3+} ions based on high affinity for oxygen-donor atoms of the phosphate ions for the lanthanide ions.

Thus, the complexation with Eu^{3+} ions resulted in an assembly that retained the emission characteristics of the Au-NCs and the lanthanide ions, which could be probed independently. In other words, the composite emission characteristics were those of distinguishable signals from individual components. Interestingly, the incorporation of lanthanide ions in the complexation-based composite provides an opportunity to extend the coordination of the central metal ions beyond the limit of transition metal ions. In addition, the oxophilic nature of the Eu^{3+} ions could be utilized for extending the assembly into further complex structures in the hierarchy. For example, the composite could be further treated with phosphate (Pi) ions in the medium, to generate a secondary assembly that may provide new structural, physical, and chemical property-based superiority. TEM analysis revealed the crystalline nature of the aggregates of Eu Au-NC and Pi. The morphologies of resultant phosphate containing Eu Au NC particles, revealed transformation from small coalesced nanoclusters to agglomerated larger size nanostructures (termed Eu Au NC Pi). (Figure 3.7) The complex deviates from the initial Eu Au NC aggregates, which were moderately dispersed. The nanostructure was analyzed by SAED and HRTEM results to examine the lattice parameters of the crystalline complex. The observed lattice spacing of 2.5 Å matched well with the edge parameter of Eu Au NC particles that were not single crystalline, to begin with. The length of each hexagonal edge in the assembled Eu Au NC Pi nanostructure was calculated to be 4.5 Å. The lattice spacing of 5.2 Å was attained from the HRTEM analysis performed on the typical crystalline nanostructure. The additional lattice fringes from the HRTEM image constituting lattice distances 3.4 Å, 2.9 Å, 2.8 Å, and 2.28 Å subsequently were also generated following IFFT analysis from the selected region. The powder X-ray diffraction (XRD) pattern, also pointed towards a crystalline phase indicated by the presence of diffraction parameter at 31.8º (2θ value). (Figure A.3.7)

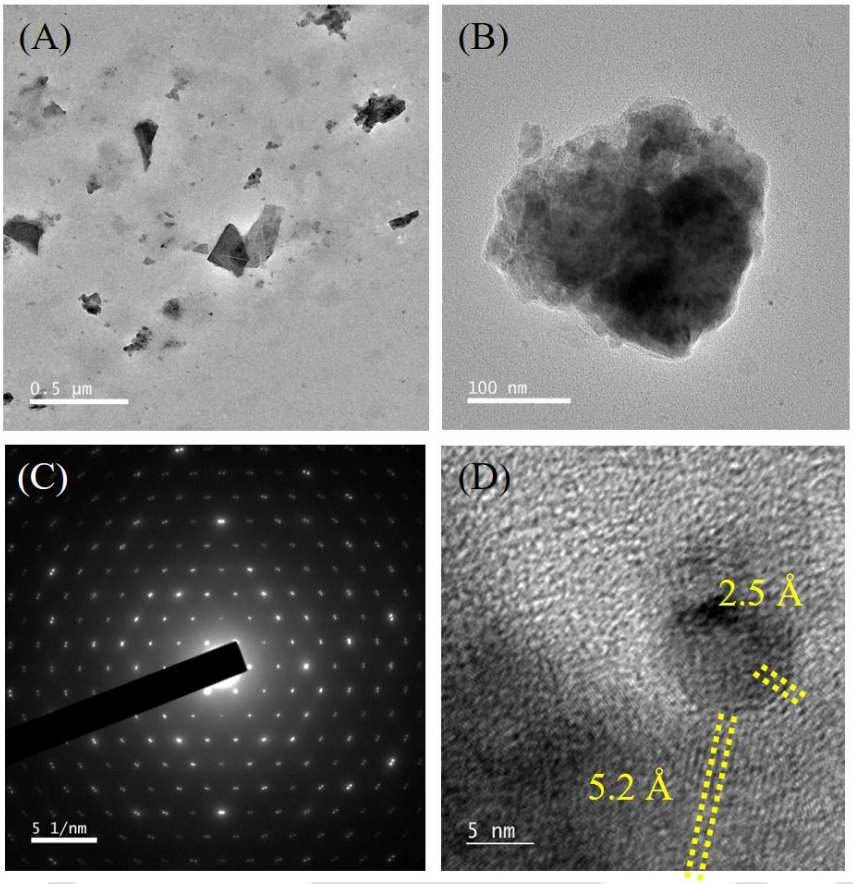

Figure 3.7. (A) TEM image of phosphate added Eu Au NC dispersion. (B) TEM image of crystalline Eu Au NC Pi complex. (C) SAED pattern obtained on crystalline complex of Eu Au NC Pi. (D) HR-TEM image of crystalline assembly of Eu Au NC Pi.

Scanning-TEM image of Eu Au NC Pi nanostructure and analysis from elemental mapping confirmed the presence of Au, Eu, N, O, P, and S (Figure A.3.8). The findings confirmed the existence of the constituent elements in the hybrid system. The characteristic peak at 31.8º in the powder XRD of Eu-Au NC-Pi revealed the formation of the rhabdophane crystal structure of (102) plane of hexagonal europium phosphate.[35,36] The corresponding plane corroborated with the lattice fringe distance of 2.8 Å from HRTEM analyses. The clearly identified lattice fringes due to (110), (200), (112), and (102) planes substantially revealed the hexagonal $EuPO_4.H_2O$ polymorph. (JCPDS Number- 020-1044) Further, based on the aforementioned TEM observation and SAED analyses, a plausible arrangement of the corresponding assembled structure of Eu Au NC Pi has been proposed.

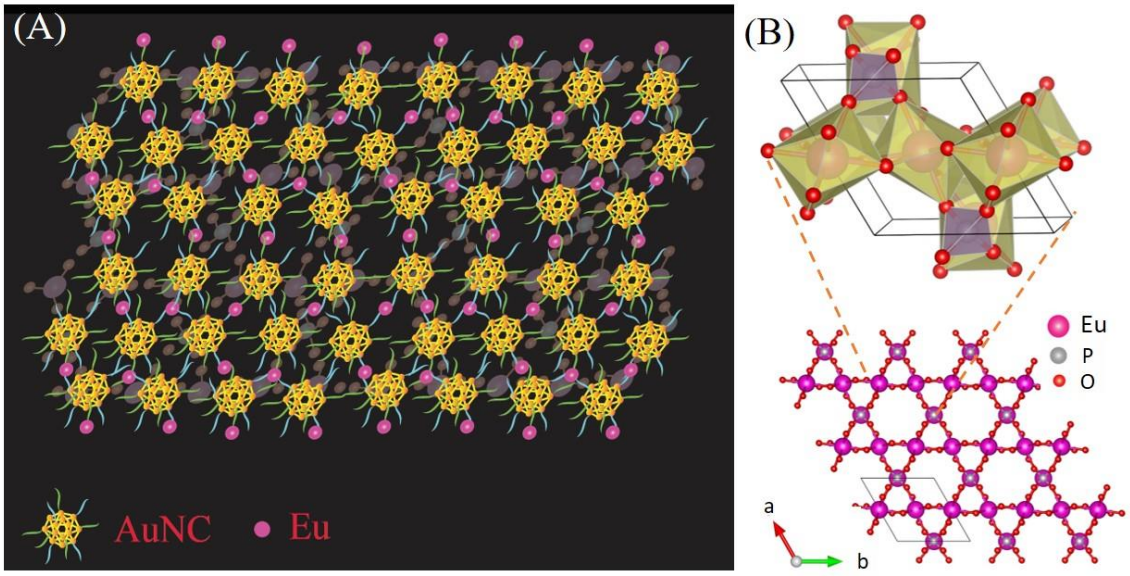

Figure 3.8. (A) Schematic illustration representing the plausible phosphate-based europium Au NC crystalline assembly. (B) Crystallographic structure representation of hexagonal $EuPO_4.H_2O$ obtained using vesta program 3.5.8.

The crystal is constituted of hexagonal close packing of ligand-stabilized Au_{14}NCs. In the arrangements. the two nearby Au_{14}NCs are connected through carboxylate group of ligands of Au_{14}NCs, coordinated via europium ion. The distance between the two Au_{14} NCs connected via tryptophan ligand to metal ion was calculated to be 5.3 Å, which was close to the experimental distance of 4.5 Å from SAED analyses. The particular distance of 2.5 Å is identical to the intra-cluster gold atoms (Au-Au) distance of Au_{14}NC. Further, unsaturated coordination of europium ion in Au_{14}NCs nanoparticles offers selective binding of free phosphate (PO_4^{3-}) group with metal ion over the surface in a hexagonal manner, resulting in europium phosphate crystallization over the Au_{14} NCs assembled nanostructures. The distance between the Au_{14}NCs connected by MPA ligands in the XY plane was calculated to be 6.5 Å, which is in close agreement with the observed distance of 5.2 Å. Thus, based on the experimental evidence, the addition of orthophosphoric acid to Eu Au NC led to the growth of europium phosphate structure over the surface of NCs which further resulted in the complexation of assisted assembly of NCs. Also, the newly generated lattice distances of 3.4 Å, 2.9 Å, 2.8 Å, and 2.28 Å were found to be similar to the d-spacing of hexagonal europium phosphate structure. A crystal structure of hexagonal europium phosphate monohydrate with cell parameters of a=b= 6.9100 Å and c=6.3400 Å

and α=β=90º, γ=120º is schematically presented (Figure 4.B). A plausible arrangement of crystalline Eu Au NC Pi corresponding to the assembled system has been proposed based on TEM evidence and computational analysis. (Figure 3.8) FESEM analyses also corroborated the larger ordered assembly of Eu Au NC Pi. (Figure A.3.10) The aforementioned TEM results assisted inferring the plausible interactions through complexation reaction that are further supported by FT-IR analysis. (Figure A.3.11) The broad peak at 920-1100 cm^{-1} is ascribed to the stretching mode of P-O bonds. The distinctive P-O asymmetric stretch band at 1057 cm^{-1} indicated a phosphoric type complex. The corresponding asymmetric triply degenerate (O-P-O) bending vibrations appeared at 540 cm^{-1}, 574 cm^{-1} and 619 cm^{-1}.[37] The (O-P-O) bending and (P-O) stretching vibrations are the characteristics bands for europium coordination to phosphate. The limited blue shift in the C-O stretching vibration of carboxylate group indicated higher affinity of Eu^{3+} ion for oxygen atoms in phosphate group. Also, the O-C=O asymmetric stretch at 1543 cm^{-1} indicated coordination to the Eu ion.

Also, the optical measurements of crystalline assembly were made to assess the fluorescence characteristics of Eu Au_{14}NC following complexation. The prompt fluorescence intensity of Eu Au_{14} NC was augmented and was accompanied by an increase in the average decay lifetime to 321.50 ns corresponding to the emission of Au NC at 590 nm. The structural stiffness induced by the molecular interaction between phosphate group and Eu ions, reduced the non-radiative transitions from excited states, which in turn affected the total decay parameters emanating from Eu Au NC-Pi crystalline nanostructure. Moreover, phosphate addition to Au NCs dispersion suggested no change in the FL emission intensity. (Figure 3.9) The results indicated the importance of the incorporated phosphate in the Eu Au NCs assembly. Thus, the addition of phosphate led to aggregated assembly, which coalesced together to form ordered arrays between the metal ion and ligands generating a crystalline superstructure. Also, the addition of europium to a solution of phosphate only led to the generation of wire-like structures that supported the formation of the crystalline structure of Eu Au NCs. (Figure A.3.12)

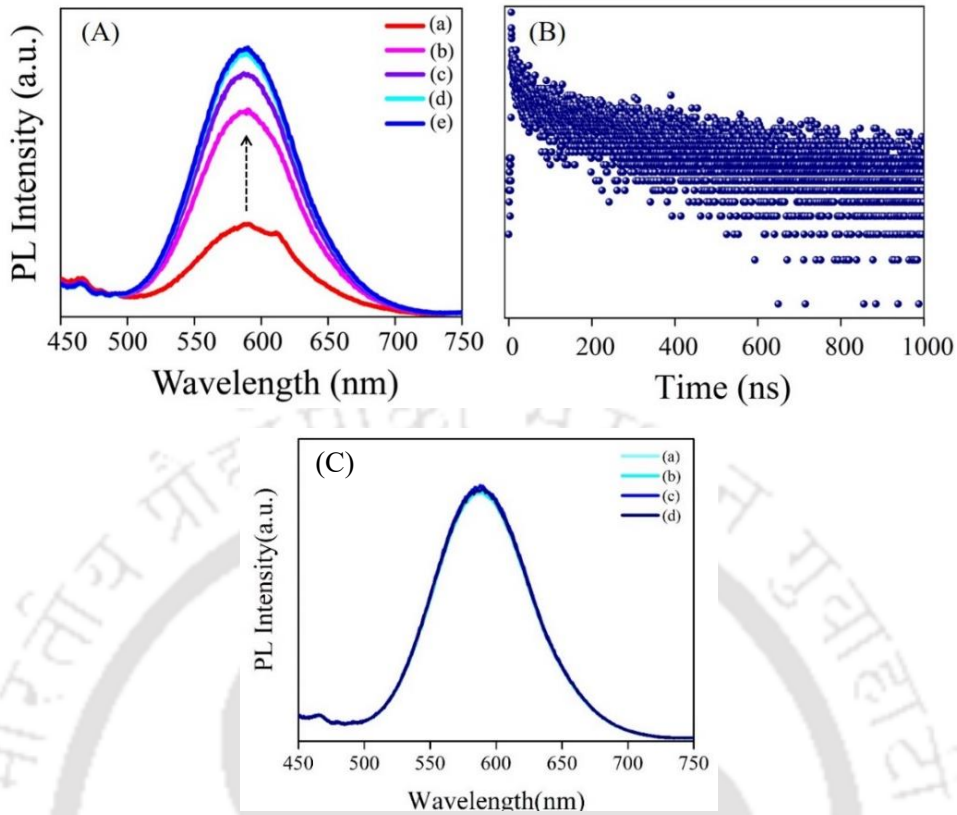

Figure 3.9. (A) Emission spectrum of (a) Eu Au NCs and those following titration (b) 50 µL, (c) 100 µL, (d) 150 µL and (e) 200 µL of 45 mM of *ortho*-phosphoric acid. (B) TRPL decay profile of Eu Au NC-Pi. (C) Emission spectrum of (a) Au NCs and those obtained following titration with (a) 50 µL, (b) 100 µL, (c) 150 µL and (d) 200 µL phosphate.

The delayed fluorescence of Eu Au NC Pi crystalline nanostructure was measured for the metal centric emission. The complexation with phosphate led to a selective decrease in luminescence intensity (615 nm) in the assembled complex (Figure 3.10.A). It is worth mentioning here that in Eu emission, the electric dipole transitions ($^5D_0 \rightarrow ^7F_2$) are hypersensitive to coordination environment while the emission due to magnetic-dipole transition ($^5D_0 \rightarrow ^7F_1$) signifies site with centre of symmetry.[8] This type of transition being independent from coordination surrounding, the extent of decrease in $^5D_0 \rightarrow ^7F_2$ emission intensity was significant as compared to $^5D_0 \rightarrow ^7F_1$ transition in the assembled nanostructure. The complex symmetry change characterized by the intensity ratio, I ($^5D_0 \rightarrow ^7F_2$) / I ($^5D_0 \rightarrow ^7F_1$) descends to the value of 1 which is lower than the value of 3 observed for Eu Au NCs. So, in the phosphate added assembled system this pointed to a transformed symmetric coordination environment around the Eu^{3+} centre. The intensity ratio of value 1

is in good agreement with the formation of hexagonal growth of europium phosphate in the crystalline system.[37] Therefore, the explanation of luminescence transition- is the formation of the hexagonal structure of europium phosphate during the reaction, has made the change in symmetry of Eu^{3+} coordination environment. The europium ion in the Au NCs medium affects the selective binding of phosphate groups with the metal ion in a hexagonal manner distributed on their surface. An intense magnetic dipole transition (J=1) indicates metal interface with inversion symmetry in the assembled state. A more symmetric environment transition from low symmetric environment leading to a crystalline nature caused the change in the $^5D_0 \rightarrow {}^7F_j$ transitions. The intensity ratios 3 and 1 of Eu^{3+} emissions are higher than that in the europium chloride solution. This phenomenon of coordination transformation from high to low value indicated initial interaction between Eu^{3+} and phosphate ions changed from low symmetry to a higher symmetry. Under an excitation of 393 nm, the intrinsic Eu^{3+} transitions to the emitting states had increased, which suggested efficient energy transfer. The decay curve is biexponential and the average lifetime of the $^5D_0$ state obtained is longer 0.339±0.005 ms. (Figure 3.10.B) This spectroscopic data indicated Eu (III) ion at a site of higher symmetry. The longer lifetime is also indicative of the effect of lowering of non-radiative decay process prior to effective shielding of Eu (III) ions by ligands and phosphate ions from the surrounding environment. The photophysical properties hence indicate through enhanced rigidity following crystal formation of Au NCs with europium phosphate growth in Eu Au NC Pi nanostructure.

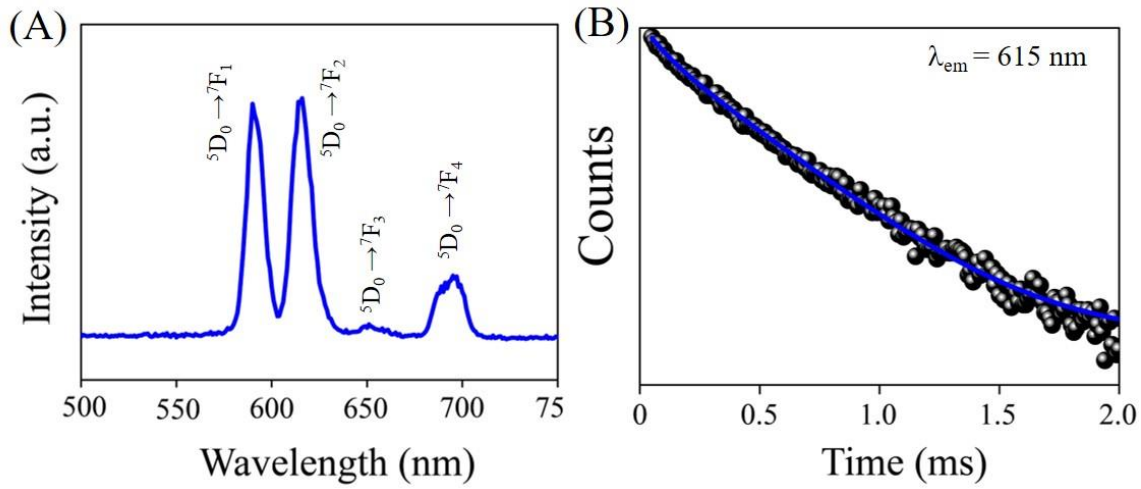

Figure 3.10. (A) Delayed fluorescence emission spectrum of Eu Au NC-Pi. (B) Time-resolved decay profile of crystalline Eu Au NC-Pi assembled particles recorded fixing emission at 615 nm. The average lifetime calculated is 0.339±0.005 ms at emission 615 nm

The delayed emission and decay spectra are in accordance with the delayed fluorescent nature of europium in the assembled complex (Figure 3.10). Altogether, the modified Eu environment via oxygen donor atom in Eu Au NC Pi enhanced the delayed PL lifetime in atomic europium ions impacted by the structural alterations. It is noteworthy that europium delayed emission could be modulated for the first time in crystalline assembled Au NC. The structural confinement established on Au_{14} clusters during assembly formation from (complexation) reaction including phosphate groups to coordinate with europium ion was characterized by radiative lifetime and symmetry transitions ($I_{j=2}/I_{j=1}$), which varied modestly. Alongside, the control set of experiments depicted the photophysical details including excitation spectra, and emission spectra. (Figure A.3.13-A.3.14) Also, an overview of the intensity ratios and lifetime of the transitions in the luminescence spectra are reported in tabulated form. (Table A.3.2, A.3.4). The overall photoluminescent quantum yield for metal centred emission upon nanocluster excitation (340 nm) for Eu Au NC Pi nanostructure was measured 25.19 ± 1.93 %. The loss in quantum yield (from 33.99 ±1.56 %) is relevant to the association of europium mediated Au NC and phosphate ions, leading to additional crystallinity.

3.5 Conclusion

In summary, we have introduced a complexation reaction-based assembly of Au_{14} NCs with lanthanide europium ions. The coordination of europium to Au_{14} NCs could effectively enhance the metal-centric properties of europium ions that could further be modulated on formation of a higher order assembly of gold nanocluster. The Eu Au_{14} NC aggregates exhibited a long- lifetime of Eu emission. The facile tailoring of delayed fluorescence of Eu in the assembled structure would enable application based on modulated intensity ratios and exploration for tailorable nanoprobe designs due to the unique optical characteristics of lanthanides. The work reported here could lead to novel materials by the organization of lanthanide metal-mediated nanoclusters and further functionalization through phosphate into the crystalline assembly.

3.6 Bibliography

1. Basu, S.; Paul, A.; Chattopadhyay, A. Zinc Mediated Crystalline Assembly of Gold Nanoclusters for Expedient Hydrogen Storage and Sensing. *J. Mater. Chem. A* **2016**, 4, 1218– 1223.
2. Basu, S.; Bhandari, S.; Pan, U. N.; Paul, A.; Chattopadhyay, A. Crystalline nanoscale assembly of gold clusters for reversible storage and sensing of CO_2 via modulation of photoluminescence intermittency. *J. Mater. Chem. C* **2018**, 6, 8205– 8211.
3. Paul, M.; Basu, S.; Chattopadhyay, A., Complexation Reaction-Based Two-Dimensional Luminescent Crystalline Assembly of Atomic Clusters for Recyclable Storage of Oxygen. *Langmuir* **2020,** *36* (3), 754-759.
4. Basu, S.; Paul, A.; Chattopadhyay, A. Zinc-Coordinated Hierarchical Organization of Ligand-Stabilized Gold Nanoclusters for Chiral Recognition and Separation. *Chem. Eur. J.* **2017**, 23, 9137– 9143.
5. Basu, S.; Chattopadhyay, A. Room-Temperature Delayed Fluorescence of Gold Nanoclusters in Zinc-Mediated Two-Dimensional Crystalline Assembly. *Langmuir* **2019**, 35, 5264– 5270.
6. Das, P.; Chattopadhyay, A., Delayed Dual Emission of Two-Dimensional Copper Nanocluster Assembly. *J. Phys. Chem. C* **2022,** *126* (2), 997-1005.
7. Das, P.; Chattopadhyay, A., Enhanced Chemical Stability in the Twisted Dodecagonal Stacking of Two-Dimensional Copper Nanocluster Assemblies. *J. Phys. Chem. Lett.* **2022,** *13* (37), 8793-8800.
8. Binnemans, K., Interpretation of europium (III) spectra. *Coordination Chemistry Reviews* **2015,** *295*, 1-45.
9. Bünzli, J.-C. G., Benefiting from the Unique Properties of Lanthanide Ions. *Acc. Chem. Res.* **2006,** *39* (1), 53-61.
10. Binnemans, K., Lanthanide-Based Luminescent Hybrid Materials. *Chem. Rev.* **2009,** *109* (9), 4283-4374.
11. Saraci, F.; Quezada-Novoa, V.; Donnarumma, P. R.; Howarth, A. J., Rare-earth metal–organic frameworks: from structure to applications. *Chem. Soc. Rev.* **2020,** *49* (22), 7949-7977.

12. de Bettencourt-Dias, A.; Barber, P. S.; Viswanathan, S.; de Lill, D. T.; Rollett, A.; Ling, G.; Altun, S., Para-Derivatized Pybox Ligands as Sensitizers in Highly Luminescent Ln (III) Complexes. *Inorg. Chem.* **2010,** *49* (19), 8848-8861.

13. Bourdolle, A.; Allali, M.; Mulatier, J.-C.; Le Guennic, B.; Zwier, J. M.; Baldeck, P. L.; Bünzli, J.-C. G.; Andraud, C.; Lamarque, L.; Maury, O., Modulating the Photophysical Properties of Azamacrocyclic Europium Complexes with Charge-Transfer Antenna Chromophores. *Inorg. Chem.* **2011,** *50* (11), 4987-4999.

14. D'Aléo, A.; Picot, A.; Beeby, A.; Gareth Williams, J. A.; Le Guennic, B.; Andraud, C.; Maury, O., Efficient Sensitization of Europium, Ytterbium, and Neodymium Functionalized Tris-Dipicolinate Lanthanide Complexes through Tunable Charge-Transfer Excited States. *Inorg. Chem.* **2008,** *47* (22), 10258-10268.

15. de Bettencourt-Dias, A.; Barber, P. S.; Bauer, S., A Water-Soluble Pybox Derivative and Its Highly Luminescent Lanthanide Ion Complexes. *J. Am. Chem. Soc.* **2012,** *134* (16), 6987-6994.

16. Bui, A. T.; Grichine, A.; Duperray, A.; Lidon, P.; Riobé, F.; Andraud, C.; Maury, O., Terbium (III) Luminescent Complexes as Millisecond-Scale Viscosity Probes for Lifetime Imaging. *J. Am. Chem. Soc.* **2017,** *139* (23), 7693-7696.

17. Bünzli, J.-C. G., Lanthanide Luminescence for Biomedical Analyses and Imaging. *Chem. Rev.* **2010,** *110* (5), 2729-2755.

18. Fang, F.; Zhao, D.; Zhang, Y.; Li, M.; Ye, J.; Zhang, J., Europium-Doped Nanoparticles for Cellular Luminescence Lifetime Imaging via Multiple Manipulations of Aggregation State. *ACS Appl. Bio Mater.* **2020,** *3* (8), 5103-5110.

19. Singh, K.; Boddula, R.; Vaidyanathan, S., Versatile Luminescent Europium (III)−β-Diketonate-imidazo-bipyridyl Complexes Intended for White LEDs: A Detailed Photophysical and Theoretical Study. *Inorg. Chem.* **2017,** *56* (15), 9376-9390.

20. Montgomery, C. P.; Murray, B. S.; New, E. J.; Pal, R.; Parker, D., Cell-Penetrating Metal Complex Optical Probes: Targeted and Responsive Systems Based on Lanthanide Luminescence. *Acc. Chem. Res.* **2009,** *42* (7), 925-937.

21. Sun, J.; Song, B.; Ye, Z.; Yuan, J., Mitochondria Targetable Time-Gated Luminescence Probe for Singlet Oxygen Based on a β-Diketonate–Europium Complex. *Inorg. Chem.* **2015,** *54* (24), 11660-11668.

22. Eichelbaum, M.; Rademann, K., Plasmonic Enhancement or Energy Transfer? On the Luminescence of Gold-, Silver-, and Lanthanide-Doped Silicate Glasses and Its Potential for Light-Emitting Devices. *Adv. Funct. Mater.* **2009,** *19* (13), 2045-2052.

23. Nath, P.; Priyadarshni, N.; Chanda, N., Europium-Coordinated Gold Nanoparticles on Paper for the Colorimetric Detection of Arsenic (III, V) in Aqueous Solution. *ACS Appl. Nano Mater*. **2018,** *1* (1), 73-81.

24. Lahtinen, S.; Wang, Q.; Soukka, T., Long-Lifetime Luminescent Europium (III) Complex as an Acceptor in an Upconversion Resonance Energy Transfer Based Homogeneous Assay. *Anal. Chem.* **2016,** *88* (1), 653-658.

25. Shavaleev, N. M.; Eliseeva, S. V.; Scopelliti, R.; Bünzli, J.-C. G., Influence of Symmetry on the Luminescence and Radiative Lifetime of Nine-Coordinate Europium Complexes. *Inorg. Chem.* **2015,** *54* (18), 9166-9173.

26. Kirby, A. F.; Foster, D.; Richardson, F. S., Comparison of $^7F_J \leftarrow ^5D_0$ emission spectra for Eu (III) in crystalline environments of octahedral, near-octahedral, and trigonal symmetry. *Chem. Phys. Lett.* **1983,** *95* (6), 507-512.

27. Shen, X.; Lu, Y.; Yan, B., Lanthanide Complex Hybrid System for Fluorescent Sensing as Thermometer. *Eur. J. Inorg. Chem.* **2015,** *2015* (6), 916-919.

28. Zhang, Q.; Wang, J.; Kirillov, A. M.; Dou, W.; Xu, C.; Xu, C.; Yang, L.; Fang, R.; Liu, W., Multifunctional Ln–MOF Luminescent Probe for Efficient Sensing of Fe^{3+}, Ce^{3+}, and Acetone. *ACS Appl. Mater. Interfaces*. **2018,** *10* (28), 23976-23986.

29. Zhan, G.; Wang, L.; Zhao, Z.; Fang, P.; Bian, Z.; Liu, Z., Highly Efficient and Air-Stable Lanthanide EuII Complex: New Emitter in Organic Light Emitting Diodes. *Angew. Chem. Int. Ed.* **2020,** *59* (43), 19011-19015.

30. Xu, L.; Li, Y.; Pan, Q.; Wang, D.; Li, S.; Wang, G.; Chen, Y.; Zhu, P.; Qin, W., Dual-Mode Light-Emitting Lanthanide Metal–Organic Frameworks with High Water and Thermal Stability and Their Application in White LEDs. *ACS Appl. Mater. Interfaces*. **2020,** *12* (16), 18934-18943.

31. Comby, S.; Surender, E. M.; Kotova, O.; Truman, L. K.; Molloy, J. K.; Gunnlaugsson, T., Lanthanide-Functionalized Nanoparticles as MRI and Luminescent Probes for Sensing and/or Imaging Applications. *Inorg. Chem.* **2014,** *53* (4), 1867-1879.

32. Li, Q.; Zhang, J.; Sun, W.; Yu, J.; Wu, C.; Qin, W.; Chiu, D. T., Europium-Complex-Grafted Polymer Dots for Amplified Quenching and Cellular Imaging Applications. *Langmuir* **2014,** *30* (28), 8607-8614.

33. Yang, C.; Xu, J.; Ma, J.; Zhu, D.; Zhang, Y.; Liang, L.; Lu, M., An efficient long fluorescence lifetime polymer-based sensor based on europium complex as chromophore for the specific detection of F^-, CH_3COO^-, and $H_2PO_4^-$. *Polym. Chem.* **2012,** *3* (9), 2640-2648.

34. Picot, A.; D'Aléo, A.; Baldeck, P. L.; Grichine, A.; Duperray, A.; Andraud, C.; Maury, O., Long-Lived Two-Photon Excited Luminescence of Water-Soluble Europium Complex: Applications in Biological Imaging Using Two-Photon Scanning Microscopy. *J. Am. Chem. Soc.* **2008,** *130* (5), 1532-1533.

35. Song, X.; Ma, Y.; Ge, X.; Zhou, H.; Wang, G.; Zhang, H.; Tang, X.; Zhang, Y., Europium-based infinite coordination polymer nanospheres as an effective fluorescence probe for phosphate sensing. *RSC Adv.* **2017,** *7* (14), 8661-8669.

36. Yang, K.-S.; Wu, A.-P.; Zhao, X.; Yan, Y.; Guo, X.-Y.; Bian, Y.-L.; Bao, J.-R.; Li, W.-X.; Zhu, X.-W., Controlled synthesis of $EuPO_4$ nano/microstructures and core–shell SiO2@$EuPO_4$ nanostructures with improved photoluminescence. *RSC Advances* **2017,** *7* (82), 52238-52244.

37. Kijkowska, R.; Cholewka, E.; Duszak, B., X-ray diffraction and Ir-absorption characteristics of lanthanide orthophosphates obtained by crystallisation from phosphoric acid solution. *Journal of Materials Science* **2003,** *38* (2), 223-228.

38. Zollfrank, C.; Scheel, H.; Brungs, S.; Greil, P., Europium (III) Orthophosphates: Synthesis, Characterization, and Optical Properties. *Crystal Growth & Design* **2008,** *8* (3), 766-770.

Appendix: A.3

Chapter 3

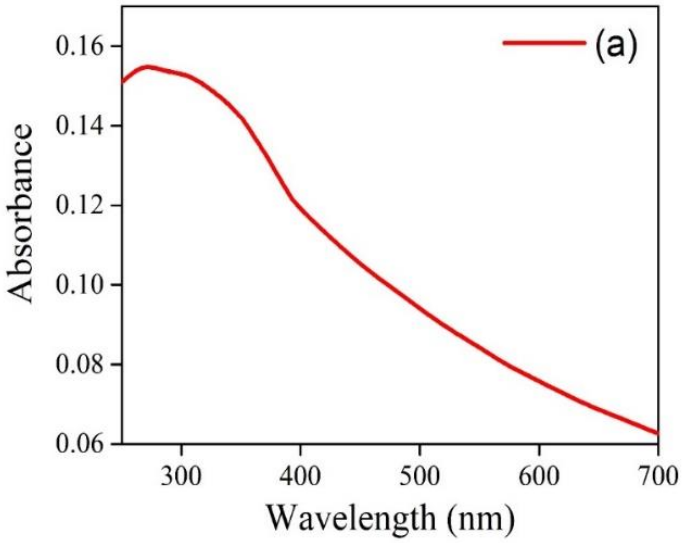

Figure A.3.1. UV-vis spectrum of MPA and D-Tryptophan Au NCs marking absence of any significant peak beyond the range 500 nm.

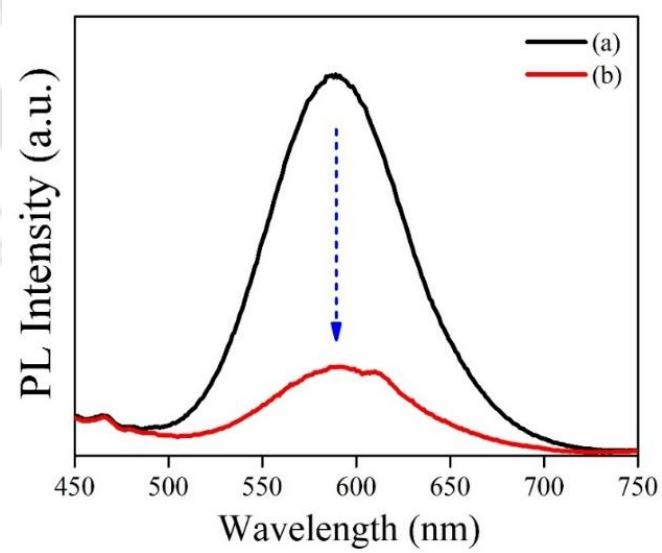

Figure A.3.2. (B) Photoluminescence spectra of (a) Au NC and (b) Eu^{3+} added Au NC showed decrease in emission intensity and a perceptible atomic peak at ~612 nm.

Table A.3.1. Decay parameters obtained from TRPL analysis monitored at 590 nm emission for Au NCs, Eu Au NCs, and Eu Au NCs Pi following tri-exponential fitting.

Sample	A_1 (%)	τ_1 (ns)	A_2 (%)	τ_2 (ns)	A_3 (%)	τ_3 (ns)	χ^2	τ_{avg} (ns)
Au NCs	3.134	1.052	7.418	22.95	89.449	245.98	1.2	244.23
Eu Au NCs	6.314	2.778	27.418	32.977	66.268	234.965	1.1	223.64
Eu Au NC Pi	3.210	0.907	6.726	21.963	90.063	323.051	1.1	321.50

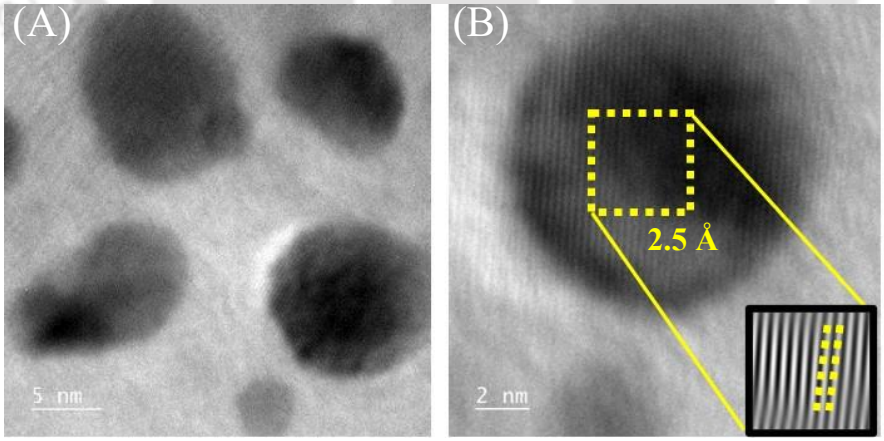

Figure A.3.4. (A) Additional FE-TEM images of europium mediated Au NCs (B) HRTEM obtained on single particle of Eu Au NCs (inset showing d-spacing of 0.25nm)

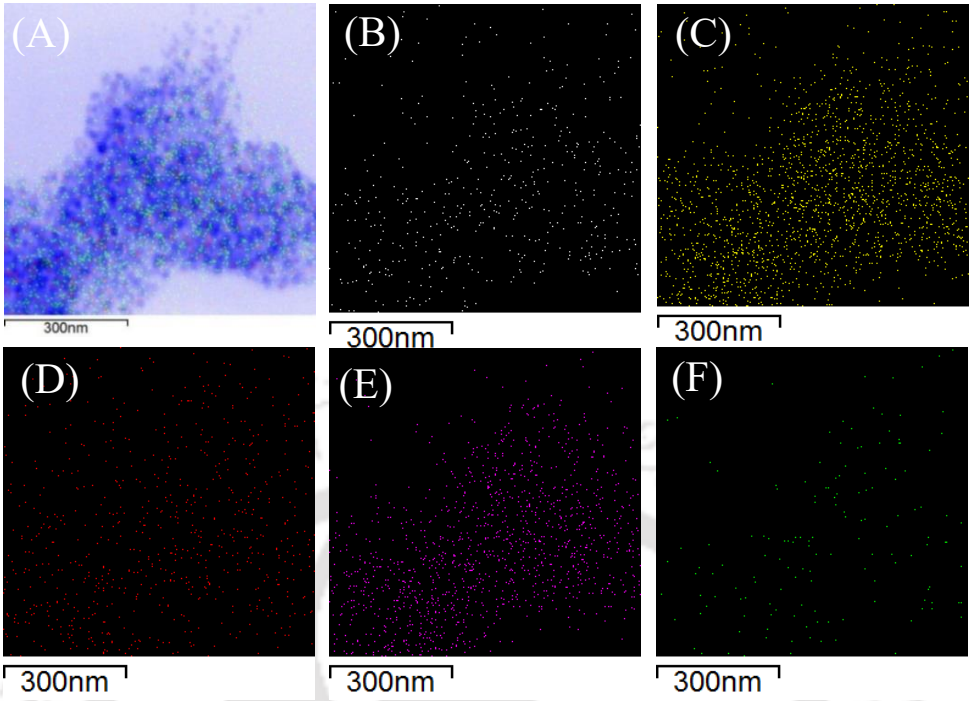

Figure A.3.5. STEM image of (A) Eu Au NCs and elemental mapping of (B) Eu, (C) Au, (D) O, (E) S, (F) N in Eu Au NCs, hence marking the presence of the elements in the Eu Au NCs.

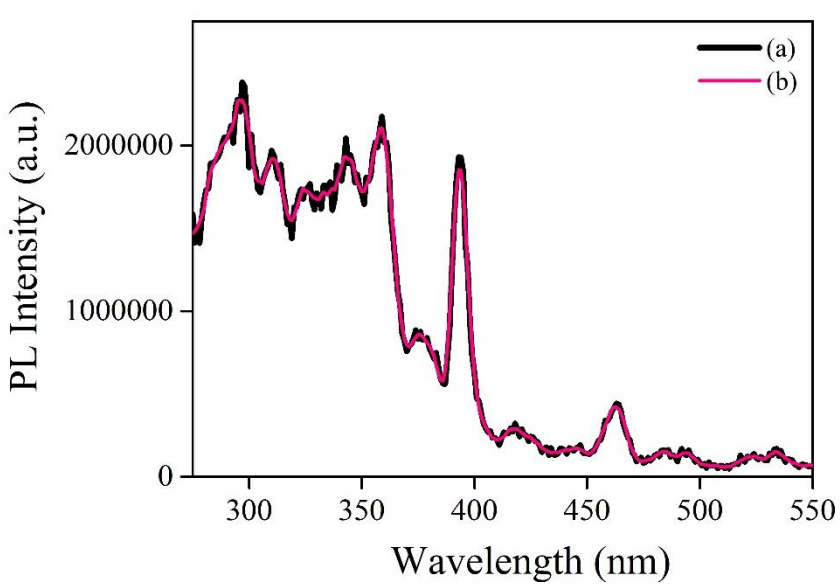

Figure A.3.6. (a) Delayed fluorescence excitation spectrum of Eu Au NCs recorded fixing emission at 615 nm.

Table A.3.2. Assessment of area ratio of $^5D_0 \rightarrow ^7F_2$ (615 nm): $^5D_0 \rightarrow ^7F_1$ (590 nm) at 393 excitation.

Sample	Asymmetric area Ratio $^5D_0 \rightarrow ^7F_2$: $^5D_0 \rightarrow ^7F_1$
Eu-Au NCs	3
Eu-Au NCs-Pi	1
$EuCl_3$	0.5
$EuCl_3$ + D-Try + MPA	0.6

Table A.3.3. Decay parameters obtained from delayed fluorescence analysis of Eu Au NCs monitored at emission of (a) 590 nm, (b) 615 nm obtained following bi-exponential fitting.

Emission	Set No.	A_1	τ_1 (ms)	A_2	τ_2 (ms)	χ^2	τ_{avg} (ms)	$\tau_{avg}\pm\sigma$ (ms)
590 nm	1	63.3%	0.249	36.7%	0.040	0.99	0.231	**0.236±0.009**
	2	57.3%	0.286	42.7%	0.117	0.99	0.247	
	3	73.9%	0.244	26.1%	0.053	0.99	0.230	
615 nm	1	39.2%	0.028	60.8%	0.240	0.99	0.225	**0.230±0.005**
	2	76.7%	0.245	23.3%	0.050	0.99	0.233	
	3	26.5%	0.075	73.5%	0.250	0.99	0.233	

Table A.3.4. Decay lifetime of Eu fluorescence monitored at excitation wavelength 393 nm.

Sample	Delayed fluorescence Lifetime (ms) at emissions (nm)	
Emission	**590**	**615**
Eu-Au NCs	0.236	0.230
$EuCl_3$	0.111	0.108
$EuCl_3$ + Ligands	0.106	0.106

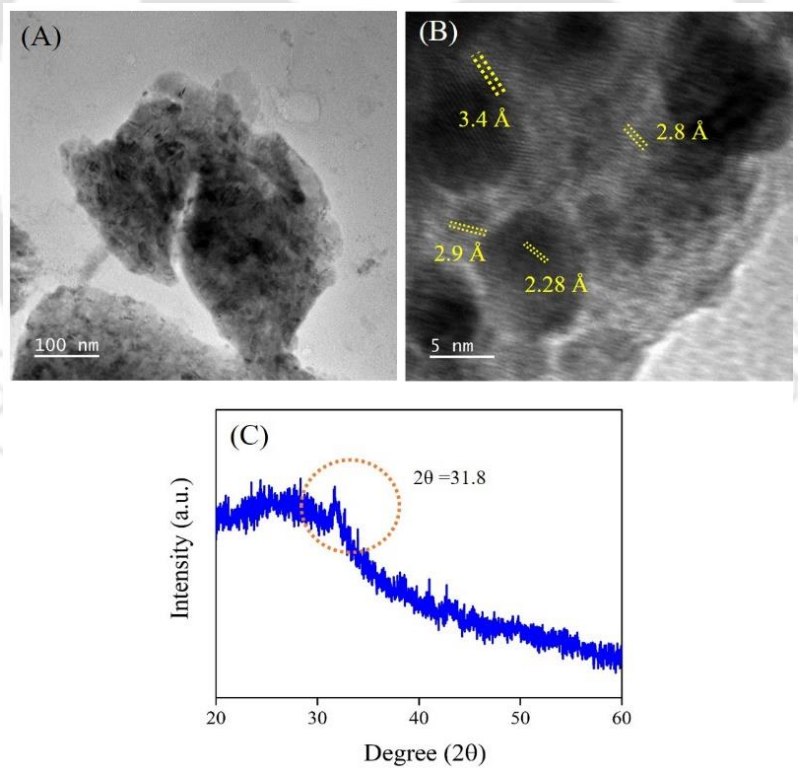

Figure A.3.7. (A) Additional TEM image of Eu Au NC-Pi nanostructure. (B) HRTEM obtained on the nanostructure signifying the lattice fringes obtained from the IFFT pattern. (C) XRD pattern of as synthesized crystalline Eu-Au NC-Pi complex.

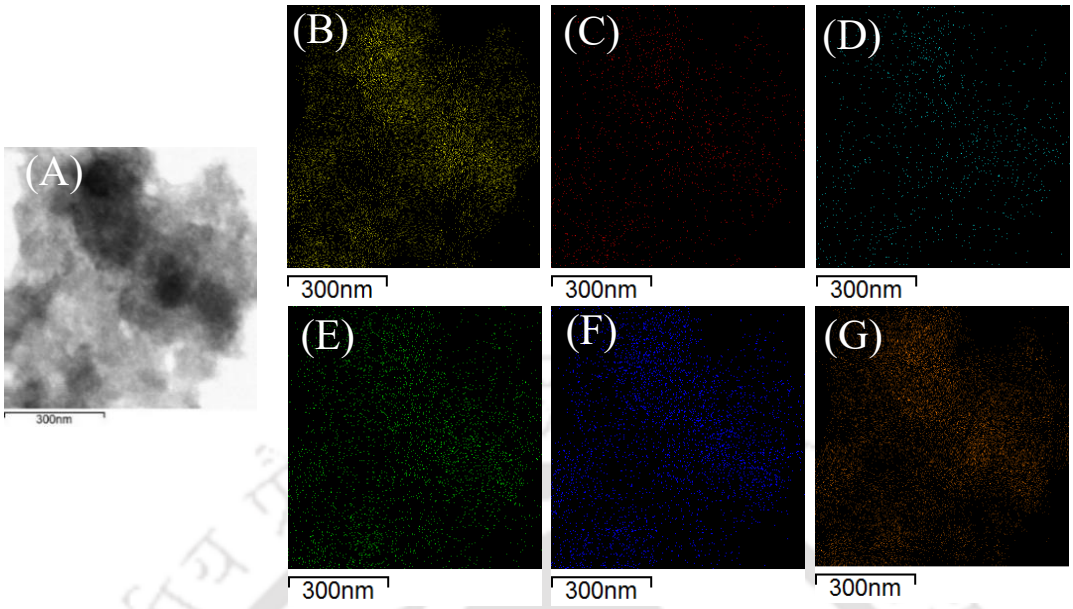

Figure A.3.8. STEM image of (A) Eu Au NCs Pi, and elemental mapping of (B) Au, (C) Eu, (D) N, (E) O, (F) P, (G) S in Eu Au NC Pi, hence marking the presence of the elements in the Eu Au NCs Pi complex.

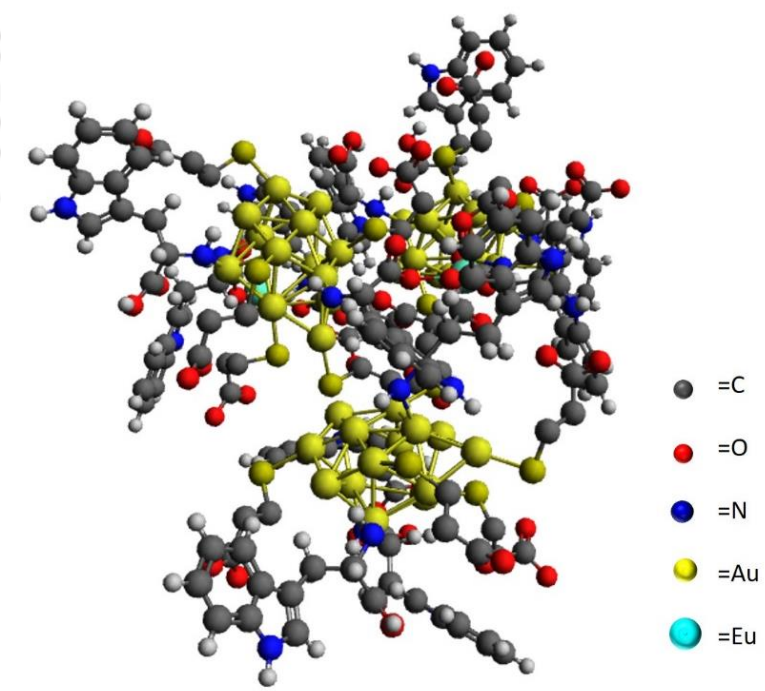

Figure A.3.9. Computationally optimized structure of assembled Eu Au NCs.

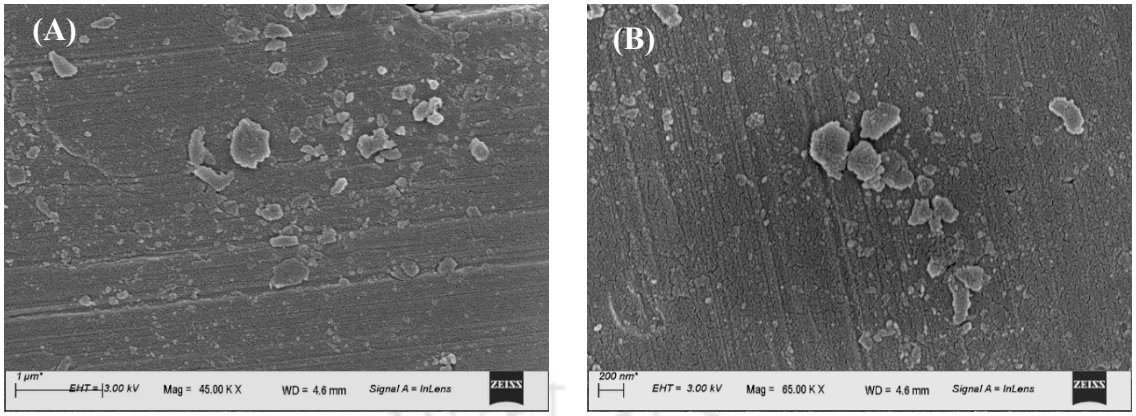

Figure A.3.10. FESEM images obtained on crystalline nanocomplex of Eu-Au NC-Pi nanostructures.

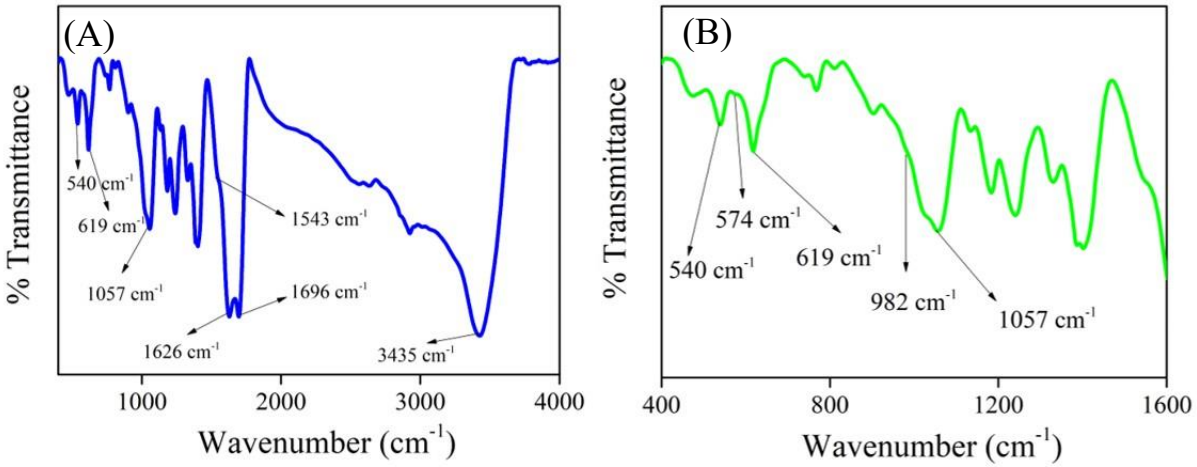

Figure A.3.11. (A) Fourier transformed infrared spectrum of Eu Au NCs Pi. (B) Magnified view in the range of 400-1600 cm^{-1}.

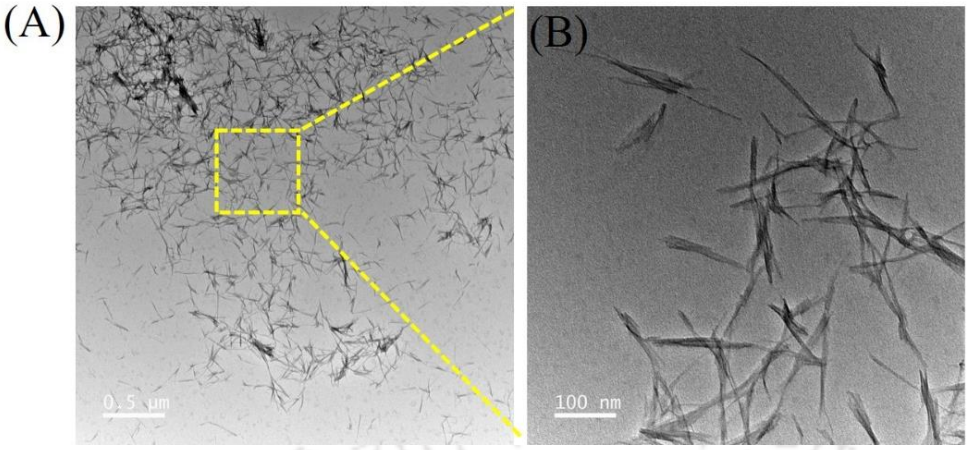

Figure A.3.12. (A) TEM images of $EuPO_4$. (B) Enlarged area with high magnification.

Table A.3.5. Decay parameters obtained from delayed photoluminescence analysis of Eu Au NCs-Pi monitored at emission (a) 590 nm (b) 615 nm obtained following bi-exponential fitting.

Emission	Set No.	A_1	τ_1 (ms)	A_2	τ_2 (ms)	χ^2	τ_{avg} (ms)	$\tau_{avg}\pm\sigma$ (ms)
590 nm	1	18.8%	0.059	81.2%	0.374	0.99	0.362	**0.360±0.012**
	2	44.9%	0.373	55.1%	0.024	0.99	0.347	
	3	38.9%	0.074	61.1%	0.405	0.99	0.371	
615 nm	1	72.5%	0.357	27.5%	0.081	0.99	0.335	**0.339±0.005**
	2	49.6%	0.408	50.4%	0.108	0.99	0.345	
	3	63.0%	0.374	37.0%	0.089	0.99	0.339	

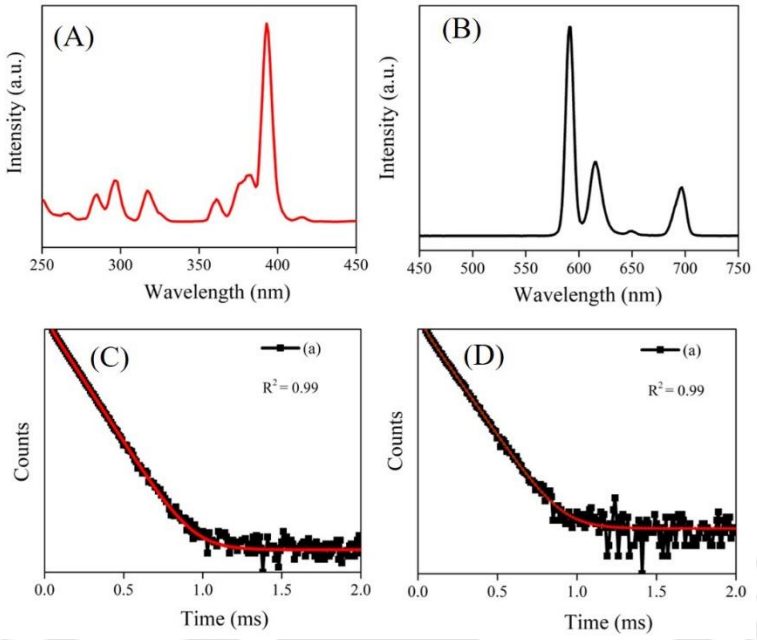

Figure A.3.13. Delayed photoluminescence (A) excitation spectrum centered at emission 590 nm. (B) Emission spectrum. Time resolved decay spectrum at (C) Emission 590 nm. (D) Emission 615 nm of $EuCl_3.6H_2O$. [(a) Decay (b) Fit]

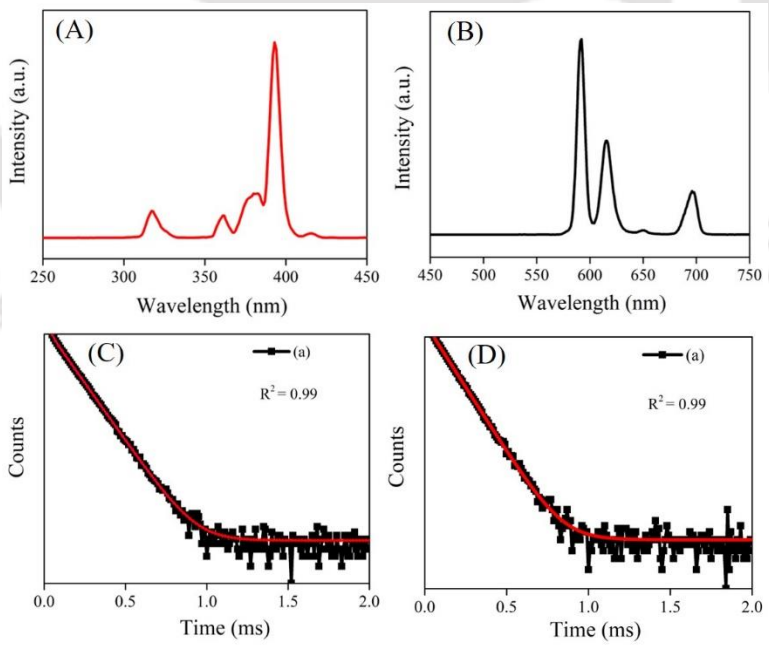

Figure A.3.14. Delayed photoluminescence (A) excitation spectrum centred at emission 590 nm. (B) emission spectrum. Time resolved decay spectrum at (C) Emission 590 nm, (D) Emission 615 nm of $EuCl_3$ + Ligands [(a) Decay (b) Fit]

Chapter 4

Gadolinium Mediated Crystalline Assembly of Gold Nanoclusters for White Light Emission

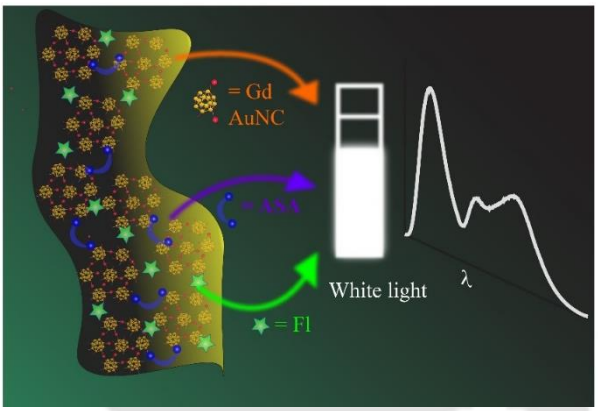

We report the formation of photo-luminescent two-dimensional (2D) crystalline nanosheets involving gadolinium ions and ligand stabilized gold nanoclusters (Gd-Au NCs). Transmission electron microscopy (TEM), selected area electron diffraction (SAED), high-resolution TEM (HR)-TEM in conjunction with FESEM analyses substantiated the 2D crystalline nature of the Au NC nanosheets. The optical and magnetic properties of the have been investigated by photoluminescence measurements and vibrating-sample magnetometry (VSM) analyses. The so-formed crystalline product was further utilized to generate a synchronous tri-colour (orange, green, and blue) emission from a single excitation wavelength through an inorganic surface complexation reaction. The independent emissions were tuneable after ligand functionalization of - acetylsalicylic acid and fluorescein with Gd Au NC assembly. Interestingly, the assembled superstructure with augmented quantum yield led to white light emission at λ_{exc} ~325 nm with CIE of (0.34, 0.33) in the liquid phase. Also, The CRI value of > 85 obtained from the white light emitting (WLE) nanostructure is important and would offer innovative entrants in the field of LEDs.

4.1 Introduction

Higher-order assembly of atomically precise metal nanoclusters (MNCs) in the form of well-defined superstructures has emerged as a class of interest in the field of nanomaterials. The tuneable size and surface chemistry of the nano-regimes are advantageous in assembled hierarchical structures. MNCs have been well-known to bridge molecular and supramolecular chemistry. In this regard, the assembly of such building blocks into "ordered aggregates" has been emphasized by numerous non-covalent interactions like-electrostatic interactions, H-bonding, van der Waals interactions, and π-π stacking. [1-4] However, the ordered assemblies of MNCs are achievable by utilizing the peripheral ligands, which influence the physical and chemical properties exclusively in the assembled crystals. Thus, the higher pattern of assembly is achievable and designable, also by the choice of metal salts and stabilizing ligands. Such supramolecular structure of MNCs provides avenues to attain collective properties from the attained new materials with myriad applications. For example, higher dimensional (3D and 2D) assemblies of NCs achieved by divalent transition metal (Zn^{2+}) have been efficient for gas storage, and sensing applications.[5-8] Also, Zn ion assemblies of atomic (Au and Cu) clusters with delayed fluorescence and near-white light properties were developed.[9,10] Considering that multivalent metal ions could be an effective choice of metal ions, which are scarcely explored to trigger assembly of thiolate Au NCs could be promising.

Rare earth-based materials with unique 4f configurations are at the forefront owing to their unique optical, magnetic, catalytic, and other physical and chemical properties. Such have attracted significant interest in the field of biological imaging, sensors, optical materials, and white light-emitting diodes.[11-13] One such element -gadolinium, from the lanthanide family with a paramagnetic nature, is eminent for clinical applications as a contrast agent (CA) for magnetic resonance imaging (MRI). Also, gadolinium-based nanosheet platforms with an extended surface area as compared to their bulk counterparts demonstrate the potential of highly efficient CAs in this regard. [14,15] Also, Au-supported Gd-doped cobalt boride nanosheets were demonstrated as remarkable electrocatalysts for water oxidation.[16] In another example, gadolinium oxide nanoclusters and rare earth-doped-Gd nanocrystals find pronounced application in optical fields. [11,17] Now, optimizing the properties of nanomaterials for multifunctionality requires parameters such as size and surface chemistry, which is necessary to improve their effectiveness. In this regard, well-

defined structures composed of multicomponent species with inherent advantages provide tuneable functionalities. Therefore, approaching a combination of Gd^{3+} ions and Au NCs with well-defined assemblies-which could create optical and magnetically sensitive nanostructures, could be of interest. Au NCs are found to be photostable and luminescent; their stability in liquid medium provides opportunity for use in optical applications. For example, Au NC for white light emission in aqueous medium initiated through energy transfer to a dye was demonstrated.[18] A white light-emitting composite of conjugated Au NCs and ZnS Qdots has also been demonstrated. [19] Among the multitude of properties of Au NCs assembly, there also remains room to develop effective multicomponent nanocrystals with tuneable emission channels. Recent results have demonstrated that introducing organic ligands on the surface of doped-ZnS Qdots produces white photoluminescence from two channels.[20] Also, surface complexation of 8-hydroxyquinoline ligand on Cu nanocluster assembled 2D crystals led to delayed near white light properties.[10] This also enables the possibility to analyze the scope of designing multiple inorganic complexes with different optical properties. In such a way, inorganic components might be crucial for the stability and adaptability of colour parameters. Hence, establishing the chemistry of inorganic complexes on the surface of higher dimensional assemblies could open new outlooks and have an impact on technologies involving sensing, bioimaging, and optical devices. Additionally, a single-component nature consisting of multicolour emission in the visible range at the same time is desirable.

4.2 Outline of the present work:

Herein, we report the generation of synchronous tri-colour (orange, green and blue) emission from a single excitation wavelength out of inorganic surface complexation reaction on gadolinium based 2D single crystalline assembly of gold clusters (Gd-Au NCs). The crystallinity of the 2D structure was established by XRD, TEM, SAED, and HRTEM analyses. The optical and magnetic properties of the nanosheets have been investigated by photoluminescence measurements and VSM analysis. The independent emissions at three colours were achieved from the Au NC assembly and the complexes with dual ligands acetylsalicylic acid and fluorescein. In this way, the assembled crystalline superstructure with augmented lifetime and quantum yield, emitted white light at λ_{exc} ~325 nm to give colour chromaticity coordinate of (0.34, 0.33) in the liquid phase. The colour rendering

index (CRI) value >85 obtained from the white light emitting (WLE) nanostructure may offer novel strategies and materials in the field of LEDs.

4.3 Experimental Section:

4.3.1 Chemicals:

Tetrachloroauric acid (Sigma-Aldrich, assay = 99.99%), D-tryptophan (Sigma-Aldrich, assay ≥ 98.0 %), mercaptopropionic acid (Sigma-Aldrich, assay ≥ 99%), gadolinium acetate hydrate (Sigma-Aldrich, assay = 99.9 %), ethanol (assay ≥ 99.9%), acetylsalicylic acid (Sigma-Aldrich, assay > 99%), fluorescein (Sigma-Aldrich), acetonitrile (Merck, assay ≥ 99.9 %), potassium bromide (Sigma-Aldrich, assay ≥ 99%), quinine sulphate (Sigma-Aldrich), sulphuric acid (Merck, assay = 95% - 98%), and Milli-Q grade water were used as procured for experimental work.

4.3.2 Analytical Method:

(a) Optical Measurements (UV-vis and fluorescence experiment): All measurements related to fluorescence studies of Au NC, gadolinium assembly of Au clusters (Gd Au NC), and Gd Au NC complex were performed using Horiba Jobin Yvon Fluoromax-4 spectrofluorometer. UV measurements for all the samples were performed using Perkin Elmer, Lamda 750 UV-visible spectrophotometer.

(b) Electron paramagnetic resonance (EPR measurement): EPR measurements were performed using JEOL, Model: JES-FA200 EPR spectrometer. The EPR spectrum was recorded by taking an aliquot of sample in a capillary tube.

(c) Vibrating-sample magnetometry (VSM analysis): VSM measurements were performed using Model 7410 series Lakeshore vibrating sample magnetometer. The product obtained was dried after centrifugation, then weighed and wrapped in Teflon tape for VSM analysis.

(d) Fourier transform infrared spectroscopy (FTIR): FTIR analyses of Au NC, and Gd-Au NCs, and Gd Au NC complex were done using Thermo scientific Perkin Elmer FTIR spectrometer.

(e) Field emission transmission electron microscopy (TEM) and selected area electron diffraction analysis: TEM and SAED analyses of all the samples were acquired using

JEOL JEM 2100F FETEM Instrument with an acceleration voltage 200 kV. Each of the aqueous dispersion of samples was drop-cast in carbon coated copper grid and allowed to dry in a vacuum.

(f) Field emission scanning electron microscope (FESEM): Instrument JEOL JSM-7610F was used to analyze Gd Au NC nanosheets. Sample were prepared by drop casting a dilute dispersion of Gd Au NCs on an aluminium foil wrapped on a glass slide, and allowed to dry overnight.

(g) Thin film X-ray diffraction study: Thin film XRD analysis of samples were recorder using Rigaku TTRAX III diffractometer running with CuKα source (λ=1.54 Å).

(h) CIE chromaticity coordinate calculation: The software "go cie" was used to calculate chromaticity points in the CIE diagram.

4.3.3 Synthesis method:

(a) Synthesis of Au nanoclusters: Au NC was synthesized based on a previously reported approach. [4] 1 mL of $HAuCl_4$ (10 mM) was added to 10 mL of ethanol, followed by 0.4 mL of MPA (0.11M), and the medium was stirred continuously, leading to a colorless dispersion. Following that, ~10 mg of D-tryptophan was added to the resultant solution and allowed to stir continuously. The luminescent dispersion obtained was centrifuged at 10 °C for 10 min at a speed of 10,000 rpm to remove the free ligands existing in the supernatant. The pellet obtained was utilized for further experiments.

(b) Synthesis of gadolinium assembly of Au NCs (Gd Au NCs): 20 mg of gadolinium acetate hydrate was added to the dispersion of Au NCs obtained after centrifugation. The dispersion was allowed to stir, which led to an increase in luminescence intensity. The resulting dispersion was centrifuged multiple times at 10 °C for 10 min at a speed of 10,000 rpm. The final pellet produced after centrifugation was re-dispersed in 1 mL water and utilized for further experiments.

4.4 Results and discussions

Higher dimensional systematic organization of dual ligand stabilised Au NCs -based on the chemistry of complexation reactions - may offer precise functionalization with enhanced stability. In this case, the coordination of negatively charged carboxylate or amide functional groups with trivalent lanthanide metal ions could produce NC-coordinated assemblies. Interestingly, at room temperature – the complexation of gadolinium ions with D-tryptophan (Try) and MPA ligands stabilizing Au_{14} NCs induced luminescence enhancement and excited state lifetime. The synthetic details of (i) Au_{14} NCs and (ii) gadolinium-mediated crystalline assembly of Au_{14} NCs are described in section 4.3.3. Briefly, Au NCs with an emission maximum of around 595 nm, were synthesized at room temperature in an ethanolic solution of $HAuCl_4$ by adding ligands (mercaptopropionic acid and Try). The prepared Au NCs showed no peak beyond 500 nm in the absorption band, marking the absence of plasmon-active large nanoparticles. (Figure A.4.1A) The fluorescent Au NCs showed an emission maximum at 595 nm at λ_{exc} 325 nm. (Figure A.4.1B) TEM and SAED results indicated the formation of Au NCs with an average particle size of 2.5 nm with no crystalline characteristics. (Figure A.4.2) ESI-MS featured the formation of Au_{14} NCs attributed to the molecular formula $[Au_{14}MPA_5Try_4+3Na]^{3+}$ (Figure A.4.3) The photoluminescent lifetime of Au NCs was measured as 252.3 ns. (Figure A.4.4)

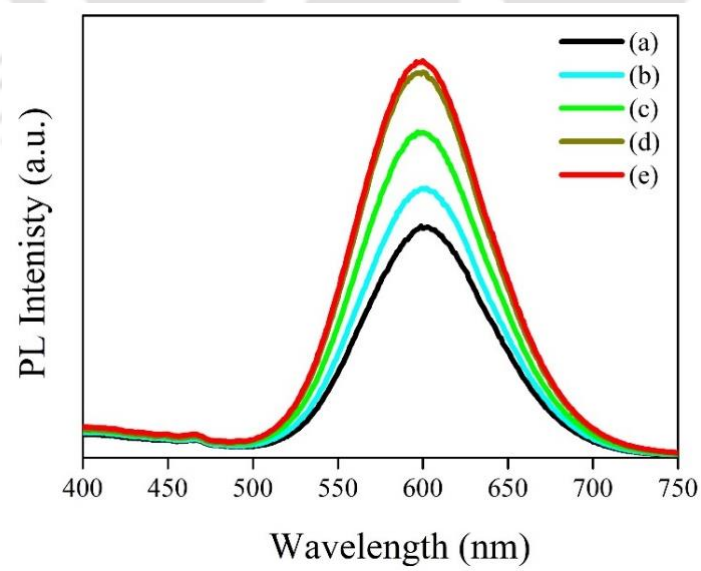

Figure 4.1. (A) Emission spectrum of Au NCs and of that following addition of (a) 5 µL, (b) 10 µL, (C) 15 µL, and (d) 20 µL of 10 mM Gd $(OOCCH_3)_3 \cdot H_2O$.

Based on supramolecular chemistry, the formation of an extended network of Au NC via the coordination of multivalent metal ions could be possible. It was observed that the luminescence intensity of Au NCs was augmented after the addition of gadolinium, which was in stark contrast to those of Au NCs. The gadolinium added dispersion of Au NCs was centrifuged multiple times, and the so obtained colloidal pellet when redispersed retained the luminescent intensity. Hence this possibly indicates the binding of Au NC with the metal ions (Gd Au NCs) (Figure 4.1). One such possible reason for binding is the coordination of ligands of NCs -Try and MPA with metal ions leading to the formation of Gd-Au NCs. The possible binding mode between MPA and Try ligands- stabilizing the clusters and Gd^{3+} in promoting the formation of assembled structures of Au NCs was verified by FT-IR spectroscopic analysis. (Figure 4.2). The C=O stretching frequency due to carboxylate group of MPA at 1696 cm^{-1} was absent in Gd-Au NC, which appeared at a lower stretching value of 1633 cm^{-1}. Also, as is evident from the peak at 1544 cm^{-1}, which was red shifted from higher stretching frequency of 1625 cm^{-1} for the C=O stretching frequency of Try ligand. The shifts in the stretching frequencies implied the important role of carboxylate groups of terminal ligands in coordination with gadolinium ion.

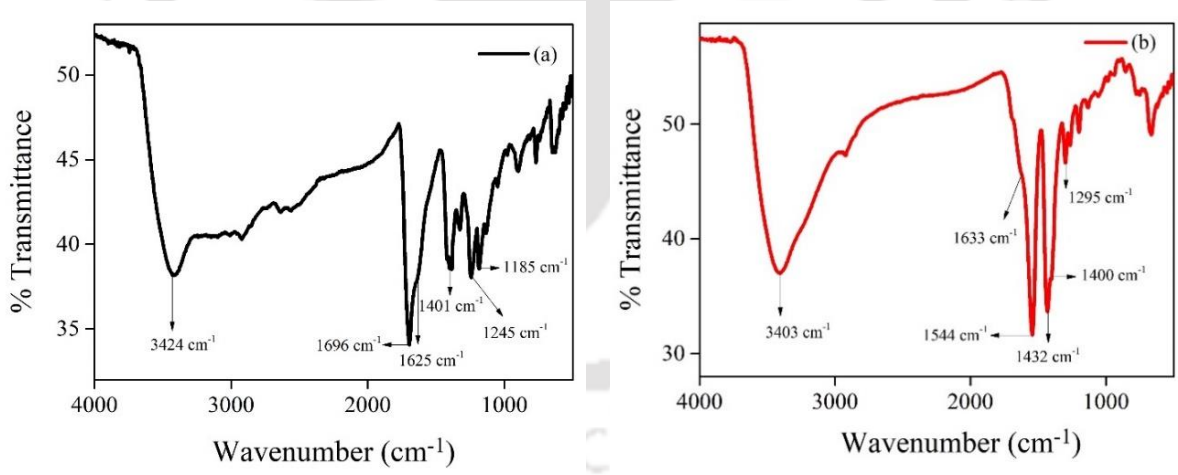

Figure 4.2. Fourier transformed infrared spectra of (a) MPA and Try stabilized Au NCs. (b) FTIR spectrum of Gd Au NCs.

Also, the UV-Vis spectrum remained unaltered following complexation with gadolinium ions, indicating a lack of formation of larger plasmonic nanoparticles. Given the practical importance of the assembly of Au NCs, the ensemble of such NCs can behave coherently/differently compared to individual components when interacting with a

common light field. Also, in the close proximity of emitting components, charge transfer is anticipated to occur which may lead to delayed fluorescence.

In addition to the prompt fluorescence properties, Gd Au NC exhibited distinct delayed fluorescence emission at 595 nm with a long-excited state lifetime. The decay profile of Gd Au NC nanosheets showed a bi-exponential decay function fit with an average lifetime of 0.91 ms at room temperature. (Figure 4.3, Table A.4.1) Also, photoluminescence intensities were significantly enhanced. The intramolecular rotations are also comprised of ligands stretching vibrations, which are suppressed by physical constraints in the "aggregated" states. Hence the excited states undergo a radiative decay (ISC or RISC) process with conspicuous delayed fluorescence and intense luminescence. As a consequence, the longer lifetime component resulted in a near millisecond lifetime. Such enhanced delayed lifetimes are of special interest in the field of light-emitting materials.

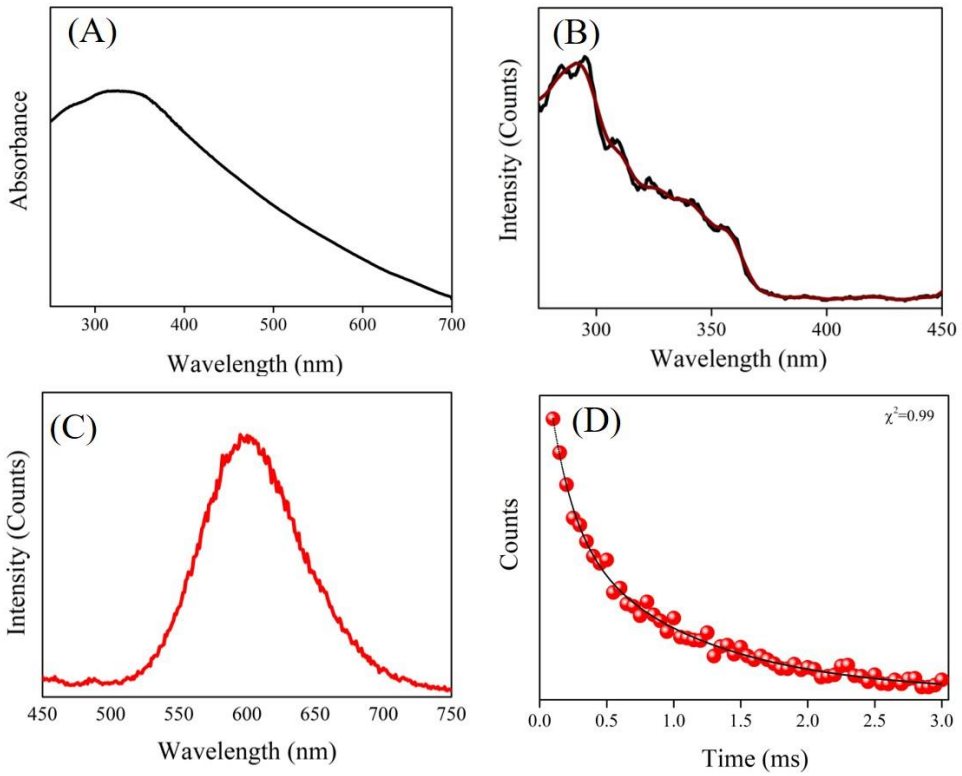

Figure 4.3. (A) UV-vis spectrum of Gd Au NCs. (B) Delayed fluorescence excitation spectrum of Gd Au NCs. (B) Delayed fluorescence emission spectrum of Gd Au NCs. (C) Time-resolved delayed fluorescence spectrum of Gd Au NCs.

Next, considering the higher coordination site of trivalent gadolinium ions, the formation of two-dimensional superstructures via a conjugated extended network of Au NCs is possible through chemical bonding. Also, from FT-IR observations, the effect of strong intermolecular bonding between carboxylate groups of ligands and gadolinium ions, molecular rigidity, and inclination towards close packing could be anticipated. Intriguingly, from TEM analysis, gadolinium ion mediated assembled structures constituting Au NC showed the presence of several segregated 2D nanosheet-like structures. (Figure 4.4.A) The typical nanosheets of Au NCs obtained had an average size of 200-300 nm. On further magnification, the typical nanosheets were found to have been composed of a few layers of 2D structures. The nanostructures, as observed from the assemblies resulted in enhanced emission properties. The SAED pattern of Gd Au NCs, which revealed the crystalline nature of 2D nanosheets indicated hexagonal lattice diffraction. The dimension analyzed from one such nanosheet from a hexagonal diffraction pattern (SAED) was calculated to be 2.9 ± 0.1 Å. (Figure 4.4.D). Also, from high-resolution TEM analysis (HRTEM), the well-resolved lattice fringes were obtained. The measured lattice spacing was 7.5 Å and 3.0 Å obtained from a typical crystalline nanosheet. (Figure 4.4.C, E) The presence of constituent Au NCs in the nanosheet was evident from the distributed small particles of size about 2.5 nm. (Figure 4.4.E) Also, the lattice parameter obtained from HRTEM analysis confirmed the finding from the d-spacing value calculated from XRD analysis. (Figure 4.4.F) The simultaneous localization of gold and gadolinium along with other constituents in the so formed nanosheets were confirmed by scanning-TEM analysis and elemental mapping. (Figure A.4.5) Hence, evidence of constituent elements in the nanosheet of Au NCs was confirmed. FESEM analysis also corroborated the simultaneous formation of Gd-Au NC layered nanosheets. (Figure A.4.6)

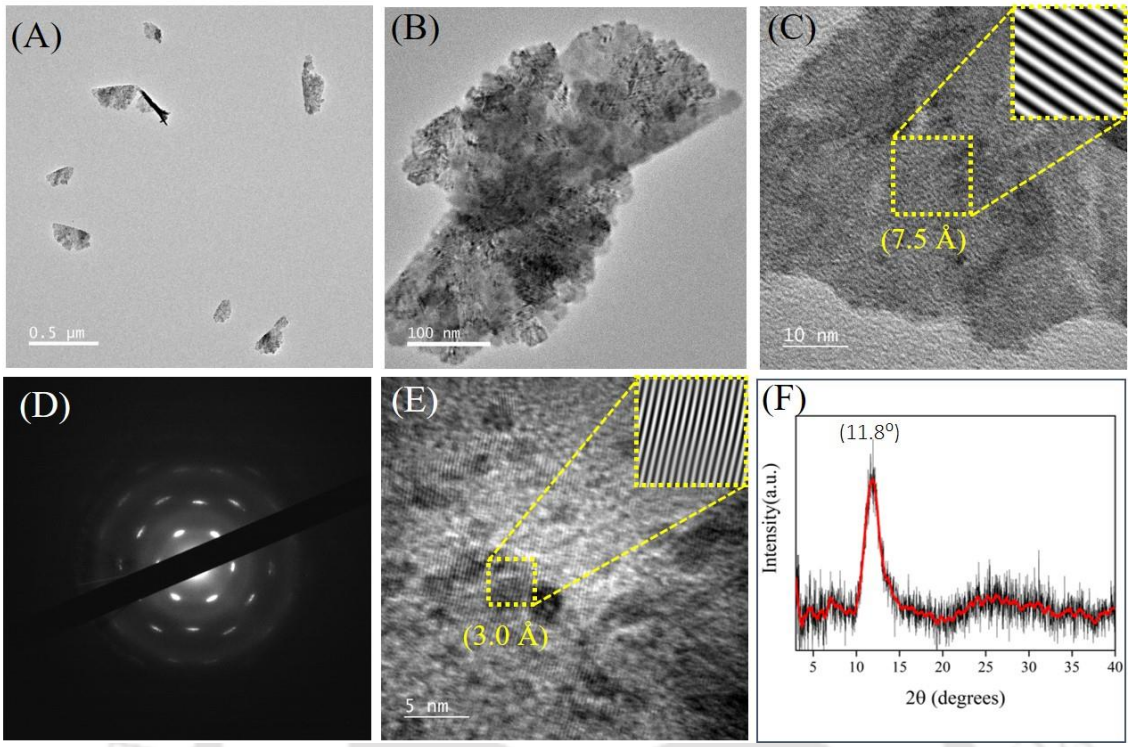

Figure 4.4. (A-B) TEM image of crystalline assembly of 2D nanosheets obtained from the reaction between ligand stabilized Au NCs and gadolinium ions. (C) High-resolution -TEM image of a typical sheet of Gd Au NCs. (D) SAED pattern of the crystalline sheet. (E) HRTEM image of a typical sheet of Gd Au NCs in 5 nm scale. (F) XRD pattern obtained from Gd Au NCs.

Based on the TEM analysis, a probable structure of nanosheets could be predicted by analyzing the diffraction pattern generated by the constituent Au NCs. The formation of nanosheets has been attributed to the chemical interaction between trivalent gadolinium ions and MPA ligands. The periodic presence of brighter spots obtained from the SAED pattern may be attributed to the network of Au_{14} clusters that are aligned at the apex of the formed hexagon in the XY plane. The observed distance was found to be similar to the calculated distance of 4.5 Å. In contrast, an extension of Au_{14} cluster in the z direction was defined by the coordination of gadolinium ions with Try, as well as π–π interaction between the aromatic moieties of ligand (Try). Based on computational calculations, the distance between hexagonally arranged clusters, that is clusters coordinated via gadolinium ions in the z direction was found to be 7.2 Å. (Using Avogadro Figure A.4.7) The calculated distance was in close resemblance with the experimentally obtained distance of 7.5 Å between adjacent planes consisting of NCs. Further, the experimentally obtained distance

of 3.0 Å was smaller in comparison to the distance obtained in the z direction, resulting in a smaller lattice parameter and could be a plausible reason for the close stacking-together of each layer of Au NC to result in 2D structural growth. A schematic illustration of the structure of Gd Au NCs from the spatial organization of Au NC and Gd^{3+} ions based on the above-mentioned observations is presented in Figure 4.5.

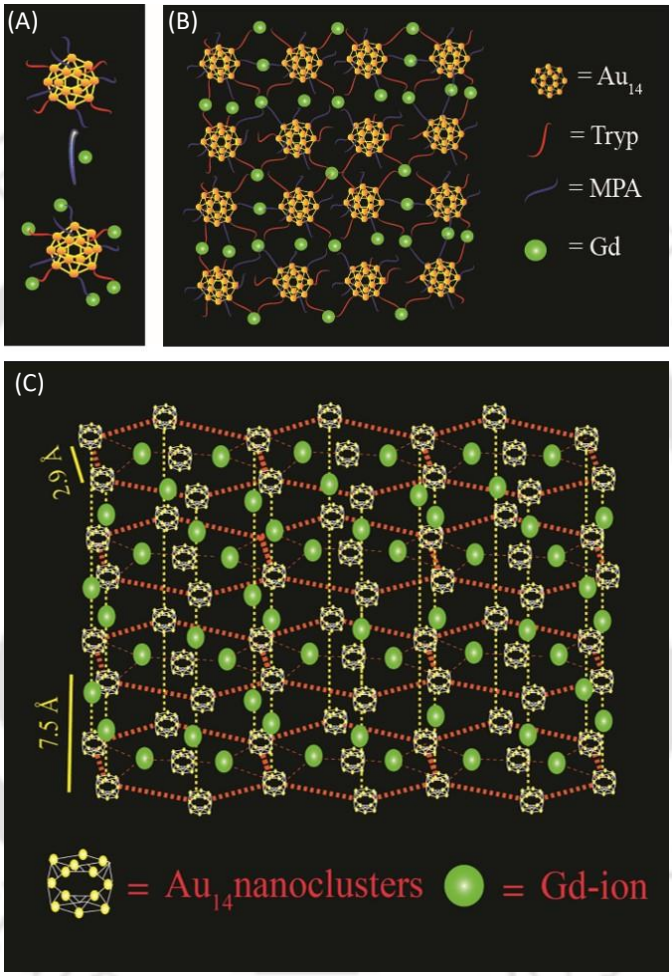

Figure. 4.5. (A) Schematic representation of ligand stabilized Au NCs prior to complexation with Gd ions. (B) Schematic representation of the possible mode of bonding between Au NC and Gd ions, (C) Plausible 2D structure representation of Gd Au NCs.

Apart from the augmented luminescence properties of Au NCs, the effect on the magnetic properties obviously on interacting with Gd ions was studied. The electron paramagnetic resonance (EPR) spectrum for the solid sample of Gd Au NCs was recorded. The experimental EPR spectrum of Gd Au NCs was slightly broad with a value of $g \approx 2.0$.

(Figure 4.6.A) Magnetic measurements were performed and the magnetic hysteresis (M-H) curve exhibits the paramagnetic behavior of Gd Au NC. The magnetization value recorded for the Gd Au NC pellet was M_s = 0.4 emu/g. (Figure 4.6.B) The significant shift in the magnetization values for Gd after complexation with Au NCs signifies a possible change in magnetic properties on assembling. Also, an experimental spectrum depicting the shift in magnetization in comparison to gadolinium salt was acquired. The results demonstrated the magnetic responsiveness evident from M-H curve with the shift in the value of M_s obtained after the assembly of Au clusters by Gd ions. (Figure A.4.8)

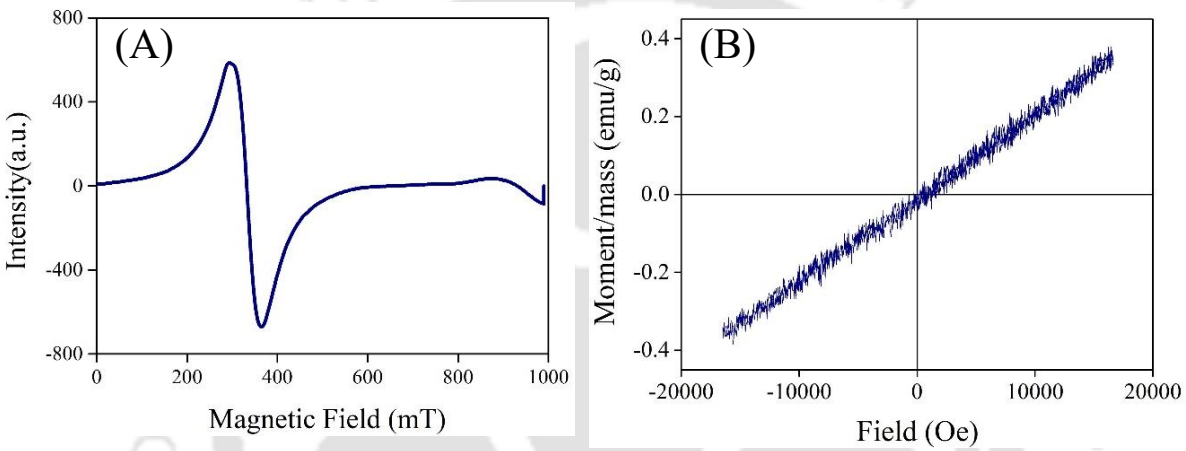

Figure 4.6. (A) EPR spectra of Gd Au NCs. (B) M-H curve of Gd Au NCs.

Complexation reaction between Au NC with Gd metal ion leading to crystalline assemblies generated superstructure with enhanced physical and chemical properties that were superior to only nanoclusters. Further, surface modifications of such crystalline nanoclusters may provide opportunities for various applications. Through surface functionalization of organic ligands on the generated Au nanosheets may generate independent emissions-integrated in a single nanostructure. Through the formation of different complexes chelated to its surface, the composition of the emission channel could be controlled. Possible engineering on the surface of Au nanosheets by forming inorganic complexes may generate different optical characteristics. The addition of ASA to an aqueous dispersion of Gd Au NCs led to the generation of a new blue emission peak at 410 nm when excited at 325 nm.

The luminescence intensity peak at 595 nm of Gd Au NCs changed after ASA complexation with metal ions. The emission peak at 595 nm was partially reduced with the enhancement of peak intensity at 410 nm, with an increase in concentration of 0.05 mM, 0.10 mM, and 0.20 mM ASA gradually. (Figure 4.7.A) Interestingly, the position of an excitation spectrum remained unaltered at an emission maximum of 595 nm, and a distinct excitation peak at 295 nm appeared with the emission maximum of 410 nm. (Figure 4.7.B) It was observed that with only ASA solution, the emission maxima at 410 nm increased upon the addition of Gd^{3+} at an excitation of 295 nm. (Figure A.4.9) The ASA added dispersion of Gd Au NCs were centrifuged and redispersed pellet obtained showed similar luminescence characteristics. Hence this also indicated a similar nature of product formation of a luminescent species on the surface of Gd Au NC nanosheets. The surface labile Gd^{3+} ions assist the coordination with ASA ligand to form $M(ASA)_3$ complex. So, it is plausible that a composition of $M(ASA)_3$ complexes (M=Gd) was attached to Au NC nanocrystals creating an independent emission channel at 410 nm. Moreover, such salicylates are potential of luminescent material for further applications.[21-23] Earlier observations based on the formation of metal and ASA complexes (M=Zn) on the surface of ZnS quantum dot are also reported.

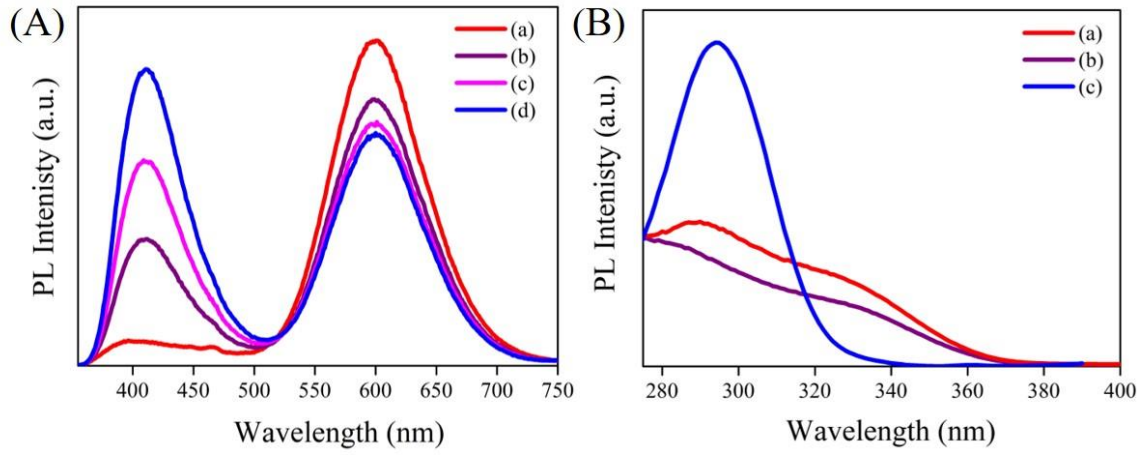

Figure 4.7. (A) Emission (λ_{ex} = 325 nm) spectra of (a) Gd-Au NCs and that following addition of (b) 0.05 mM, (b) 0.10 mM, and (C) 0.20 mM of ASA. (C) Excitation spectra of (a) Gd-Au NCs at λ_{em} = 595 nm, and (b, c) ASA-added Gd-Au NCs at λ_{em} = 595 and 410 nm, respectively.

The as-synthesized Gd Au NCs upon complexation into $M(ASA)_3$ on the nanosheet surface emitted in the blue region at 410 nm, and orange region at 595 nm. Now, for a white light-

emitting source - a green emitting organic fluorophore is desirable. Hence, the dual emitting Gd Au NC-ASA complex was conjugated with green emitting species fluorescein (FL) by coordination with gadolinium ions. Earlier reports of gadolinium-fluorescein complex formation as dual mode probe for fluorescence sensing have been reported. [24] This could provide an ideal choice of independent tri-colour emitting channel from a single nanocomplex entity. The emergence of a new green luminescent maximum at 510 nm, in addition to luminescent maxima of ASA complex at 410 nm, and Au NC nanosheets at 595 nm, was observed at an excitation of 325 nm. (Figure 4.8.A) Notably, the luminescence intensity of only FL was enhanced compared to the intensity prior to addition of Gd salt. Hence, this indicates the green emitting peak (510 nm) is a result of FL ligand coordination with Gd ions. (Figure A.4.10) Additionally, when FL interacted with dual emitting Gd Au NCs complex, there was a change in intensity observed for Au NC and metal ASA complex- suggesting preferential interaction with metal ions. Also, the spectra were obtained following centrifugation and redispersion in water, and the three-emitting channels in the same nano-entity consisted of the Gd Au NCs and metal complexes on the surface of nanosheets. The emission intensity was tuneable at 595 nm by the extent of complexation of the components. Because, with the addition of either of the ligands (ASA and FL), the emission intensity at 595 nm was reduced, and the emission intensities at 410 nm and 510 nm were commensurate with changing concentration. Upon excitation at 325 nm, the nearly perfect white light emission was achieved following a reaction with ASA (of 0.20 mM concentration) and FL (of 0.0015 mM concentration). Also, the presence of three emitting species was confirmed further from excitation spectra recorded at three different emissions. (Figure 4.8.B) The overlapping excitation peaks following centrifugation and redispersion supported the single excitation wavelength origin for tri-emissions at 410 nm, 510 nm, and 595 nm. The excitation peak at 295 nm corresponded to ASA complexation; the additional excitation range also beyond the range of 340 nm corresponded to FL coordination. Also, the UV-Vis spectra of the Gd Au NCs, and after complexation with ASA and FL ligands showed equivalent absorption with non-functionalized Gd Au NCs. (Figure A.4.11) This also indicated signifies similar behaviour with Gd Au NCs nanosheets from the little contribution of the ligands to the absorption characteristics. (Figure A.4.10) Moreover, the increase in photoluminescence quantum yield from 0.7% to 1.3%, measured at 325 nm excitation was observed. Importantly, the preservation of the 0.75 nm lattice spacing from XRD analysis supported no change in morphologies of the surface functionalized Gd Au

NCs nanosheets. (Figure A.4.12) EPR spectral data, also signified the functionalizing of the ligands on the surface of nanosheets with unaltered properties of gadolinium in the complex. (Figure A.4.13)

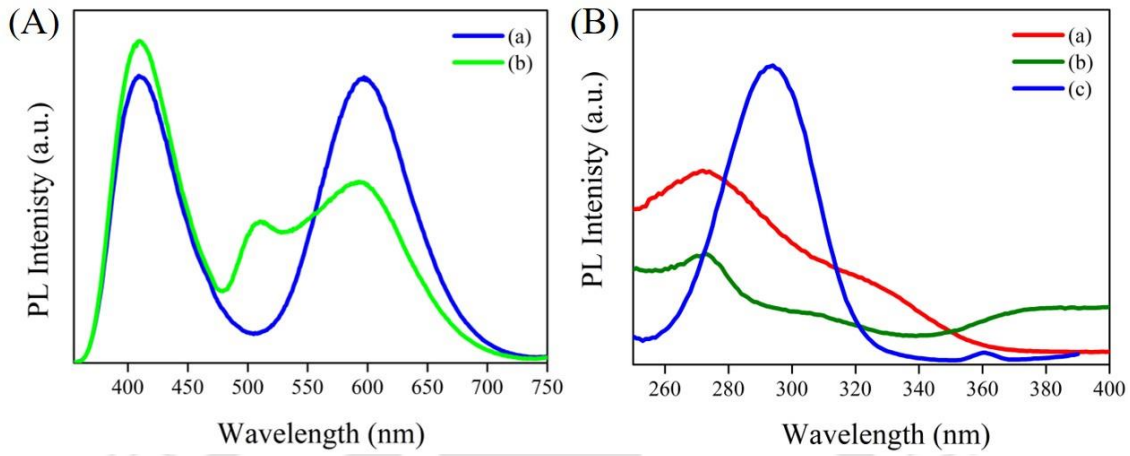

Figure 4.8. (A) Emission spectrum of (a) ASA (0.20 mM) added Gd-Au NCs at 325 nm excitation and (b) the emission spectrum following the addition of FL (0.0015 mM) to ASA-Gd Au NCs. (B) Excitation spectra of Gd-Au NC-ASA-FL complex at emission wavelengths of (a) 595 nm, (b) 510 nm, and (c) 410 nm, respectively.

The Fourier transform infrared spectroscopic data revealed the characteristic frequencies of ligands (ASA and FL) present in the Gd Au NCs complex, which were absent in the Gd Au NCs nanosheets. (Figure A.4.14, Table A.4.2) The FT-IR spectra were compared to the un-interacted ligands (ASA and FL), showing a number of additional bands in the range of 1750-500 cm^{-1}, in order to detect the change caused by ligands. The stretching frequency at 1631 cm^{-1} due to carboxylate group of ASA was shifted to 1709 cm^{-1}. Also, the appearance of a new peak at 1300 cm^{-1} is attributed to the carboxylic group of ASA due to the chelation through two oxygen. The emergence of a new peak at 1592 cm^{-1} in the complex also suggested the coordination of oxygen atoms (of the carboxylate group) with Gd^{3+} ions. Similar results were obtained for the rare earth metal complex of salicylates.[25] Additionally, the disappearance of the peak at 1635 cm^{-1}, which is characteristic of carboxylate group of Fl, revealed the coordination through oxygen. The spectra of Gd Au NC complex as expected due to low FL concentration also showed weak bands caused by FL. The results shown above supported the formation of new products via

complexation of independent dual emissive ligands on the surface of Gd Au NCs nanosheets.

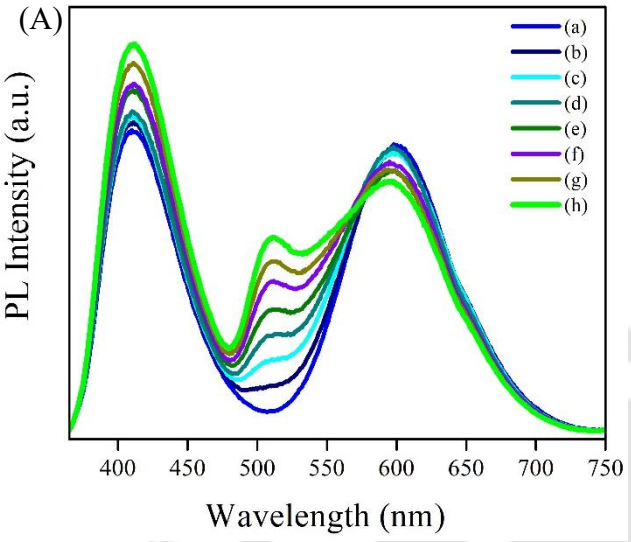

(B)

Sample at λ_{exc} 325 nm	CIE coordinates	
	X	Y
Gd Au NC	0.46	0.43
ASA-Gd Au NC	0.41	0.30
FL-ASA-Gd Au NCs	0.34	0.33

Figure 4.9 (A) Emission spectra (at λ_{exc} 325 nm) of (a) ASA Gd Au NCs and that upon treatment with (b) 1 µL (c) 5 µL, (d) 10 µL, (e) 15 µL, (f) 20 µL, (g) 25 µL, and (h) 30 µL of fluorescein ligand (0.05 mM). (B) Tabulated form comparing the CIE coordinates of Gd, Au NCs, and ligated Gd Au NCs.

Importantly, at a fixed concentration the dual emissive Gd Au NC complex was treated with 0.05 mM fluorescein ligand. The emission intensity at 510 nm of FL added solution increased and the other emission intensities at 595 nm and 410 nm changed accordingly. This led to changes in WLE parameters correspondingly like- CIE coordinates and CRI values. (Figure 4.9.A) Thus, tunability in photophysical properties was observed with the surface complexation of additional FL ligands. For example, dual emissive ASA Gd Au NCs exhibited chromaticity of (0.41,0.30) and CRI of 63. With increase in concentration, the FL treated Gd Au NCs complex displayed white light emission with CIE coordinates of (0.34, 0.33) and CRI 87, when excited at 325 nm. (Figure 4.9.B) Also, for a fixed concentration of FL, the tunability in luminescence, CIE values, and CRI were observed following the change in excitation wavelength. (Figure 4.10) This indicated the excitation-dependent tuneable photophysical parameters of complexed Gd Au NCs. However, only Gd Au NCs and ASA added Gd Au NCs did not lead to products with such parameters, indicating the importance of both the ligands in Gd Au NC complex. (Figure 4.9.B)

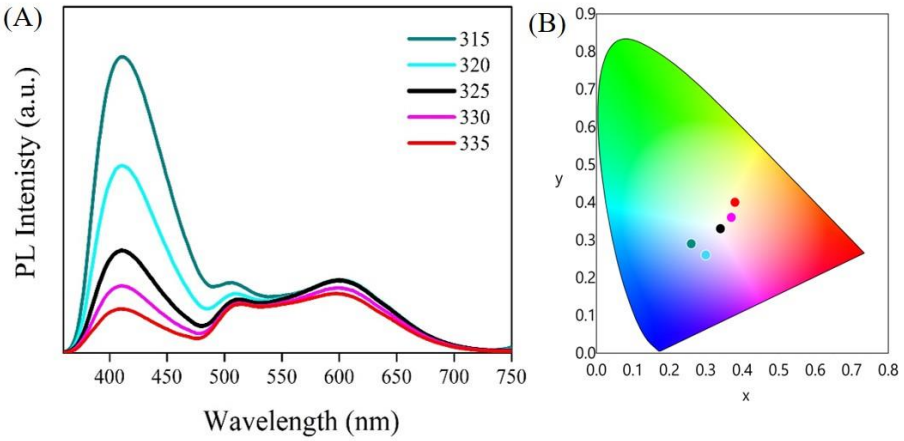

(C)

Sample at λ_{exc}	CIE coordinates		
	X	Y	CRI
315	0.26	0.29	n/a
320	0.30	0.26	81
325	0.34	0.33	87
330	0.37	0.36	87
335	0.38	0.40	84

Figure 4.10. (A) Variation in emission intensity. (B) Chromaticity coordinates of Gd Au NC complex at different excitation wavelengths as indicated in the legends. (C) Tabulated form of chromaticity coordinates of Gd Au NC complex at different excitation wavelengths.

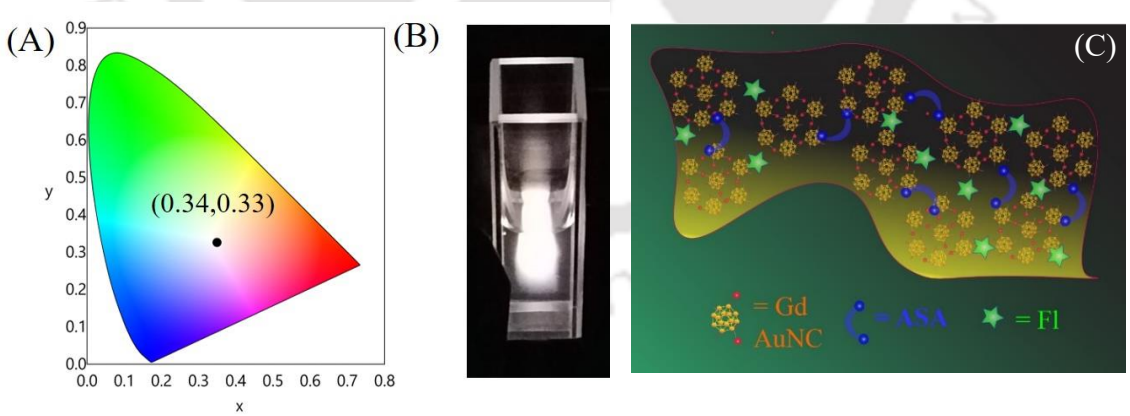

Figure 4.11. (A) CIE chromaticity diagram of Gd Au NCs complex at 325 nm excitation. (B) Digital photograph of Gd-Au NC Complex at λ_{exc} 325 nm. (C) Schematic representation of Gd Au NCs nanosheet complexation with ASA and FL is represented.

The white light emission (0.34, 0.33) for Gd Au NCs complex at 325 nm excitation was observed visually and photographed. A schematic representation of ASA and FL complexation on the surface of Gd Au NC nanosheets is represented. (Figure 4.11) Also, the complex was photostable under constant illumination of 325 nm excitation with respect to the emission at 410 nm, 510 nm, and 595 nm. (Figure A.4.15)

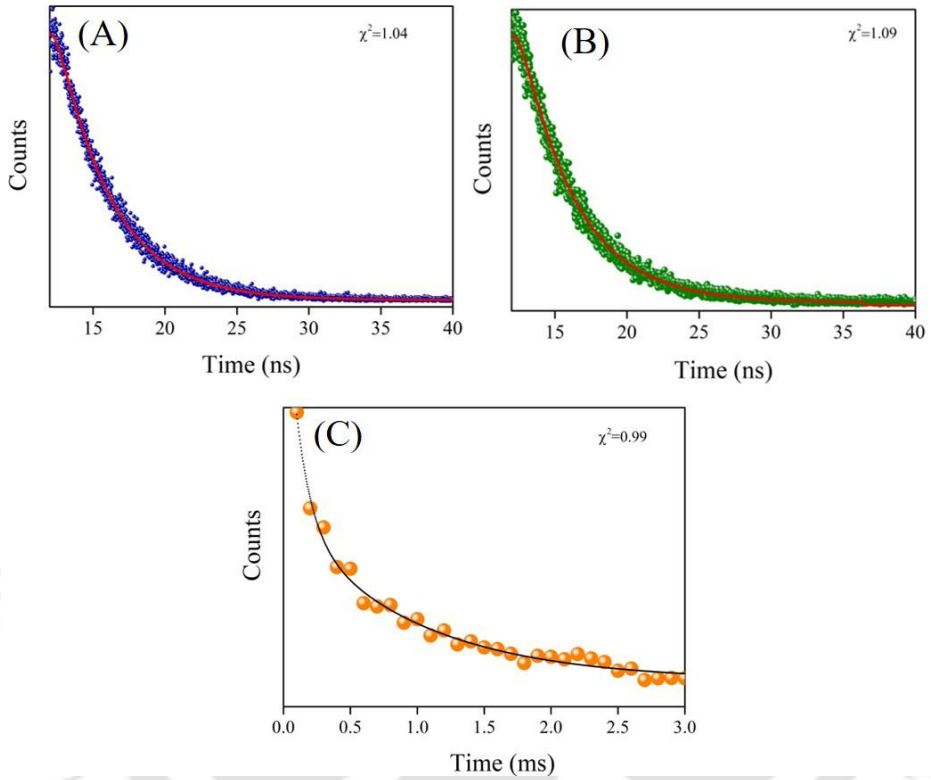

Figure 4.11. (A) TRPL decay profile at (A) 410 nm, (B) 510 nm, of Gd Au NCs WLE complex (C) TRPL decay profile at 595 nm emission of Gd Au NC complex.

Table 4.1 Tabulated form of TRPL lifetime of Gd Au NCs complex at three different emission wavelengths.

Emission (nm)	A_1(%)	τ_1 (ms)	A_2(%)	τ_2 (ms)	Avg. lifetime (ms)	χ^2
595	0.455	0.116ms	0.544	0.947 ms	0.870 ms	0.99
510	2.9	0.13 ns	97.1	3.82 ns	3.82 ns	1.09
410	3.37	0.40 ns	96.63	3.77 ns	3.76 ns	1.04

Further, Gd Au NCs complex after bi-exponential fit showed average lifetimes of 3.82 ns at emission 510 nm, and 3.76 ns at emission maximum 410 nm. On the contrary, only fluorescein dye and ASA ligand gave single exponential fitting curves. This indicates the presence of both ligands on the surface of the nanosheets. Also, a long lifetime of 0.870 ms was observed at an emission maximum of 595 nm for Gd Au NCs. Overall, the surface modification of Au NC nanosheets via metal complexation with organic ligands led to better white light emission.

4.5 Conclusion

In summary, the complexation with two ligands (acetylsalicylic acid and fluorescein) on gadolinium-based 2D crystalline assembly of gold clusters (Gd-Au NCs) was demonstrated. The crystalline 2D nanosheets of Au NCs were characterized by XRD, FESEM, and systematic TEM, SAED, and HRTEM analyses. PL measurements and VSM analyses evaluated the optical and magnetic properties of the synthesized 2D nanosheets. The independent emitting channel exhibited tri-colour emission based-white light, from the Au NC assembly and the chelation with dual ligands ASA and FL. The 2D crystalline superstructure exhibited an augmented lifetime and photoluminescent quantum yield. The synchronous tri-colour emitting white light at λ_{exc} ~325 nm could be achieved from a single nanocomponent with colour chromaticity coordinate of (0.34, 0.33) and CRI >85 in the liquid phase. The present work could bring new chemistry and strategies for the functionalization of higher-order nanostructures with a scope in light-emitting materials.

4.6 Bibliography

1. Wei, X.; Kang, X.; Yuan, Q.; Qin, C.; Jin, S.; Wang, S.; Zhu, M., Capture of Cesium Ions with Nanoclusters: Effects on Inter- and Intramolecular Assembly. *Chem. Mater.* **2019,** *31* (13), 4945-4952.
2. Nonappa; Ikkala, O., Hydrogen Bonding Directed Colloidal Self-Assembly of Nanoparticles into 2D Crystals, Capsids, and Supracolloidal Assemblies. *Adv. Funct. Mater.* **2018,** *28* (27), 1704328.
3. Wu, Z.; Dong, C.; Li, Y.; Hao, H.; Zhang, H.; Lu, Z.; Yang, B., Self-Assembly of Au15 into Single-Cluster-Thick Sheets at the Interface of Two Miscible High-Boiling Solvents. *Angew. Chem. Int. Ed.* **2013,** *52* (38), 9952-9955.
4. Higaki, T.; Liu, C.; Zhou, M.; Luo, T.-Y.; Rosi, N. L.; Jin, R., Tailoring the Structure of 58-Electron Gold Nanoclusters: $Au_{103}S_2(S\text{-}Nap)_{41}$ and Its Implications. *J. Am. Chem. Soc.* **2017,** *139* (29), 9994-10001.
5. Basu, S.; Paul, A.; Chattopadhyay, A. Zinc Mediated Crystalline Assembly of Gold Nanoclusters for Expedient Hydrogen Storage and Sensing. *J. Mater. Chem. A.* **2016**, 4, 1218– 1223.
6. Basu, S.; Bhandari, S.; Pan, U. N.; Paul, A.; Chattopadhyay, A. Crystalline nanoscale assembly of gold clusters for reversible storage and sensing of CO_2 via modulation of photoluminescence intermittency. *J. Mater. Chem. C* **2018**, 6, 8205– 8211.
7. Paul, M.; Basu, S.; Chattopadhyay, A., Complexation Reaction-Based Two-Dimensional Luminescent Crystalline Assembly of Atomic Clusters for Recyclable Storage of Oxygen. *Langmuir* **2020,** *36* (3), 754-759.
8. Basu, S.; Paul, A.; Chattopadhyay, A. Zinc-Coordinated Hierarchical Organization of Ligand-Stabilized Gold Nanoclusters for Chiral Recognition and Separation. *Chem. Eur. J.* **2017**, 23, 9137– 9143.
9. Basu, S.; Chattopadhyay, A. Room-Temperature Delayed Fluorescence of Gold Nanoclusters in Zinc-Mediated Two-Dimensional Crystalline Assembly. *Langmuir* **2019**, 35, 5264-5270.
10. Das, P.; Chattopadhyay, A., Delayed Dual Emission of Two-Dimensional Copper Nanocluster Assembly. *J. Phys. Chem. C* **2022,** *126* (2), 997-1005.

11. Hossain, M. K.; Ahmed, M. H.; Khan, M. I.; Miah, M. S.; Hossain, S., Recent Progress of Rare Earth Oxides for Sensor, Detector, and Electronic Device Applications: A Review. *ACS Appl. Electron. Mater.* **2021,** *3* (10), 4255-4283.

12. Zheng, B.; Fan, J.; Chen, B.; Qin, X.; Wang, J.; Wang, F.; Deng, R.; Liu, X., Rare-Earth Doping in Nanostructured Inorganic Materials. *Chem. Rev.* **2022,** *122* (6), 5519-5603.

13. Bouzigues, C.; Gacoin, T.; Alexandrou, A., Biological Applications of Rare-Earth Based Nanoparticles. *ACS Nano* **2011,** *5* (11), 8488-8505.

14. Tang, T.; Ma, X.; Bian, Y.; Yuan, Z.; Zou, D.; Chen, N., Composite of Gadolinium-Labeled Dendrimer Nanocluster and Graphene Oxide Nanosheet for Highly Efficient Liver T1-Weighted Imaging Probe. *ACS Biomater. Sci. Eng.* **2019,** *5* (4), 1978-1986.

15. Yuan, C.; Li, Y.; Xu, Z.; Wang, C.; Zhang, J.; Jin, Y.; Chen, Z.; Sun, H.; Wu, F.; Zhang, Q.; Tang, Y.; Wang, S., Imaging-Guided Synergistic Photo-Chemotherapy Using Doxorubicin-Loaded Gadolinium Porphyrin-Based Metal–Organic Framework Nanosheets. *ACS Appl. Nano Mater.* **2022,** *5* (10), 15318-15327.

16. ul Haq, T.; Mansour, S. A.; Munir, A.; Haik, Y., Gold-Supported Gadolinium Doped CoB Amorphous Sheet: A New Benchmark Electrocatalyst for Water Oxidation with High Turnover Frequency. *Adv. Funct. Mater.* **2020,** *30* (16), 1910309.

17. Erdem, M.; Örücü, H.; Cantürk, S. B.; Eryürek, G., Upconversion $Yb^{3+/}Er^{3+:}$ Gadolinium Gallium Garnet Nanocrystals for White-Light Emission and Optical Thermometry. *ACS Appl. Nano Mater* **2021,** *4* (7), 7162-7171.

18. Maiti, D. K.; Roy, S.; Baral, A.; Banerjee, A., A fluorescent gold-cluster containing a new three-component system for white light emission through a cascade of energy transfer. *J. Mater. Chem. C* **2014,** *2* (32), 6574-6581.

19. Bhandari, S.; Pramanik, S.; Khandelia, R.; Chattopadhyay, A., Gold Nanocluster and Quantum Dot Complex in Protein for Biofriendly White-Light-Emitting Material. *ACS Appl. Mater. Interfaces* **2016,** *8* (3), 1600-1605.

20. Bhandari, S.; Roy, S.; Pramanik, S.; Chattopadhyay, A., Double Channel Emission from a Redox Active Single Component Quantum Dot Complex. *Langmuir* **2015,** *31* (1), 551-561.

21. Yang, X. W.; Sun, W.-J.; Ke, C.-Y.; Zhang, H. G.; Wang, X.-Y.; Gao, S. L., Thermochemical properties of rare earth complexes with salicylic acid. *Thermochim. Acta* **2007,** *463* (1), 60-64.

22. Sun, W.; Yang, X.; Zhang, H.; Wang, X.; Gao, S., Thermochemical Properties of the Complexes $RE(HSal)_3 \cdot 2H_2O$ (RE = La, Ce, Pr, Nd, Sm). *J. Rare Earths.* **2006,** *24* (4), 423-428.

23. Yang, Y.-t.; Zhang, S.-y., Study of lanthanide complexes with salicylic acid by photoacoustic and fluorescence spectroscopy. *Spectrochim. Acta A Mol. Biomol*. Spectrosc. **2004,** *60* (8), 2065-2069.

24. Dong, D.; Jing, X.; Zhang, X.; Hu, X.; Wu, Y.; Duan, C., Gadolinium (III)–fluorescein complex as a dual modal probe for MRI and fluorescence zinc sensing. *Tetrahedron* **2012,** *68* (1), 306-310.

25. Xuwu, Y.; Wujuan, S.; Congyu, K.; Li, Z.; Hangguo, Z.; Shengli, G., Synthesis and characterization of the rare-earth complexes with salicylic acid. *Chem. Pap.* **2006,** *60* (2), 132-137.

Appendix: A.4

Chapter 4

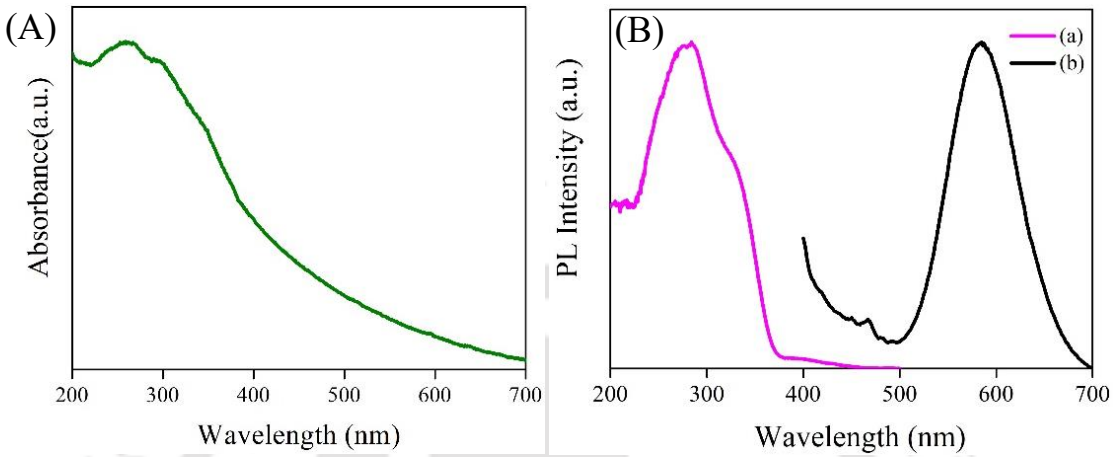

Figure A.4.1. UV-vis spectrum of Au NCs marking absence of any significant peak beyond the range 500 nm. (A) Photoluminescence (a) excitation and (b) emission spectra of MPA and D-tryptophan Au NCs.

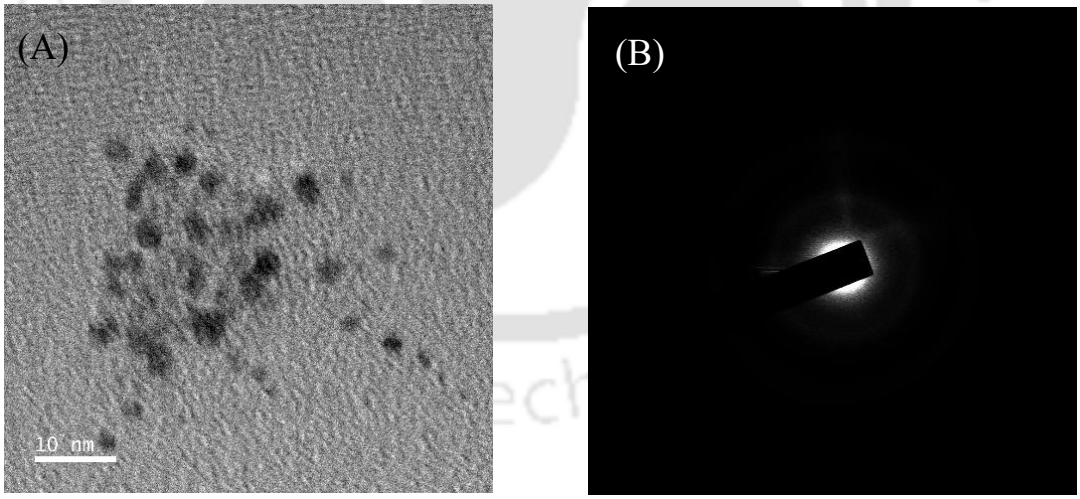

Figure A.4.2 (A) TEM image of Au NCs. (B) SAED image obtained on Au NCs.

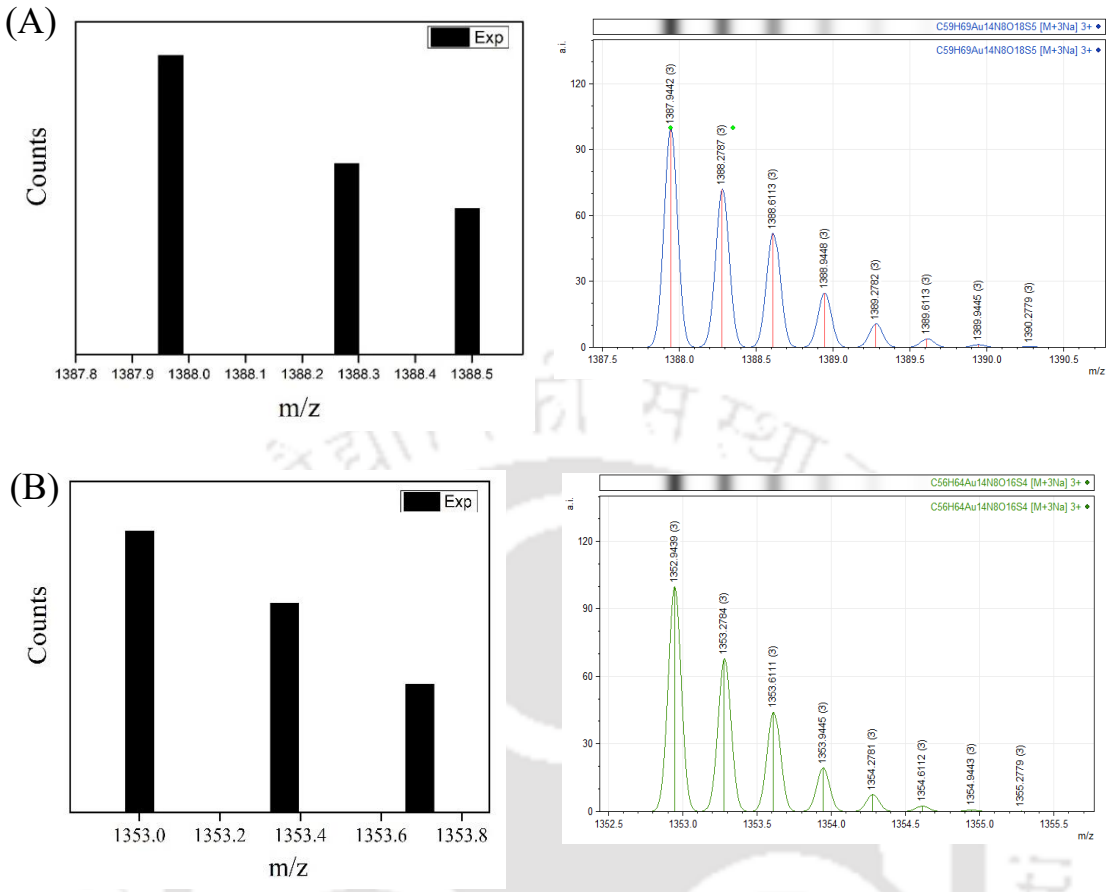

Figure A.4.3. Experimental and simulated histogram depicting the isotopic distribution of gold nanocluster species with formulas (A) $[Au_{14}(MPA)_5(Try)_4 + 3Na]^{3+}$ and (B) $[Au_{14}(MPA)_4(Try)_4 + 3Na]^{3+}$.

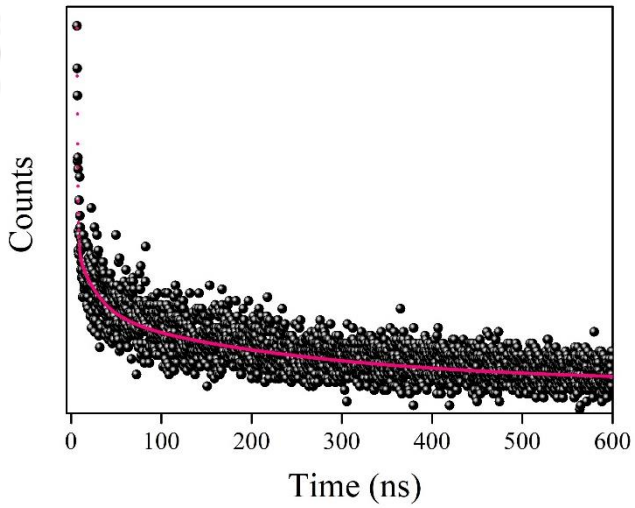

Figure A.4.4. TRPL decay profile of MPA and D-tryptophan stabilized Au NCs.

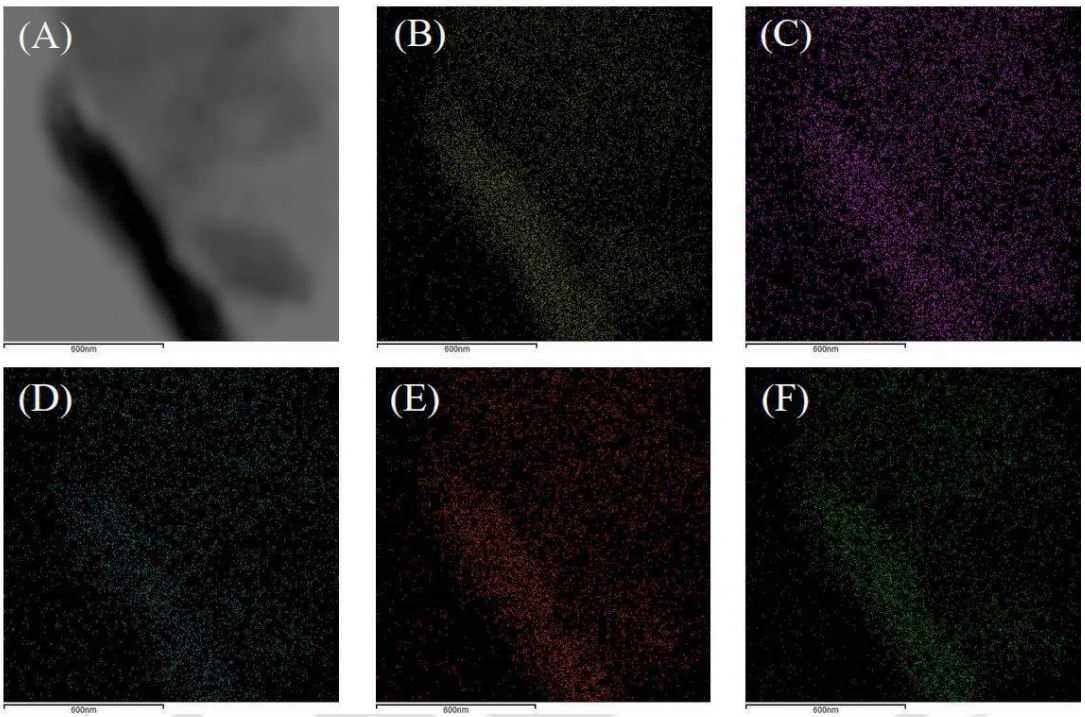

Figure A.4.5. (A) STEM image of Gd Au NC nanosheet and elemental mapping of (B) Au, (C) Gd, (D) O and (E) N (F) S in Gd Au NCs, corroborating the associated abovementioned elements in Gd Au NCs.

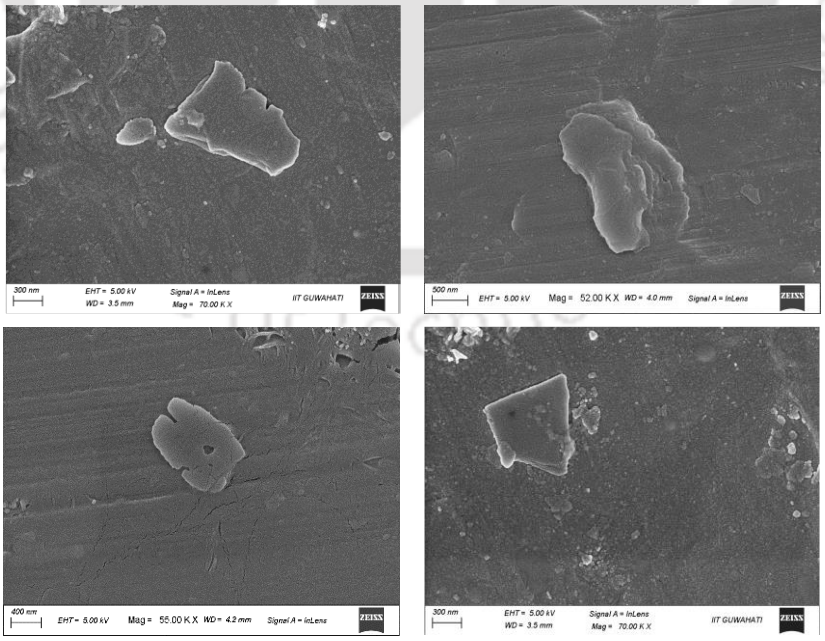

Figure A.4.6. FESEM image of Gd Au NC nanosheets.

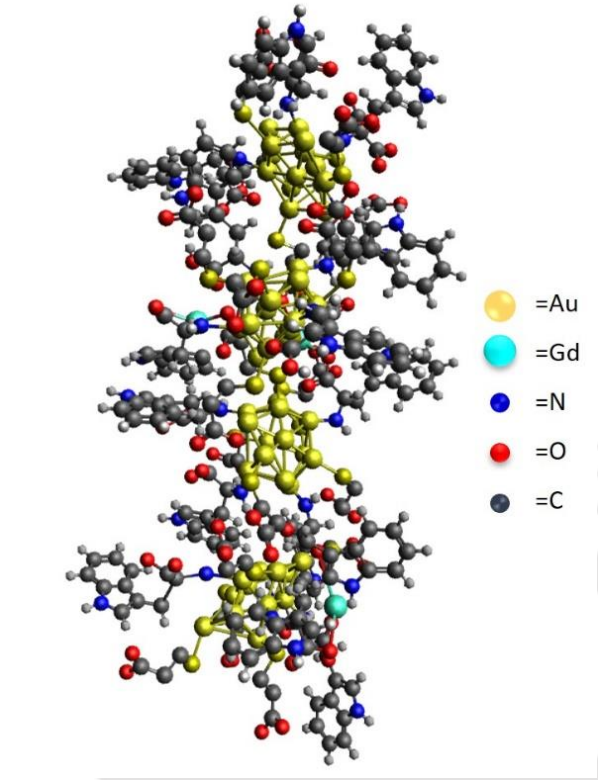

Figure A.4.7. Simulated structure of Gd Au NCs. The structure was generated using Avogadro 1.2.0 software.

Table A.4.1. Time-resolved delayed photoluminescence (TRPL) decay parameters of Gd-Au NCs.

Excitation (nm)	Emission (nm)	Sample	A_1	τ_1 (ms)	A_2	τ_2 (ms)	Avg. lifetime (ms)	χ^2
325 nm	595	Gd-Au NCs	0.416%	0.172	0.584%	0.998	0.91	0.99

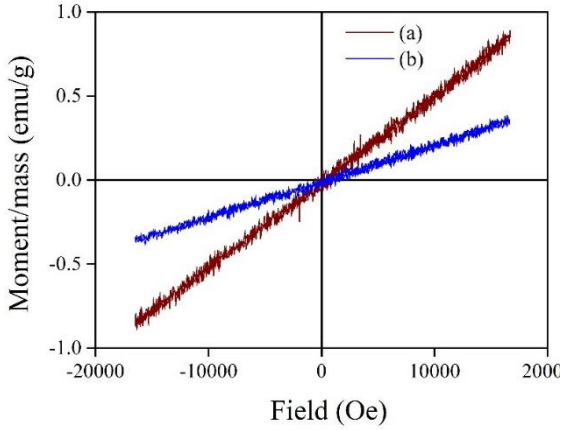

Figure A.4.8. MH curves for (a) Gd salt and (b) Gd Au NC complex.

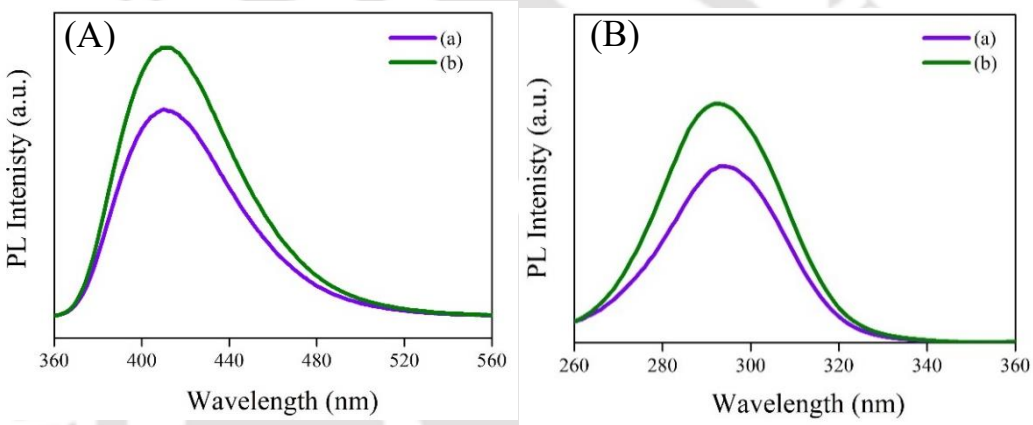

Figure A.4.9. (A) Emission spectra of (a)ASA, and (b) addition of Gd^{3+} salt at 295 excitations. (B) Excitation spectra of (a) ASA, and (b) addition of Gd^{3+} salt at 410 emissions.

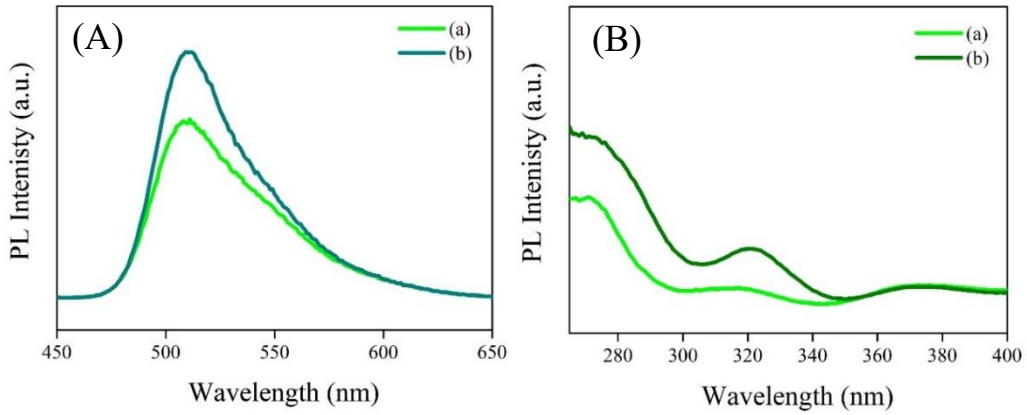

Figure A.4.10. (A) Emission spectra of (a) FL and (b) addition of Gd^{3+} salt. B) Excitation spectra of (a) FL and (b) addition of Gd^{3+} salt at 510 emissions.

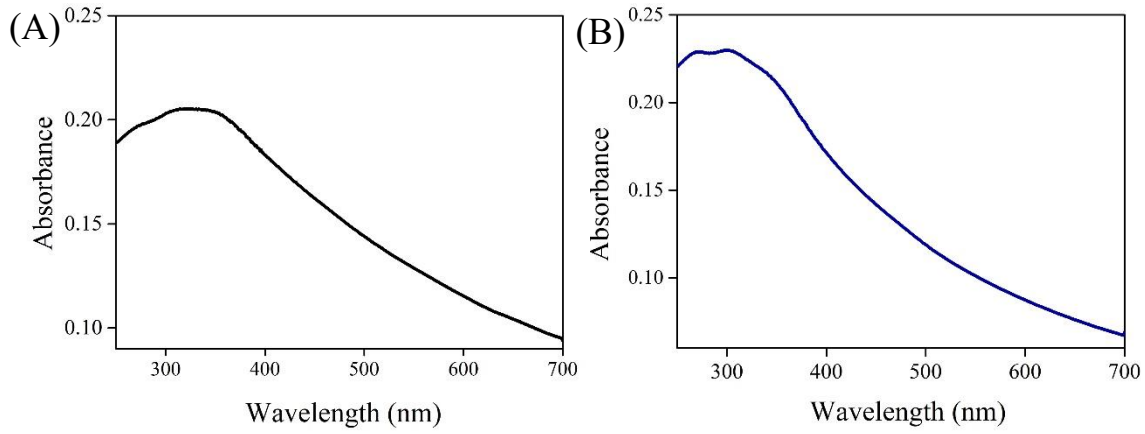

Figure A.4.11. UV-vis spectra of (A) Gd Au NC and (B) Gd Au NC complex.

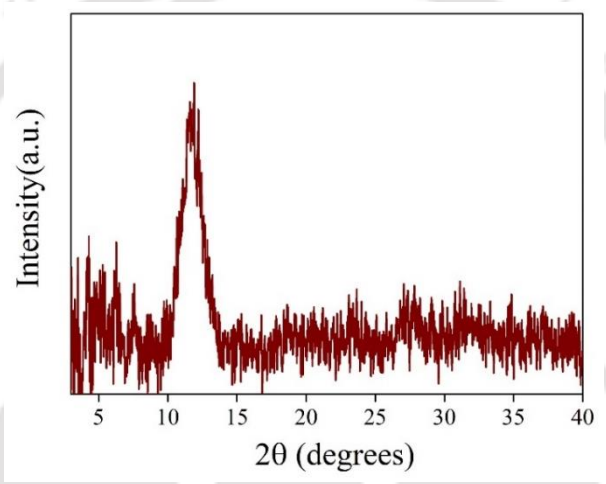

Figure A.4.12. XRD pattern of Gd Au NC complex with ASA and FL.

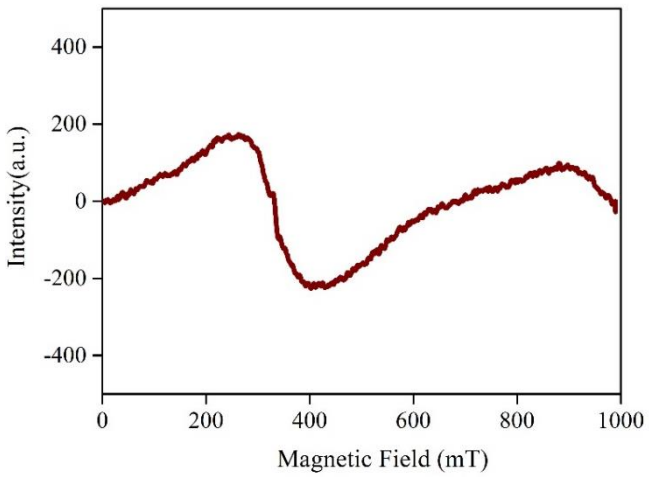

Figure A.4.13. EPR of Gd Au NC complex.

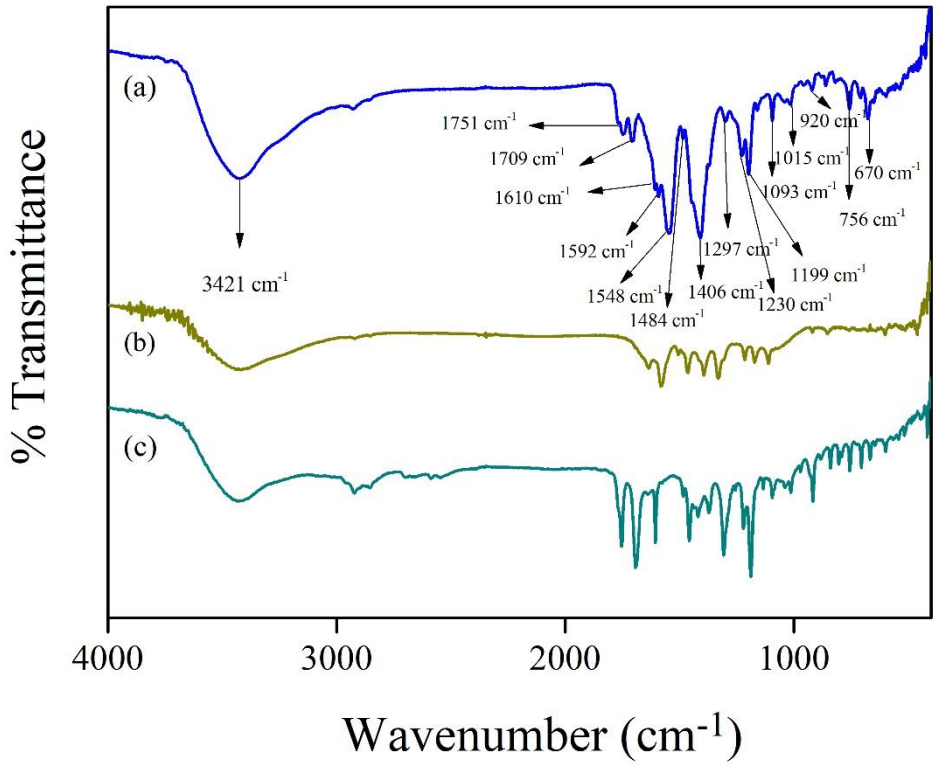

Figure A.4.14. FT-IR spectra of (a) Gd Au NC complex, (b) only FL ligand, and (c) only ASA ligand.

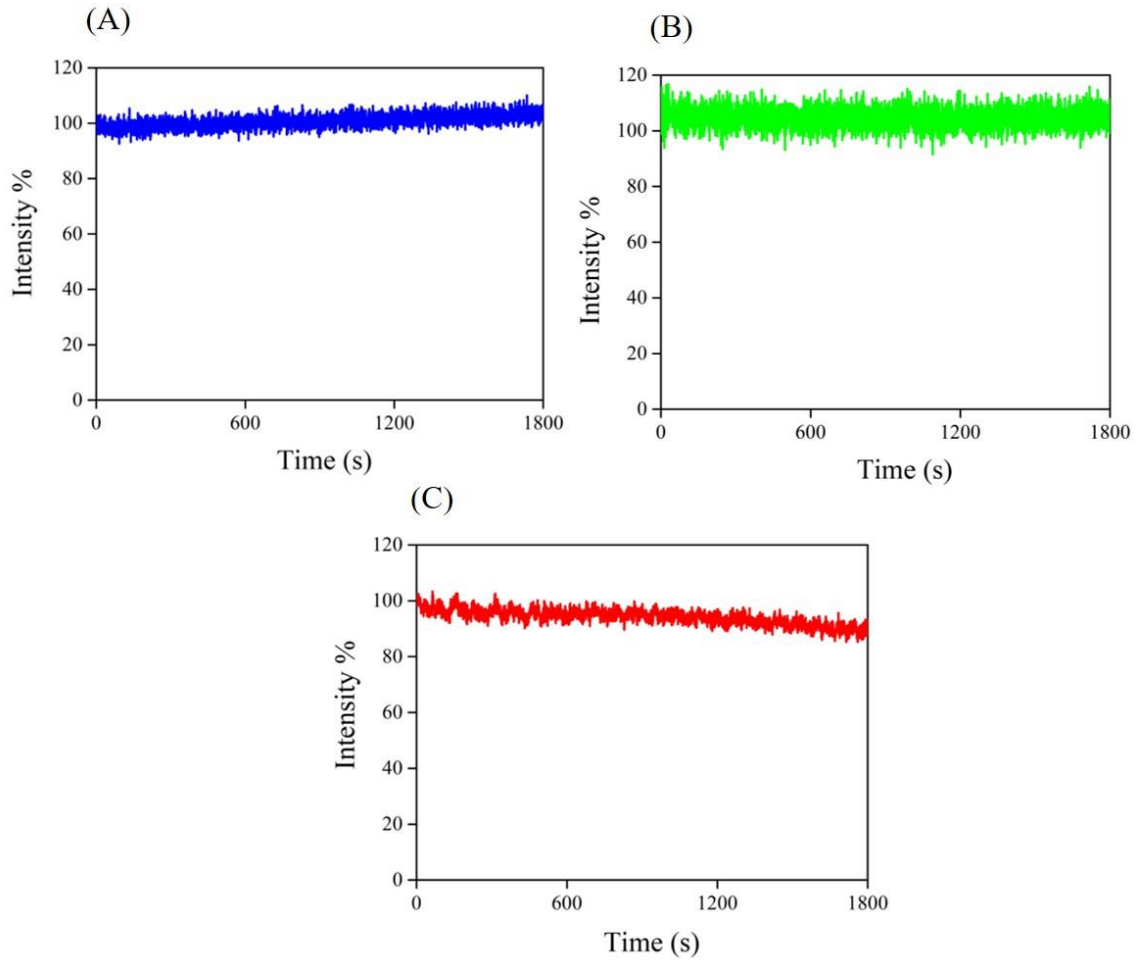

Figure A.4.15. Photostability study under constant irradiation of 325 nm excitation for 1800 sec of tri-emissive Gd Au NCs with respect to emission channel at (A) 410 nm, (B) 510 nm, and (C) 595 nm.

Table A.4.2. Tabulated peaks of vibrational frequencies obtained from FT-IR spectra of Gd Au NC complex.

Vibrational frequency (cm^{-1})	Band assignment	Vibrational frequency (cm^{-1})	Band assignment
1751	C=O (ester group)	1230	C-H deformation (in plane)
1709	C=O (carboxylate group)	1093	C-H deformation (in plane)
1610	C=O stretching, C-C stretching (ring)	1015	C-H deformation (in plane)
1592	COO asymmetric stretching	920	C-H deformation (out of plane deformation)
1457	C-C stretching (phenyl group)	860	C-H deformation (out of plane deformation)
1406	COO symmetric stretching	756	C-H deformation (out of plane deformation)
1300	C-O stretching	670	C-H bending vibration
1297	C-H asymmetric stretching		

Chapter 5

Summary and Future Prospects

5.1 Summary

The present dissertation work focuses on developing metal ion-mediated crystalline assembly of gold NCs through chemical reactions allowing the development of functional nanomaterials with tailored properties. Through the assembly formation of such gold NCs, it was possible to demonstrate superior and new properties in higher dimensional assembled nanostructures. In the first work, the formation of two-dimensional (2D) nanostructures from zinc-assisted assembly of gold NCs has been achieved. The experimental demonstration of photoluminescent 2D layered nanosheets of zinc Au NCs was efficient to store molecular oxygen with a capacity of 0.266 ± 0.004 mM/g of Zn Au NCs, which could be used reversibly at an ambient condition of 20 ºC and pressure limit ranging from 0 to 20 bar. Also, the thesis work explored the potential of crystalline nanostructures for constructing multifunctional optical nanostructures through the integration of atomic clusters and lanthanide (europium and gadolinium) ions. For example, another work demonstrated the delayed fluorescence enhancement of europium ion with a prolonged lifetime through the interaction of ligand-stabilized Au NCs. The photoluminescent (PL) properties - that included delayed Eu emission - from each component could be modulated through the functionalization of phosphate ions (Pi) leading to crystallization. By combining atomic luminous probes and molecular NCs, this concept provides the opportunity to create an optical system that might be used in a variety of applications. Further, a single nanocomponent tri-colour white light emission could be possible from a 2D crystalline assembly of gadolinium-gold NCs through surface complexation with augmented properties. The optical and magnetization properties of the nanosheet with experimental observations have been investigated by photoluminescence measurements and VSM analysis. This thesis presents a thorough investigation of the tuneable properties

of gold nanoclusters (NCs) and explains the complex process of NC assembly assisted by metal ions. Through investigation, the study provides valuable insights into the controlled manipulation of gold NCs, showcasing their potential for diverse applications in nanotechnology and materials science.

5.2 Future prospects

The present thesis guides the assembly of NCs assisted by a few of the important transition metal ions like zinc, europium, and gadolinium. Given the advantages of assembled gold clusters, a substantial effort could be accelerated towards enhancement in energy harvesting and storage by using species like europium with extended coordination that is useful for complexation. Thus, with enhanced long emissions and tunable luminescent properties, lanthanide-based assembled superstructures of NCs can also be utilized in luminescence imaging. The concurrent luminescence arising from the atomic clusters and the incorporated metal ion species represents a groundbreaking aspect of these assemblies. This simultaneous luminescence introduces a dual functionality, expanding the scope of potential applications. The correlated individual luminescence of atomic clusters and metal ion species enable the nanomaterials to serve in dual functionalities and bring new aspects to multifunctional applications ranging from sensors to optoelectronics. Such assemblies with multifunctional properties could be utilized to further detect important biomolecules by independently studying the multichannel emissions. The specific functionalities of the modified assembled superstructure can be created for multiplexed sensing platforms for the detection of multiple analytes, valuable in food safety and medical diagnostics. By guiding the assembly of nanoclusters with selected transition metal ions, the research not only unlocks new possibilities in energy-related technologies but also opens avenues in luminescence imaging, multifunctional applications, and advanced sensing platforms. The multifaceted nature of these assembled structures, combined with their tunable properties, positions them as versatile tools with the potential to revolutionize diverse scientific and technological domains. This thesis lays the groundwork for future research endeavors, offering a blueprint for harnessing the full potential of nanocluster assemblies in addressing complex challenges across various disciplines.

Publications

1. **Paul, M**.; Basu, S.; Chattopadhyay, A. Complexation Reaction-Based Two-Dimensional Luminescent Crystalline Assembly of Atomic Clusters for Recyclable Storage of Oxygen. *Langmuir* 2020, *36* (3), 754-759.
2. **Paul, M**.; Chattopadhyay, A. Modulating Photoluminescence of Europium Through Crystalline Assembly Formation with Gold Nanoclusters and then Phosphate Ions. *J. Phys. Chem. Lett.* 2023, 14, 50, 11250–11257
3. **Paul, M**.; Chattopadhyay, A. Gadolinium Mediated Crystalline Assembly of Gold Nanoclusters for White Light Emission. (*Manuscript under preparation*)
4. Pal, S.; Dutta, A.; **Paul, M**.; Chattopadhyay, A., Plasmon-Enhanced Chemical Reaction at the Hot Spots of End-to-End Assembled Gold Nanorods. *The Journal of Physical Chemistry C* 2020, *124* (5).

Conferences

1. Presented a Poster at International Conference on Advanced Nanomaterials and Nanotechnology, ICANN-**2021**, organized by Centre of Nanotechnology, IIT Guwahati, India.
2. Received Second Place in Poster Presentation: Scientifique under Department of Chemistry, IIT Guwahati in Research and Industrial Conclave, RIC-Integration' **2022**, held at IIT Guwahati, India.
3. Presented a Poster in Research and Industrial Conclave, under Department of Chemistry, IIT Guwahati in RIC-Integration' **2023**, held at IIT Guwahati, India.

Permissions

Visible to Infrared Luminescence from a 28-Atom Gold Cluster

Author: Stephan Link, Andrew Beeby, Simon FitzGerald, et al
Publication: The Journal of Physical Chemistry B
Publisher: American Chemical Society
Date: Apr 1, 2002

PERMISSION/LICENSE IS GRANTED FOR YOUR ORDER AT NO CHARGE

This type of permission/license, instead of the standard Terms and Conditions, is sent to you because no fee is being charged for your order. Please note the following:

- Permission is granted for your request in both print and electronic formats, and translations.
- If figures and/or tables were requested, they may be adapted or used in part.
- Please print this page for your records and send a copy of it to your publisher/graduate school.
- Appropriate credit for the requested material should be given as follows: "Reprinted (adapted) with permission from {COMPLETE REFERENCE CITATION}. Copyright {YEAR} American Chemical Society." Insert appropriate information in place of the capitalized words.
- One-time permission is granted only for the use specified in your RightsLink request. No additional uses are granted (such as derivative works or other editions). For any uses, please submit a new request.

If credit is given to another source for the material you requested from RightsLink, permission must be obtained from that source.

BACK CLOSE WINDOW

SPRINGER NATURE

Thermodynamic stability of ligand-protected metal nanoclusters

Author: Michael G. Taylor et al

Publication: Nature Communications

Publisher: Springer Nature

Date: Jul 7, 2017

Au38S2(SAdm)20 Photocatalyst for One-Step Selective Aerobic Oxidations

Author: Zhimin Li, Chao Liu, Hadi Abroshan, et al
Publication: ACS Catalysis
Publisher: American Chemical Society
Date: May 1, 2017

PERMISSION/LICENSE IS GRANTED FOR YOUR ORDER AT NO CHARGE

This type of permission/license, instead of the standard Terms and Conditions, is sent to you because no fee is being charged for your order. Please note the following:

- Permission is granted for your request in both print and electronic formats, and translations.
- If figures and/or tables were requested, they may be adapted or used in part.
- Please print this page for your records and send a copy of it to your publisher/graduate school.
- Appropriate credit for the requested material should be given as follows: "Reprinted (adapted) with permission from {COMPLETE REFERENCE CITATION}. Copyright {YEAR} American Chemical Society." Insert appropriate information in place of the capitalized words.
- One-time permission is granted only for the use specified in your RightsLink request. No additional uses are granted (such as derivative works or other editions). For any uses, please submit a new request.

If credit is given to another source for the material you requested from RightsLink, permission must be obtained from that source.

BACK CLOSE WINDOW

JOHN WILEY AND SONS LICENSE TERMS AND CONDITIONS

Aug 22, 2023

This Agreement between Miss. Manideepa Paul ("You") and John Wiley and Sons ("John Wiley and Sons") consists of your license details and the terms and conditions provided by John Wiley and Sons and Copyright Clearance Center.

License Number	5611780081171
License date	Aug 18, 2023
Licensed Content Publisher	John Wiley and Sons
Licensed Content Publication	Angewandte Chemie International Edition
Licensed Content Title	Template-Free Supracolloidal Self-Assembly of Atomically Precise Gold Nanoclusters: From 2D Colloidal Crystals to Spherical Capsids
Licensed Content Author	Olli Ikkala, Hannu Häkkinen, Tiia-Riikka Tero, et al
Licensed Content Date	Nov 23, 2016
Licensed Content Volume	55
Licensed Content Issue	52
Licensed Content Pages	4
Type of Use	Dissertation/Thesis
Requestor type	University/Academic
Format	Print and electronic
Portion	Figure/table
Number of figures/tables	1
Will you be translating?	No
Title	Metal Ion Based Assemblies of Gold Nanoclusters with Tuneable Photoluminescence
Institution name	IIT Guwahati
Expected presentation date	Nov 2023
Portions	Graphical abstract
Requestor Location	Miss. Manideepa Paul IIT Guwahati, Assam Guwahati, 781039 India Attn: Miss. Manideepa Paul
Publisher Tax ID	EU826007151
Total	**0.00 USD**
Terms and Conditions	

TERMS AND CONDITIONS

This copyrighted material is owned by or exclusively licensed to John Wiley & Sons, Inc. or one of its group companies (each a"Wiley Company") or handled on behalf of a society with which a Wiley Company has exclusive publishing rights in relation to a particular work (collectively "WILEY"). By clicking "accept" in connection with completing this licensing transaction, you agree that the following terms and conditions apply to this transaction (along with the billing and payment terms and conditions established by the Copyright Clearance Center Inc., ("CCC's Billing and Payment terms and conditions"), at the time that you opened your RightsLink account (these are available at any time at http://myaccount.copyright.com).

Terms and Conditions

- The materials you have requested permission to reproduce or reuse (the "Wiley Materials") are protected by copyright.

Modulating the hierarchical fibrous assembly of Au nanoparticles with atomic precision

Author: Qi Li et al

Publication: Nature Communications

Publisher: Springer Nature

Date: Sep 24, 2018

Creative Commons

Self-Nucleation and Self-Assembly of Highly Fluorescent Au5 Nanoclusters for Bioimaging

Author: Lina Yang, Huili Wang, Danyang Li, et al
Publication: Chemistry of Materials
Publisher: American Chemical Society
Date: Aug 1, 2018

PERMISSION/LICENSE IS GRANTED FOR YOUR ORDER AT NO CHARGE

This type of permission/license, instead of the standard Terms and Conditions, is sent to you because no fee is being charged for your order. Please note the following:

- Permission is granted for your request in both print and electronic formats, and translations.
- If figures and/or tables were requested, they may be adapted or used in part.
- Please print this page for your records and send a copy of it to your publisher/graduate school.
- Appropriate credit for the requested material should be given as follows: "Reprinted (adapted) with permission from {COMPLETE REFERENCE CITATION}. Copyright {YEAR} American Chemical Society." Insert appropriate information in place of the capitalized words.
- One-time permission is granted only for the use specified in your RightsLink request. No additional uses are granted (such as derivative works or other editions). For any uses, please submit a new request.

If credit is given to another source for the material you requested from RightsLink, permission must be obtained from that source.

BACK CLOSE WINDOW

Complexation Reaction-Based Two-Dimensional Luminescent Crystalline Assembly of Atomic Clusters for Recyclable Storage of Oxygen

Author: Manideepa Paul, Srestha Basu, Arun Chattopadhyay
Publication: Langmuir
Publisher: American Chemical Society
Date: Jan 1, 2020

PERMISSION/LICENSE IS GRANTED FOR YOUR ORDER AT NO CHARGE

This type of permission/license, instead of the standard Terms and Conditions, is sent to you because no fee is being charged for your order. Please note the following:

- Permission is granted for your request in both print and electronic formats, and translations.
- If figures and/or tables were requested, they may be adapted or used in part.
- Please print this page for your records and send a copy of it to your publisher/graduate school.
- Appropriate credit for the requested material should be given as follows: "Reprinted (adapted) with permission from {COMPLETE REFERENCE CITATION}. Copyright {YEAR} American Chemical Society." Insert appropriate information in place of the capitalized words.
- One-time permission is granted only for the use specified in your RightsLink request. No additional uses are granted (such as derivative works or other editions). For any uses, please submit a new request.

If credit is given to another source for the material you requested from RightsLink, permission must be obtained from that source.

BACK CLOSE WINDOW

Modulating the Photoluminescence of Europium through Crystalline Assembly Formation with Gold Nanoclusters and Then Phosphate Ions

Author: Manideepa Paul, Arun Chattopadhyay
Publication: Journal of Physical Chemistry Letters
Publisher: American Chemical Society
Date: Dec 1, 2023